SPUTTERING OF URANIUM

Thesis by

Ron Gregg

In Partial Fulfillment of the Requirements

for the Degree of

Doctor of Philosophy

California Institute of Technology

Pasadena, California

1977

(Submitted May 13, 1977)

ACKNOWLEDGEMENTS

For motivating this experiment in the first place, for his undiminished interest in it, and especially for allowing me to pursue the research in my own style, my greatest thanks to Tom Tombrello. I also wish to thank Don Burnett and his crew in Mudd for initiating me into the mysteries (if not the joys) of the fission track technique. Ziggy Switkowski is also deserving of a special mention for his constant enthusiasm and for good advice on many occasions. Conversations with Bob Weller, Joe Griffith, and others in Kellogg proved quite useful at times. The helpfulness and general friendliness of the many staff members in Kellogg was greatly appreciated.

This section would not be complete without acknowledging the denizens of Page House, Chester's Jesters, and the many other friends here at Caltech (who shall remain nameless for their own protection) who have made the last few years so enjoyable.

The person deserving of the most gratitude of all is Sue, who gave up so much that I might pursue graduate studies at Caltech.

I would also like to acknowledge the efforts of the scanners, Sharon Streight, Robert Thornton, Dave Walker, Norm Murray and Joel Okazaki, who spent many hours at the microscope counting tracks.

ABSTRACT

Sputtering yields for uranium metal under bombardment by 13 - 120 keV protons and by 20 - 120 keV He+ are presented. Angular distributions of the material sputtered by these ions are also given. Sputtering yields for 40 and 80 keV Ar+ were measured as well.

The technique employed to make these measurements was the detection of fission tracks in mica produced by ^{235}U sputtered onto collector foils which were subsequently exposed to a high fluence of thermal neutrons. The technique is extremely sensitive and allowed the measurement of sputtering yields less than 10^{-4} atoms per ion. It also made possible a detailed study of the emission of chunks from the uranium targets during sputtering. Mass distributions of chunks emitted during bombardment by 40 - 120 keV protons and by 80 keV argon are presented.

Comparisons are made between the experimental results and those predicted by the Sigmund theory of sputtering.

TABLE OF CONTENTS

I. INTRODUCTION

Sputtering, to put it as succinctly as I can, is the ejection by a flux of particles of some of the constituent atoms of an object from one of the surfaces of that object. The principal quantity which characterizes sputtering is the sputtering yield "S" defined as the number of atoms ejected per incident particle. Scientific investigation of sputtering extends back many decades and has grown into a vigorous and multifaceted field, as one may quickly determine by consulting one of the many recent books and review articles on the subject.[2,30] Design considerations for thermonuclear reactors provide some of the strongest motivation for studying sputtering today.[20] This is due to the fact that bombardment of the first wall of the reactor vessel by energetic particles will erode the wall and may sputter enough material to poison the plasma. Sputtering of the lunar surface by the solar wind[31,47] and sputtering of such diverse astrophysical surfaces as those found on Io[33] and on interstellar grains[51] are also topics stimulating current interest in the field.

My own involvement in this sputtering business developed out of another experiment--an attempt to measure the cross-section at energies near 100 keV for $^{10}B(p,\alpha)^{7}Be$ using very thin ^{10}B targets. It was realized by Ziggy Switkowski that it was probable that the large proton bombardments contemplated would sputter away a large fraction of the target. It would therefore be necessary to measure the amount of sputtering, which was just fine as far as Ziggy was concerned since the measurement would be perfectly suited to the use of a very sensitive

technique--namely, the use of plastic track detectors and the $^{10}B(n,\alpha)$ reaction to determine the amount of sputtered ^{10}B collected on a foil. I must digress for a moment to comment that the interest in sensitive techniques is largely motivated by the low sputtering yields typically produced by light ions. The interest in sputtering by light ions (such as neutrons, protons, and α particles) is largely motivated by the fact that they are the primary constituents of the solar wind and contemplated first-generation CTR plasmas.

In any event, Ziggy took his enthusiasm for this sensitive technique to a typical gathering of the minds in Lauritsen Library in Kellogg, where Tom Tombrello proposed that sputtering of ^{235}U would be even more sensitive, and easier. One would still use the nuclear track detection method to measure the amount of sputtered material collected on a foil, but in this case exposure of the collector foils to a high neutron fluence would result in ^{235}U-fission fragments which would register in pieces of mica placed against the collector foils. The tracks would be made visible by etching in HF and could be counted with the aid of a microscope. The attractiveness of this proposal was enhanced by the presence in the Caltech community of one of the leading experts on the use of nuclear track detectors--Don Burnett. It also just so happened that Don had some 99% pure ^{235}U metal foils left over from the lunar neutron probe experiment.[6] My fate was sealed. Having been sidetracked from $^{10}B(n,\alpha)^{7}Be$ by proton sputtering of boron, I now found myself pursuing proton sputtering of uranium.

The feasibility of the experiment depended on the magnitudes of a few physical and empirical quantities which are connected by a couple of simple equations. The fission track density on the micas placed next to the collector foils during neutron irradiation is the quantity which must ultimately be determined by microscopic scrutiny of said pieces of mica. The number of tracks per square centimeter is given by

$$N_T = N_U N_n \sigma_f \qquad (1\text{-}1)$$

where N_U = number of ^{235}U atoms/cm^2 on the collector foil

N_n = neutron fluence from irradiation in the reactor (= thermal neutrons per cm^2)

σ_f = ^{235}U fission cross section at 2200 m/sec = 580 bn

The density of ^{235}U atoms collected is given approximately by

$$N_U = \frac{SN_p}{2\pi r^2} \qquad (1\text{-}2)$$

where S = sputtering yield (atoms/ion)

N_p = total number of incident ions

r = distance from target to collector foil

Equations (1-1) and (1-2) can be combined to yield

$$N_T = \frac{SN_p N_n \sigma_f}{2\pi r^2} \qquad (1\text{-}3)$$

For the experiment to work, this equation must yield a track density which is greater than the background track density due to ^{235}U in the

mica, in the collector foils, or acquired on the surface of either from the environment. Using information supplied by Don Burnett's group in Caltech's Mudd Laboratory, I estimated that $N_T = 10^5 cm^{-2}$ would be sufficiently above background and would provide a convenient track density for the microscopic scanning. (Both of these conjectures proved to be correct).

Now for the right-hand side of equation (1-3). Based on the work of Finfgeld et al.[10] on the sputtering of several metals by 0.5-8 keV protons, I guessed that the yield for 100 keV protons on uranium would be on the order of 10^{-4} (which turned out to be true). It was also known that a fluence of 10^{14} neutrons/cm^2 was readily obtainable in the thermal column at the UCLA reactor. A practical distance r from target to collector foil is about 3 cm, determined from considerations of ion-beam size and sputtering chamber geometry. Plugging these numbers into (1-3) then implies that a total incident proton dose of $\sim 10^{18}$ would be required to produce a final track density $N_T = 10^5 cm^{-2}$. This in turn implies bombarding the target with 10 μA of beam for 5 hours, which is possible with the ion source available in Kellogg. The conclusion was, therefore, that the experiment would be feasible.

In actual practice 10 μA of 100 keV ions was found to deposit more energy than the .001" foil targets could tolerate without severe thermal crinkling. Beam currents of about 1 μA were employed instead. It was also found that collector foils and mica track detectors were just small enough to fit in a small plastic container which could be lowered into the core of the UCLA reactor, affording neutron fluences

of up to $10^{16} cm^{-2}$. This compensated for the reduced ion-beam current and permitted hydrogen sputtering runs of between 15 minutes and 5 hours (depending on choice of N_p and N_n). Due to the much larger sputtering yield from helium ($S \sim 10^{-2}$), a typical helium run was 1 μA for 60 seconds. For argon the sputtering yield is on the order of 2, which meant runs with argon lasted less than a minute with ∿10 nA of beam to avoid too large a track density* in the mica detectors.

It was realized in the beginning (by Tom and Don at least) that the experiment held promise in a number of ways. First of all, it ought to be sensitive enough to measure the sputtering yield for protons with energies near 100 keV. It was also expected that angular distributions for the sputtered material could be obtained. Both of these expectations have been fulfilled. Sputtering yields and angular distributions have been measured for 13-120 keV protons. Additionally, angular distributions and sputtering yields for 40-120 keV ^4He have been obtained. It was further hoped that the technique would prove to be sensitive enough to imply the feasibility of doping various materials with ^{235}U to allow low-sputtering-yield studies of other materials utilizing the same technique. The technique has in fact proved to be sensitive enough, and this is discussed in some detail in Appendix A. Another area in which results were looked for was the area of chunk emission, since chunks collected on the foils would show up as star-bursts of fission tracks in the micas. This would permit one to actually determine the chunk size. In fact many chunks have been seen on the collector foils, and data on the amount

*for convenient scanning in an optical microscope

of chunk emission and distributions of chunk size are presented. One final bit of information that is presented is some limited data on molecular sputtering by H_2 and H_3.

Inasmuch as there are a number of parameters that one may vary in a sputtering experiment, I will summarize here what was and what was not varied.

1. The effect of beam energy on sputtering yield was investigated for 10-120 keV ^1H and 40-120 keV ^4He.
2. The angular distribution of the sputtered uranium was determined.
3. The angle of incidence of the beam was not varied; all sputtering was done with perpendicular incidence of the beam on target.
4. A comparison between the sputtering yield from slightly oxidized target surfaces and sputter-cleaned target surfaces is presented, but there was no investigation of yield as a function of surface finish. All the targets were more or less uniformly rough at the 1μ level.
5. There was no systematic study of dose effects; new target areas were used for each run to eliminate possible effects from non-uniform dose.
6. No effect from varying target temperature was looked for; beam flux was always kept low enough that heating of the target was negligible. (See p.19)

Before we plunge ahead into the experimental procedures, a few words should be said about why the sputtering is performed in ultrahigh vacuum. The primary concern is that the target surface be as clean as possible during the sputtering runs. Cleanliness of the surface is important because the sputtered atoms originate from within only a very few monolayers at the surface. If the surface is oxidized or has various substances adsorbed on it, then the sputtering yield of uranium will decrease as energy is expended to sputter atoms other than uranium. Provided that the surface is clean at the atomic level at the beginning of a sputtering run, it will remain so if the rate of adsorption of gases is small compared with the rate at which they are sputtered away by the ion beam. Since the intrinsic sputtering rates for keV protons are quite low, and since the beam current density must be kept low to prevent overheating of the targets, the vacuum must be quite good to avoid accumulation of surface contaminants during hydrogen sputtering runs. The vacuum requirements for sputtering by keV helium and argon ions are less stringent because of their much greater sputtering yields. This is all discussed quantitatively in Appendix C. The conclusion is that the vacuum employed (on the order of 10^{-9} torr) is good enough to prevent decrease of the sputtering yield from 100 keV protons by more than a few percent, as an upper limit.

Initial cleanliness of the targets is obtained by washing them in HNO_3 and then sputter-cleaning them in vacuo with an argon ion beam. (See Chapter II for details). The nitric acid bath is necessitated by the fact that uranium oxidizes progressively in air; which is to say

that an acquired oxide layer affords no protection against further oxidation. This means that over a period of weeks uranium targets stored at atmospheric pressure acquire an oxide layer which is too deep to be removed conveniently by presputtering, but which dissolves in HNO_3 in a few minutes. The uranium foils used in this experiment had been stored in atmospheric conditions for an extended period and were given, therefore, the complete cleaning treatment.

II. EXPERIMENTAL PROCEDURES

A. An Overview

The basic apparatus in which the uranium sputtering was conducted is pictured in Fig. 1, and the important elements are sketched in Fig. 2. The positions of the bands of sputtered uranium as they are collected on the catcher foils are displayed in Fig. 3.

Approximately 40 sputtering runs were made to gather the data for this thesis. The primary steps required for each run are presented here:

(1) A metallic ^{235}U target roughly 1.5 cm x 1.0 cm x .0025 cm is cleaned by dipping it in 35% HNO_3 for a few minutes.

(2) The target and others like it are mounted on a movable target plate which in turn is mounted on the sputtering assembly (Fig. 6).

(3) A cylinder designed to collimate the sputtered uranium is attached to the assembly (Fig. 7). Clean collector foils (5.0 cm x 3.75 cm x .005 cm) are installed in a cylinder which is attached to a manipulator (Fig. 8) so that a number of sputtering runs may be made each time the assembly is placed in the ultrahigh vacuum (UHV) chamber (Fig. 9).

(4) The assembly is placed in the UHV chamber which is then pumped down to 10^{-9} torr.

At this point most of the targets are sputtered by 80 keV Ar to remove any lingering surface contamination. Ion beams are provided by a 135 keV ion source.

(5) The sputtering runs themselves are now made using beams of H_1^+, H_2^+, H_3^+, He^+ or Ar^+; the collector foils are moved between runs so that the sputtered uranium is collected in bands (Fig. 3).

(6) The collector foils are removed from the assembly and interleaved with mica foils of the same dimensions in a plastic container. NBS standards containing known quantities of ^{235}U are also placed between mica sheets in the container.

(7) The container is exposed to a high fluence of neutrons (typically 10^{15}-$10^{16}/cm^2$) in the R-1 nuclear reactor at UCLA to fission some fraction (typically 10^{-6} to 10^{-5}) of the collected ^{235}U.

(8) The mica foils are then etched (typically for 15-60 min) in 48% HF to make the fission tracks visible.

(9) The micas are scanned with the aid of a microscope (at 450X usually) to obtain the raw data.

(10) The track density in the micas next to the NBS standards is used to compute the neutron fluence which in turn is used in conjunction with track densities to compute the amount of ^{235}U collected at various places on the collector foil. Finally, the angular distribution and sputtering yield are determined.

B. Sputtering

In this section I will discuss the relevant aspects of the sputtering assembly, the ultrahigh vacuum system, the ion source and associated beam line, beam integration, target preparation, and the actual sputtering.

The Sputtering Assembly

This appears in various stages of assembly in Figs. 4-8. Figure 4 shows the portion of the assembly which remains in the atmosphere. It consists of an 8" OD UHV flange on which are mounted two precision manipulators. The left-hand one is a bellows-sealed 6-inch linear travel feed-through designed by Jon Melvin and constructed in the Kellogg shop. It is used to position the cylinder carrying the collector foils. The right-hand one is a VF-172-2 rotating/translating manipulator with 2" travel manufactured by Huntington Mechanical Laboratories. It is used to position the target plate. The vacuum side of the 8" OD flange is pictured in Fig. 5. The end of the 6" travel manipulator protrudes through the hole on the right. Mounted on the end of the other manipulator is a stainless steel block to which the target plate is mounted. The block is electrically isolated from the manipulator by the boron nitride piece seen directly below it.

In Fig. 6 the target plate which was used for most of the sputtering runs is shown attached. It was machined from 1/8" OFHC copper to provide a good heat sink for the targets. The targets were mounted by clamping with pairs of copper bars, two of which are shown in position. A piece of quartz glass for viewing the beam spot is also shown attached.

This target plate supplanted one made from 1/8" aluminum, on which the targets were clamped behind 8 mm holes by single 1/8" bars of aluminum.

The sputtering assembly is next shown in Fig. 7 with the collimation cylinder in place on its insulating glass ring. This stainless steel cylinder has a 3/8" wide slot extending 180° around to limit the collection area on the collector foils for a given run. It also has two pairs of vertical side bars to ensure that the target plate is kept perpendicular to the beam.

Figures 1 and 8 display the entire sputtering assembly, which has been completed by the addition of the collector-foil holder. This cylinder (which is also stainless steel) holds the collector foils with the edges nearest the beam butted against the inwardly-protruding frame around the vertical slot, and with the outer edges clamped by vertical bars (see Fig. 2). The collector-foil holder is moved by the 6-inch travel feed-through to position the foils for different sputtering runs. The resulting arrangement of bands of sputtered uranium is shown in Fig. 3.

The Ultrahigh Vacuum System

A photograph of the UHV system appears in Fig. 9 and a sketch of the important components comprises Fig. 10. All connections between components are sealed with OFHC copper gaskets. The only materials used in the system (i.e., stainless steel, copper, aluminum, glass, mica, and boron nitride) are low vapor pressure materials which may be baked at high temperature to drive adsorbed gases from the inner walls. Except for the ion pump, the entire system may be baked at 450°C; the ferrites

in the ion pump's magnets limit its bake-out temperature to 250°C. Proper cleaning of the components (see Appendix B for cleaning procedures) and baking enable a vacuum of $<10^{-9}$torr to be routinely achieved.

The sputtering chamber is a 6" ID stainless steel tee, 11" high, which was manufactured by Ion Equipment Corp. It has three 8" flanges to which the sputtering assembly, a large viewport, and the UHV pump attach. The pump is a COV-500 by Ion Equipment which is attached directly below the sputtering assembly for maximum pumping speed in the vicinity of the targets. It contains both a titanium sublimation getter-ion pumping assembly and a 25 ℓ/sec differential sputter-ion pump. The combination is rated at 500 ℓ/sec for N_2 at 10^{-8}torr and 6ℓ/sec for argon at the same pressure. When the system is reasonably clean the pump is capable of bringing the pressure from 10^{-3}torr to 10^{-9}torr in 12 hours.

The pressure rises to about 4×10^{-9}torr when a 1 μA H^+ ion beam is brought into the chamber and to about 2×10^{-7}torr for a 1 μA argon beam. A μA of beam implies 1 ℓ/sec of particles entering the system at 2×10^{-7}torr and 50 ℓ/sec at 4×10^{-9}torr. It is quite likely that most of both the argon and hydrogen diffuse back out of the targets within seconds and contribute to the gas load. In addition, an unknown quantity of gas is desorbed from the target surface while being bombarded by the beams and must also be pumped. In the case of argon bombardment the amount of desorbed gas is likely to be several times the amount of argon. It appears, therefore, that the observed pressure rises are consistent with the expected pumping speed of the system.

The system is roughed to 10^{-3}torr by an Ion Equipment Corp. SP-11 molecular sieve sorption pump. The SP-11 consists basically of a fancy bucket of zeolite which is immersed in a simple dewar of LN_2 to promote adsorption of gases. It is capable of pumping the vacuum system down from atmospheric pressure to 10^{-3}torr in less than 30 minutes. When the SP-11 is not in use it is isolated from the ultrahigh vacuum portion of the system by an Ion Equipment Corp BVV-152 copper-sealed right-angle valve.

The UHV system is connected to the rest of the beam line through a 40-cm-long cold trap with a 1 cm ID central beam tube. A Huntington MS-075 5/8" ID copper-sealed in-line valve serves to isolate the sputtering system from the low vacuum (typically 3×10^{-6}torr) of the beam line when beam is not being run. With the cold trap filled with LN_2 and the UHV system pumped down to 10^{-9}torr there is essentially no change in pressure in the sputtering chamber when the MS-075 valve is opened. Thus, contamination of the system by oil vapor from the diffusion-pumped beam line is virtually eliminated.

Another component of the vacuum system which should be mentioned is the Faraday cup at the end of the beam line (see Figs. 9 and 10). This was made by Ion Equipment Corp. and has a very short section of glass in the middle to electrically isolate the end flange. Checks of beam integration accuracy in the sputtering chamber can be made by bringing the beam through to the Faraday cup. In addition, the end flange normally has a window mounted on it so that the beam spot may be viewed on a piece of quartz glass installed on the target plate. This

was very important in this experiment, since the beam optics are such that a wide variety of beam spot shapes and sizes is available at the target plate, and an appropriate spot must be selected for each run.

The Ion Beams

Views of the ion source and beam line appear in Figs. 11 and 12. Beams of positive ions of hydrogen, helium, argon, and other gases were extracted from the 135 kV duoplasmatron ion source located in the Kellogg Radiation Laboratory at Caltech. The beams were energy analyzed by a 31° deflection magnet. The beam energy was calibrated by direct measurement of the ion source voltage using a precision resistive divider. Beam focusing was provided by a doublet quadrupole magnet which was located between two sets of x-y steering magnets.

Final collimation of the ion beam was provided by a pair of 3 mm apertures in .020" stainless steel disks mounted in the beam tube between the cold trap and the MS-075 in-line valve. The downstream aperture was 12 cm from the other and 30 cm from the target. The beam optics were such that the focus position of the beam could be moved a considerable distance to either side of the apertures, hence the apertures did not completely determine the beam spot, but only limited it to between 3 and 6 mm in diameter. This actually proved useful in this experiment: for sputter-cleaning of the targets a large (6 mm diameter) argon beam spot was used, while a smaller 3-4 mm spot employed during the data runs ensured that the portion of the target being sputtered was well within the sputter-cleaned area. As mentioned earlier, selection of beam spot size was facilitated by viewing the beam

on a piece of quartz glass attached to the target plate.

Beam integration was performed using an Ortec model 439 digitizing current integrator. The target plate, collimation cylinder, and catcher-foil carrier were all connected together and isolated from ground so that an effective Faraday cup was formed. Secondary electrons knocked out of the target by the ion beams could only escape from the sputtering assembly through the 1 cm^2 beam entrance aperture, which amounted to <1% of the 2π solid angle available to them. This meant that the beam integration was very insensitive to application of a bias voltage. There was no change in hydrogen beam current at the most sensitive level that could be read on the beam current monitor (2%) when a +300V bias was applied to or removed from the sputtering assembly. There was also no change at the level of repeatability for argon beam current readings (4%) when a +300V bias was applied or removed. In addition, there was no detectable change (< 2%) in hydrogen beam currents when the target plate was moved so that the beam impinged on a uranium target rather than the imaging quartz. There appeared to be an increase in measured beam current of about 5% when an argon beam was moved from quartz to uranium target.

Secondary electrons emitted from the edges of the final collimation apertures were suppressed by small magnets placed near the beam tube just before the sputtering chamber. The magnets were brought almost close enough to the beam being run to just barely deflect it. Here also the beam currents were very insensitive to placement or removal of a suppressor magnet, implying that very few secondary electrons were making

it from the final collimator to the sputtering assembly even without suppression. For argon beams the current reading changed by only 1% when a magnet was brought close enough to deflect the beam a bit, and for hydrogen beams there was no detectable variation in beam current.

Target Preparation

Basic cleaning of the uranium targets was accomplished by dipping them in 35% HNO_3 for approximately 5 minutes. The acid bath was followed by a rinse in distilled water and an acetone bath. Targets which had been stored in atmospheric conditions were covered with a macroscopic layer of black oxide which presumably is mostly UO_2. Nitric acid has a much faster attack rate for the oxide than for the metal. Most of the oxide dissolved within two minutes, leaving a semi-shiny silvery surface. Occasionally a few tiny black streaks aligned with the cold-rolling grain of the foils were visible after cleaning.

After cleaning, the targets were typically at atmospheric pressure for 30-60 minutes before pump-down began, and another few hours was required for the vacuum to reach 10^{-9}torr. During this period the foils acquired a definite yellowish cast indicative of the formation of an oxide layer on the order of 100Å thick.[14] Just prior to most of the sputtering runs this oxide layer was removed by sputtering with an 80 keV argon beam. For this presputtering the argon beam spot was a uniform diffuse blob approximately 7 mm in diameter. For sputtering runs in series 2 and 3 the targets received a presputter fluence of nearly 1.5×10^{16} argon ions, and series 4-7 targets received a fluence of 5×10^{16}. The sputtering yield for 80 keV argon is $\sim$2 (as measured

in this experiment), and the average interatomic distance in uranium is 2.75Å.[24] Thus, roughly 140Å (50 monolayers) of the target surface was removed from series 2 and 3 targets, and about 400Å (150 monolayers) was removed for series 4-7. That should have been more than enough to ensure removal of all surface oxidation and other contamination. In all cases the appearance of the beam-spot area of the target foils was very silvery after sputter cleaning.

Scanning electron micrographs of typical target surfaces appear in Figs. 15-22; they are discussed in Section IIIA. In Appendix C the possibility of some re-oxidation of the foils after sputter cleaning is discussed.

The Sputtering Runs

Figure 3 displays the positions of the catcher foils and their data bands as seen from the position of a target. The foils were $1\frac{1}{2}$" x2" pieces of .005" thick 5052 aluminum for runs in series 1-3 and $1\frac{1}{2}$" x2" pieces of .002" Indian ruby muscovite mica for runs in series 4-7. Mica was substituted for aluminum to take advantage of its lower ^{235}U content after it was discovered that mica could be placed in the sputtering chamber without degrading the vacuum. The data bands resulted from collimation of sputtered ^{235}U by the 3/8" wide slot in the collimation cylinder. During presputtering cleaning runs the foils labeled GL and GR were in front of the slot.

Before each sputtering run the appropriate ion beam was carefully focused and centered on a piece of quartz mounted below the targets. The beam spot was 5 mm maximum width to ensure that it was well within

the sputter-cleaned area. Moving the target plate with the precision Huntington manipulator allowed the accurate positioning of the beam on target.

During all sputtering runs the beam current was kept low enough (< 3 μA) so that no overheating of the target foils occurred. A trial run with 20 μA of 100 keV H_1^+ on target had produced thermal crinkling of the foil, and a run at 5 μA had produced some discoloration (but no crinkling), but 3 μA produced no visible effects. Hydrogen ion beam currents were usually 1-2 μA which meant 3-5 hours to accumulate the fluence of 10^{17} ions in series 1-3 runs and less than 15 minutes to accumulate 5×10^{15} ions for series 4-7. Due to the much higher sputtering yield from argon, a typical argon sputtering run was 10 nA of beam for 15 seconds. Helium sputtering was done with 1 μA of beam on target for ∿60 seconds.

The pressure in the sputtering chamber was always $\leq 10^{-9}$ torr before any sputtering began. It rose to as much as 5×10^{-7} during argon beam sputter-cleaning and dropped to 5×10^{-9} immediately afterward. The pressure was always a few times 10^{-9} torr during hydrogen sputtering runs and dropped back down to 10^{-9} torr shortly after completion of the last run in a series.

When a series of 5 or 6 runs was finished the catcher foils were removed from the sputtering assembly and placed in individual plastic boxes to await exposure to neutrons at the UCLA reactor.

C. Track Detection

This section will be concerned with the details of the nuclear track detection technique employed to ascertain the surface density of sputtered ^{235}U on the collector foils. The basis of the technique is that mica in contact with the collector foils during neutron irradiation will record a fission-fragment damage track for each ^{235}U atom that fissions. These tracks are later etched in HF to render them visible under transmitted-light microscopy and are counted to determine the amount of ^{235}U on the collector foils.

The Mica

The muscovite mica employed in this experiment is an ideal track detector for fission fragments for a number of reasons. In the first place, it has 100% registration efficiency for fission fragments.[11] In addition, it does not register tracks at all for elements with $Z < 10$,[12] which avoids any possible background of tracks from α-particles, protons, etc. Further, the counting efficiency for the tracks produced by a surface source of fission fragments is virtually 100%. This is due primarily to the distinctive shape of the etched tracks (see Fig. 13); long (15μ full length), thin tubes with diamond-shaped cross sections. With a moderate etch (> 15 minutes in 48% HF), even tracks seen end-on are unmistakable under the microscope. This distinctive shape makes possible accurate track counting even in the presence of a substantial background of random pits, bubbles, cracks and tiny dirt particles. An important virtue of muscovite is that, since the surface is dissolved

away by the etchant at a rate which is completely negligible compared with the etching rate for tracks, it can be etched for very long times (order of hours) to make even short fission tracks unmistakable without erasing tracks having a very low angle to the surface. (See Fleischer, Price, and Walker, Ch. 2 for a detailed discussion of the etching process.)

A significant attribute of the high quality Indian ruby mica used in this experiment is an effective surface density of ^{235}U which was negligible compared with the amounts collected on the catcher foils. This low ^{235}U concentration, combined with great sensitivity for ^{235}U through induced fission makes possible measurement of some extremely low sputtering yields, which is discussed in Appendix A.

Additional advantages of mica are that it suffers little radiation damage and, quite significantly, no track fading during neutron irradiation.[41]

The only disadvantage of mica is its susceptibility to neutron activation. At a fluence of $10^{16} n/cm^2$ the resultant activity decays to a negligible level in a period of a few days, hence it is not a serious drawback.

Neutron Irradiation

When a group of collector foils was accumulated they were interleaved with 1-1/2" x 2" pieces of muscovite mica and placed in a small plastic container for transport to UCLA and subsequent neutron irradiation. All pieces of mica had the surface layer on each side stripped off with adhesive tape to minimize possible environmental uranium

contamination. The mica placed up against each foil recorded the uranium distribution on the foil by registering one of the fission fragments from each ^{235}U that was fissioned. In the cases where sputtered ^{235}U was collected directly on mica foils, two copies of each data band resulted.

Neutron irradiations were performed at the R-1 nuclear reactor at UCLA's Nuclear Energy Laboratory. This reactor produces a peak flux of $2 \times 10^{7} n/(cm^2\text{-sec-watt})$ and is therefore capable of delivering a fluence of $10^{16} n/cm^2$ in a period of 90 min at its full operating power of 100 kW. For runs in series 1-3 a fluence of $\sim 10^{15} n/cm^2$ was employed, and for series 4-7 the fluence was $\sim 10^{16} n/cm^2$.

The fluences were determined with the aid of NBS glass standards containing known quantities of ^{235}U. These standards are available in four nominal uranium concentrations (500, 50, 1, and 0.07 ppm), the higher concentrations being appropriate for use with lower neutron doses and vice-versa. The primary technique employed to ascertain the neutron fluence was simply to place a standard between two sheets of mica in the package of catcher foils being irradiated and count the number of fission tracks per cm^2 that were produced in the mica. The fluence is then calculated from

$$N_n = \frac{N_t}{N_u \sigma_f}$$

where N_t = number of tracks per cm^2

N_u = effective number of ^{235}U atoms / cm^2 in the standard

σ_f = fission cross section = 582 bn

N_u in turn is given by

$$N_u = \frac{1}{2} R_f n_u$$

where n_u = number density of ^{235}U in standard

R_f = average single fission-fragment range in the standard glass

and the factor of $\frac{1}{2}$ accounts for the fact that only half the fissioned ^{235}U atoms within a distance R_f of the surface of the standard glass produce a fission fragment which leaves the surface (given that the thickness of the glass is greater than R_f).

The accuracy of this technique depends on two things: 1) careful counting of all fission tracks produced in the mica, which is difficult because the actual track lengths are distributed all the way down to zero due to the fact that the source of the fission fragments is thicker than R_f, and 2) knowledge of the value of R_f itself. For each reactor run I personally counted a minimum of 1000 tracks (under direct microscopy at 450X) spread over a large area on the micas which were in contact with the glass standards. I feel confident that the counting efficiency was at least 95% and that the counting accuracy (involving resolution of short tracks and discrimination against tiny features which are not tracks) was about $\pm$5%. It has been reported,[41] however, that discrepancies in neutron flux determination due to differences in track counting criteria may be expected to be as large as 20%.

A range R_f appropriate to the soda-lime glass composing the NBS standards was calculated by Haines[18] using the range and energy-loss

relations of Lindhard.[25,26] The calculation was normalized to the range of n-induced fission tracks in fluorapatite as measured by Bhandari et al.[4] Their measurement of the mean etchable track length yielded a value of 15.3 ± 1μ (2.37 ± 0.15 mg/cm^2). The range derived by Haines for soda-lime glass is 2.24 mg/cm^2. Other calculated values (including 2.22 mg/cm^2 for pure SiO_2 and 2.29 mg/cm^2 for phlogopite mica) make it clear that the range is not strongly sensitive to the exact atomic composition of such silicates. In addition, the measured etchable range of fission fragments in muscovite mica is very close to 15μ.[11] It is apparent, therefore, that calculational errors in deriving R_f are smaller than the error quoted by Bhandari, and a value of 2.24 ± 0.15 mg/cm^2 is thus employed. Combining this error (± 6.5%) with the stated counting error (± 5%) yields an overall uncertainty in the value of the neutron fluence of less than ± 10%.

As a check on this neutron fluence determination method, the included glass standard wafer from one of the neutron exposures was compared with an identical pair of standards which had received prior irradiations in the NBS reactor and been certified by the NBS as to neutron dose. These are sold by the NBS as "calibrated glass standards for fission track use" in the same four uranium concentrations as the non-irradiated standards. The pair of standards used contain 0.823 ± 0.002 ppm (by weight) uranium with 0.2792 atom % ^{235}U and is designated "SRM 963" by the NBS. The two wafers are separately designated RT-3 and RT-4 corresponding to the different positions in which they were irradiated in the NBS reactor. The RT-4 position is farther

from the reactor core center, and the neutron flux is better thermalized there than in position RT-3. This is indicated by the cadmium ratios of 10.2 for gold foils and 65 for copper foils at RT-3 and ratios of 87 for gold foils and 536 for copper foils at position RT-4.[8] The neutron fluxes measured by the NBS for SRM 963 are shown in Table 1; total neutron fluence is found by multiplying by the exposure times given in footnote b. The wafer identification numbers for the standards I used are 614016 for RT-4 and 614141 for RT-3.

After irradiation of the blank wafer, which I designated SRM-A, all three wafers were ground, polished, etched, and counted as detailed in Appendix D. Results are tabulated in Table 2. The neutron fluence values determined here for the UCLA reactor run are a bit lower than the value of $1.08 \pm .10 \times 10^{16} n/cm^2$ found by counting fission tracks in mica sheets placed against SRM-A during irradiation. However, the proportion of fast neutron flux in the center of the UCLA reactor is somewhat higher than found even in the RT-3 position of the NBS reactor. This is indicated by a cadmium ratio for 40 mgm/cm^2 gold foils (as measured by Bruce Taylor, private communication) of 3.3 in the UCLA reactor center as compared with 10.2 for gold foils* at RT-3 and 87 at RT-4. The values determined by comparing SRM-A with RT-3 thus actually underestimate the neutron dose received by SRM-A by a few percent. The conclusion, therefore, is that agreement between the two methods of fluence determination is within the error quoted for the primary method due to counting error and uncertainty in R_f, and no correction is applied to fluences derived by the primary technique.

*also 40 mgm/cm^2

Etching

After the neutron irradiation, and after the resultant radioactivity decayed to a reasonable level, the micas were etched in 48% HF at room temperature to render the fission tracks visible. Etching times of 15 to 60 min were employed; a short etch was used for micas where it was desired to make star bursts of tracks easy to count, and a long etch was given to the standards to enhance the visibility of the many short tracks. The etching action of the HF was stopped after the desired time by immersing the micas in full strength NH_4OH for 10-15 min. This was followed by rinsing for a few hours in running water to remove all traces of HF.

Results of etching a typical mica detector appear in Fig. 13. The etching time in this case was 15 min. The magnification is $\sim$1000X and the actual track lengths are close to 15μ. This particular photo contains a small "star" of about 30 tracks resulting from fissions of 10^{-6} of the ^{235}U atoms in a chunk of approximately 3×10^7 atoms. Figure 14 displays a large fission star at the same magnification.

Scanning

Once a mica has been etched, all that remains to extract the raw data from it is to count the tracks in given areas. Since the tracks are $\sim$15μ in length it is necessary to use a microscope to do this. The microscopes utilized in this experiment were equipped with precision x- and y-deflection gauges on the stage to enable given points on the data bands to be accurately located. They also possessed precision grids in the eyepieces which permitted accurate determination of track densities.

The areas of the grids were calibrated using a Zeiss objective micrometer engraved with a scale 1 mm long marked off every 10μ.

Scanning was often facilitated by viewing the areas to be counted on a closed-circuit TV attached to one of the microscopes. Track size and contrast were sufficient that the TV could be employed for routine work with perfectly adequate results. The resolution was not quite enough for counting the standards (with many short tracks) or counting the number of tracks in a given star-burst, and in these cases direct viewing through the microscope was always used.

A small number of scanners were employed at one time or another in the tedious counting operation. Their results were checked frequently and found to be consistent and reproducible to within 10%, which is smaller than the scatter in the data. Generally, a minimum of 400 tracks were counted at each data area, which was typically an area 1 mm high and .15 mm wide in the long direction of a data band. Each data area supplied one data point on an angular distribution of sputtering yield curve. Thus the error from counting statistics was ±5% for the angular distributions. Since the sputtering yield for each ion-target combination summed over 7 data areas, the statistical error on the values of S(E) due to counting was $<2\%$.

III. EXPERIMENTAL RESULTS

A. Target Surfaces

Before looking at the results of the sputtering measurement, it would be useful to have an idea of the condition of the surfaces being bombarded. To this end a number of the targets were examined with a small scanning electron microscope (SEM). A series of photographs of a typical target were taken and will be discussed here.

Figure 15 shows the target at a magnification of 240X. Striations due to cold rolling of the uranium foil are clearly visible. They are also visible at 2400X (Fig. 16). It is seen here that gross surface features on the target are on the order of a few microns in size. The dark pits presumably result from nitric acid dissolution of oxides during the surface-cleaning baths. This same area is seen at 8400X in Fig. 17. Here it becomes evident that the targets are quite rough at the 0.1μ level, in addition to being lumpy at the 1μ level. This is significant because the projected range of 120 keV protons is on the order of 0.1μ [40] and the other ions have even shorter ranges. This implies that even though the ion beams always impinged perpendicularly to the target surface, the sputtering yields are actually averaged over a very wide range of incident angles.

An area of this same target which has been sputter-cleaned with a fluence of $\sim 10^{17}$ 80 keV argon ions appears in Fig. 18 at a magnification of 8400X. In this case the surface roughness is very great and fairly uniform on the scale of 1μ. Here it is quite clear that the ion beam impinges on the target at effectively all angles of incidence. This same spot is seen in Fig. 19 at 2400X. A similar area which was

also sputter-cleaned in the same fashion is shown in Fig. 20 at the same magnification. Also at 2400X is another photo of an unsputtered area of this target (Fig. 21).

A couple of sputtering runs were made on a target which was not cleaned at all. This target had been stored in a small plastic box inside a larger plastic box at atmospheric pressure for more than a year. It was fully oxidized to a depth of about 10μ (as revealed by thickness measurements before and after washing it in HNO_3). An SEM photo of it at 800X appears in Fig. 22.

B. Angular Distributions of Sputtered Atoms

Although the basic Sigmund theory predicts an isotropic distribution for the sputtered flux,[43] experimentally determined angular distributions tend to be near $\cos \theta$,[2] for perpendicular incidence and θ measured relative to the beam direction. Results on proton sputtering of various metals reported by Finfgeld[10] include distributions that are peaked more sharply than cosine. Having seen in the previous section that the uranium surfaces bombarded in this experiment are very rough on the scale of the collision-cascade size, one might expect that the angular distributions would be smeared out considerably from a cosine form. Such as the case, as can be seen in Figs. 23-26.

The angular distributions are not quite isotropic, which may well be due to self-shadowing (i.e., atoms sputtered from a low area of the target cannot leave the surface at a large angle without impacting high areas nearby), but they are clearly not cosines. $\cos^{1/4}\theta$ gives

a fit whose accuracy is commensurate with the scatter in the angular distribution data and with the errors on the individual data points. Figures 23 and 24 display respectively the best and the worst fits of $\cos^{1/4}\theta$ to the proton sputtering angular yields. Figure 25 gives a typical fit to the molecular hydrogen results, and Fig. 26 is a typical fit for the helium sputtering case. In all cases $\cos^{1/4}\theta$ was chosen for purposes of calculating total sputtering yields and is not intended to represent any underlying physics. It is possible, of course, that one might be able to show that such a distribution arises naturally, given an intrinsic isotropic distribution and some reasonable model of a rough surface. In any case it would be interesting to study the angular distribution as a function of surface finish. This would be difficult for light-ion sputtering of uranium, however, because the sizes of the collision cascades are so small. 120 keV protons have a projected range in uranium of approximately 1000Å (see Schiøtt 1966), implying collision cascades of that extent. This implies a surface finish on the order of 100Å would be required for the surface to appear planar to the cascade.

C. Total Sputtering Yields

The total sputtering yield results are summarized in Tables 3 and 4 and Figs. 27-29. The yields were calculated with the formula

$$S = \frac{8\pi r^2}{5} \frac{N_t^o}{N_p N_n \sigma_f} \qquad (3\text{-}1)$$

where N_t^o = number of fission tracks per cm^2 on the collector foil

extrapolated to $\theta = 0°$

N_p = number of incident atoms (not ions; e.g., an H_3^+ ion has 3 atoms)

N_n = neutron fluence to which the collector foils were exposed

σ_f = cross section for fission of ^{235}U by thermal neutrons

r = distance from target to catcher foil.

The factor $8\pi/5$ arises from fitting the angular distribution results by $N_t(\theta) = N_t^o \cos^{1/4}\theta$, as discussed in the previous subsection. It may be instructive to observe that this factor would be 2π if an isotropic distribution was fitted. This would increase the calculated values of S by 25% if the same values of N_t^o were employed. If one attempted instead to fit a $\cos\theta$ curve to the differential yield results, the factor would be π and the total yields calculated would be reduced by 37.5% using the same N_t^o values. To obtain even a rough fit to the angular distributions with $\cos\theta$ it would be necessary to use a substantially higher N_t^o value, so the reduction in calculated values of S would be more like 15%.

Looking now at Fig. 27, three sets of hydrogen sputtering data can be seen. The upper set of points was obtained by sputtering targets which had just been sputter-cleaned in vacuo with an 80 keV argon beam. The total proton fluences in these runs were on the order of 5.0×10^{15}. The middle set of points are from bombarding sputter-cleaned targets with 10^{17} protons. The reduction in yield may be due to accumulation of surface oxides during the runs (3-5 hours here as opposed to 15 minutes in the previous case). This point is discussed in detail

in Appendix C. It may also be that the increased proton dose has some effect, since strong dose effects have been observed elsewhere.[2] The lowest yields were obtained with the same proton dose on targets which had not been sputter-cleaned. These targets were cleaned in HNO_3 immediately prior to placement in the UHV system, but acquired many monolayers of oxide before being sputtered.

It could be argued that the increased surface roughness of the sputter-cleaned targets was responsible for the increased yields. There are two arguments against that, however. First of all, the electron micrograph of Fig. 17 demonstrates that all of the targets are quite rough at the 1000Å level, which is the relevant scale here because the collision cascades (for the energy and mass-ratio regimes we are concerned with) are of this extent. Second, the theoretical prediction is that the sputtering yield will not vary much with incident angle when $M_2 >> M_1$ (see Sigmund 1969, p. 404). It is true, though, that the theory is not sophisticated enough to handle large-angle incidence by ions accurately, particularly for light ions on heavy targets.

To try to get a better idea of the effect of surface oxidation on the sputtering yield, a pair of runs were made on targets that were heavily oxidized. An average area of one of them appears in Fig. 22. As discussed in Section IIIA, the oxidation extended to a depth of 10μ or so. Due to the storage conditions it is expected that the surface consists primarily of UO_2, but the precise stoichiometry and the amounts of any contaminants are unknown. The sputtering yields

(presented in Table 3) are approximately 10 times lower than those of sputter-cleaned targets also bombarded by 10^{17} protons. This sets an approximate lower limit to the sputtering yield of UO_2 due to protons near 50 keV; if the surface is completely UO_2 to a depth of $\sim 10\mu$ then these numbers are sputtering yields for UO_2 (assuming the sputtering proceeds stoichiometrically). If, however, there are other materials present, the sputtering yield has been reduced accordingly, since the fission track technique is insensitive to them.

The energy dependence of each of the three sets of hydrogen sputtering data follows the trend predicted by the Sigmund theory and indicated by the curve (see Section IV). Exceptions are the two points at 13 keV and 20 keV which were due to sputtering with 40 keV H_3^+ and 40 keV H_2^+ respectively. No cause to doubt the validity of these measurements was discovered, and the reason for the disagreement with theory is unknown. The other proton yields derived from H_2^+ and H_3^+ bombardment agree well with the H_1^+ yields with equal energies per proton. These results are shown in Fig. 28. They agree with previous results of H_2^+ and H_3^+ sputtering of several metals obtained by Kenknight and Wehner (1964), who found that the sputtering yield per proton of a given energy was the same for H_2 and H_3.

Sputtering yields due to helium ion beams are displayed in Fig. 29 and tabulated in Table 4. It is immediately apparent that the yields are about 30 times those from proton sputtering on similar sputter-cleaned surfaces. The energy dependence appears to be somewhat flatter than Weissman and Sigmund's prediction (solid curve; see Section IV).

Here, too, the magnitudes of the yields are much lower (by a factor of about 10) than predicted by the theory.

A couple of data points for uranium sputtering by argon were also obtained, as seen in Tables 3 and 4. In this case the theory comes much closer, being high by only a factor of 3.

D. Chunk Emission

It has been discovered in recent years that sputtered material does not always emerge as single atoms. There are instances in which some of the material is ejected as agglomerates of many atoms, commonly referred to as "chunks".

Chunk emission from niobium during sputtering by 14 MeV neutrons has been reported by Kaminsky[19] and Kaminsky and Das.[21,22] Biersack, et al,[5] have studied chunk ejection during neutron irradiation of UO_2 utilizing the same mica detection of fission tracks as employed in this experiment. The technique is particularly appropriate to investigation of chunk emission from materials containing ^{235}U because of the striking "star-burst" signature left in the mica by a chunk during neutron irradiation. Two examples appear in Figs. 13 and 14. The number of fission tracks in more than 1000 such stars was counted to yield the chunk emission data summarized in Tables 5 and 6 and Figs. 30-32. The number of ^{235}U atoms per chunk is obtained by dividing the number of tracks in the corresponding star by the fraction of ^{235}U atoms fissioned: 8.5×10^{-7} for runs in series 1-3; 8.0×10^{-6} for runs in series 4-7.

The mass distribution of chunks emitted during the first five proton sputtering runs of Table 5 is shown in Fig. 30. The lower cutoff

at 5×10^6 atoms per chunk is due to the fact that smaller chunks normally produced less than 5 tracks in the mica and could not be recognized. The distribution displays a long tail, indicated by the two bars at the right, extending out to 10^9 atoms per chunk. The curves represent visual fits to the data of the forms $N(n) = a/n^2$ and b/n. The former fit represents the histogram fairly well for larger n but diverges badly from it at small n. The latter fit, on the other hand, is not as bad for small n but is quite a bit high at larger n. An exponential actually fits the histogram much better, as seen in Fig. 31. More data would be required to ascertain whether or not the exponential adequately represents the tail of the distribution, which has been omitted from Fig. 31. Fits to the mass distribution will be discussed further in Section IVC.

The mass distribution of chunks ejected during sputtering by 80 keV argon is shown in Fig. 32. The low number of stars with 5-10 tracks is rather surprising but evidently quite real. No data on chunks of smaller size is yet available to confirm the existence of the apparent maximum in the distribution. It is also worth noting that the distribution is somewhat flatter here than in the H_1 case and the tail is longer--several chunks with a few times 10^9 atoms were counted.

This size ($\sim 10^9$ atoms) is typical of the many chunks of UO_2 seen by Biersack, et al[5], but I do not know what sort of size distribution their experiment produced. The average chunk of niobium sputtered by neutrons, as reported by Kaminsky and Das,[21] contained 2×10^{12} atoms,

and chunks as small as 10^7 atoms were seen. The median chunk size seen here was $\sim 2.5 \times 10^7$ atoms, for 80 keV argon sputtering, and $\sim 2.0 \times 10^7$ atoms for proton sputtering; the mean sizes were 6.6×10^7 atoms and 4.3×10^7 atoms respectively. These values are of course influenced by the arbitrary cutoff at 5×10^6 atoms/chunk and by the low statistics for large chunks. Assuming a spherical shape, a chunk containing 5×10^7 ^{235}U atoms would be $\sim 0.1\mu$ in diameter.

The observed chunk size for protons at reduced dose (5×10^{15} instead of 10^{17} incident ions per target) was only $\sim 10^6$ (see Table 5). The statistics here are very poor, however, since a reduction in dose by a factor of 20 resulted in a reduction in chunk yield by a similar amount. This reduction is probably significant in itself, since it indicates that the chunk emission is not due to release by the first wave of H_1^+ ions of energy stored in the target surface. A great deal more information on dose dependence is necessary before anything definitive can be said.

The observed median size of chunks emitted during helium sputtering was $\sim 2 \times 10^6$. Here again the He^+ dose was down by an order of magnitude from what it would have been in conjunction with a neutron fluence of $10^{15} cm^{-2}$ ($10^{16} cm^{-2}$ was the neutron fluence for the helium sputtering runs), but the dose effect is unknown.

Looking now at Table 6, it is apparent that the efficacy of chunk emission correlates roughly with the efficacy of single atom sputtering. The He^+ sputtering yield is ~ 50 times greater than for H_1^+, and roughly 50 times the H_1^+ fluence was required to eject an amount of ^{235}U

in chunks comparable to that ejected by He^+ (taking into account the fact that the chunks were smaller in the He^+ case). S for argon sputtering is two orders of magnitude greater than S for helium, and two orders of magnitude more He^+ fluence yielded a number of chunks comparable to that ejected by argon ions. Since the He^+-ejected chunks were smaller, the amount of uranium ejected as chunks was considerably greater for the argon case. This agrees with the observation that chunks composed a much greater fraction of the total sputtering yield for argon ($\sim$ 10%) than for hydrogen or helium ($\sim$ .3% and $\sim$ .1% respectively). This fraction is determined in each case by multiplying the average chunk size by the observed number of chunks per cm^2 and dividing by the number of ^{235}U atoms/cm^2 (see Table 6), with the assumption that all single tracks represent single atoms. If the size distribution of chunks does in fact follow an exponential dependence, then this assumption has very little effect on the calculated fractions (see Section IVC).

Another observation of possible importance is that the amount of chunk emission under H_1^+ bombardment seems to increase with ion energy, which is the reverse of the energy dependence of the total sputtering yield. Here again more data is needed to establish this trend.

Before closing this topic, a few words are in order concerning possible spurious contributions to the chunk distribution on the micas. As a test of environmental contamination, a 3 cm^2 area on the back of data band LL2-1 was scanned very carefully at 450X. A total of two stars were found (see "Blank" entry in Table 5), while the same area

on the front contained >300 stars. This argues strongly against general environmental contributions or spurious stars internal to the mica. Actually, on rare occasions a uranium-rich inclusion near enough to the mica surface to be etched was encountered. An internal star is readily told apart from a star due to a surface deposit by focusing the microscope up and down, so none of those were counted.

Scans at low power (25X and 100X) were made of the relevant micas to see if any patterns that would suggest contamination could be found. None were, except for broad bands of stars along the sides of micas in series 6, (He^+ sputtering) where enough uranium had accumulated (during the sputter-cleaning runs) on the clamping bars to scrape off on the micas when they were installed. The scanning area for series 6 was accordingly reduced to avoid the contaminated area by more than 1 cm.

A final argument that spurious stars do not make a large contribution is that data bands on micas which have been through identical processes, and even data bands on the same mica, display very different chunk densities, but which are uniform within each data band.

All things considered, there is undoubtedly some contamination included in the data, but it is expected to be only a small portion.

E. Error Analysis

The primary sources of error in determination of values for the yield S were uncertainty in N_n (the neutron fluence) and error in determining the track density N_t^o (see eq. (3-1)).

As discussed in Section IIC the error in N_n was due to counting error (±5%) in determining the number of tracks in the standard micas

and to uncertainty (of ±6.5%) in the established fission-fragment range R_f. The overall error in N_n is then ±8.5%.

The error in N_t^o had three sources: 1) counting statistics (±2%) (see Section IIC); 2) error in fitting the $\cos^{1/4}\theta$ curve to the angular distribution data due to scatter in the data (varied from ∿±5% to ±10%); and 3) background subtraction. The amount of background subtraction varied considerably. For most runs in series 4-7 it was zero, due to collecting the sputtered uranium directly on mica (see Section IIC). In series 1-3 the sputtered uranium was collected on aluminum which contributed ∿30 background tracks per field of view, which had typically 100-300 tracks total. Uncertainty in the background determination was ∿±10%, which contributed typically ±1% to ±4% to N_t^o.

Another source of background on some data bands was ^{235}U atoms bouncing or drifting up onto them during the sputter-cleaning runs. Although the uranium being sputtered during the cleaning runs was well collimated, the amount was so great that a small fraction finding its way up to LL and LR foils (see Fig. 3) instead of sticking to GL and GR foils gave rise to a non-negligible background "fog" of tracks on some of the low-numbered data bands. This background subtraction was handled by scanning vertically across the data bands and plotting the fall-off of the track density with distance away from the lower edges of LL and LR micas. In the worst cases the subtraction amounted to 25% and is responsible for the relatively large error bars on the Ar^+ sputtering yields.

The result of the foregoing is that the error in N_t^o had to be determined individually for each sputtering run. Values were typically ±10%. Once the error on N_t^o was obtained for a given sputtering run it was added (in quadrature) to the error on N_n to produce the quoted error on the value of S for that run. Quoted errors are typically ±15%.

All other sources of error in S were determined to be negligible compared with those discussed, but a couple of them deserve mention. One of those is beam integration error, which was found to be <1% for hydrogen ion beams and perhaps as large as 5% (systematic error) for the argon beams (see Section IIB). Another possible source of systematic error is the sticking fraction for the sputtered ^{235}U atoms on the catcher foils, since a sticking fraction less than 1 would reduce the measured values of S accordingly. The sticking fractions for sputtered ^{235}U atoms on both aluminum and mica have been measured in the Kellogg Laboratory by Bob Weller and Joe Griffith (private communication) and found to be >.97 in both cases.

IV. THEORY AND SPECULATION

A. The Collision Cascade Theory

In view of the complexity of the atomic processes involved, it is not surprising that a definitive theory of sputtering has not yet emerged. The collision cascade theory due to Sigmund[43,49] is the most satisfactory theory to date; it makes definite predictions concerning the important quantities measured in sputtering experiments and has proved to be quite accurate in many cases. It also serves to bring into focus the primary physical interactions at the atomic level which occur during sputtering. Before examining the quantitative predictions of the Sigmund theory, a brief qualitative look at the sputtering process is in order.

An impinging ion suffers a series of collisions with target atoms, creating a number of primary recoil atoms which in turn collide with other target atoms, and so on. This collision cascade continues until none of the recoiling atoms has sufficient energy (on the order of 20 eV) to displace another atom from its position in the lattice. Typically, the cascade proceeds through many steps, and a large number of atoms are set in motion with very low energies. The fact that the cascade progresses through many generations of recoiling atoms implies that momentum information about the original projectile is lost, and the cloud of low energy atoms becomes essentially isotropic. This makes the theoretical solution of the sputtering problem much more tractable. In any event, atoms in the cascade which arrive at a surface of the target with enough energy to overcome the surface binding (typically a few eV) are

sputtered. So many atoms are set in motion with very low energies that they account for the bulk of the sputtering yield, even though energetic recoils and backscattered ions account for most of the sputtered energy.[42] Experimental energy spectra of sputtered atoms peak strongly at a few eV (see, for example, Thompson 1968). The low energy of most sputtered atoms also implies that they originate within a few Ångstroms of the surface.

In addition to losing energy via collisions with target atoms ("nuclear stopping") an ion loses energy to the electrons in the target ("electronic stopping"). Due to the enormous mass difference between atoms and electrons, energy once lost to the system of electrons is never returned to the collision cascade. In calculations of sputtering it is necessary, therefore, to determine and subtract out this energy loss. For heavy ions on moderate atomic-weight targets, nuclear stopping of the ion predominates and electronic stopping is neglected, but for light ions on heavy targets, electronic stopping is greater and must be taken into account. As a pertinent example, the electronic stopping power for 100 keV protons in uranium is 330 times the nuclear stopping power.

Sigmund's basic approach to the calculation of sputtering yields is to make use of transport theory to determine the distribution of energy deposited in atomic motion in the target. This energy is then converted into a distribution of low energy recoils, and it is determined how many of them arrive at the surface with sufficient energy to overcome the surface binding forces. Knowledge of certain quantities

is essential to the procedure: the cross sections for scattering of high-energy ions and atoms (Rutherford cross-sections for higher energies and Thomas-Fermi cross-sections for lower energies), cross sections for low energy target-atoms scattering from each other (Thomas-Fermi for most energies and Born-Mayer cross sections for the lowest energies), electronic stopping powers (Lindhard's expression[25,26] $S_e(E) = KE^{1/2}$ is used except when the ion velocity is high enough to warrant use of an $S_e(E) \propto 1/E$ approximation to the Bethe-Block formula)[3], and the surface binding energy U_o (sublimation energy is generally used for lack of better information). The procedure is applicable only to amorphous targets, but should provide a reasonable approximation to sputtering from polycrystalline targets. It also applies only to bombarding ions with energy much greater than the surface binding energy, i.e., to ion energies of at least 100-200 eV. In addition, the energy threshold E_d ($\sim$ 20 eV) for displacement of an atom from its lattice position and binding energy lost to the lattice by recoiling atoms are neglected. One final approximation that may be significant is that the target surface is a smooth plane.

The depth distribution $F_{(1)}(x,E,\eta)$ of energy deposited in atomic motion satisfies the equation[44,45,49,53]

$$-\eta \frac{\partial F_{(1)}}{\partial x} = NS_e \frac{\partial F_{(1)}}{\partial E} + N \int d\sigma_n (F_{(1)} - F_{(1)}(x,E-T,\eta') - F(x,T,\eta")) \tag{4-1}$$

where E = initial ion energy

$\eta = \cos\theta$ and θ is the angle between the ion beam and the target surface-normal (the x-direction)

η' = cos θ' and θ' is the polar angle for a scattered ion

η'' = cos θ'' and θ'' is the polar angle for a scattered target atom

$F(x,T,\eta'')$ is the deposited-energy profile due to a target atom with energy T; it is computed from a similar transport equation.[45]

$d\sigma_n = d\sigma_n(E,T)dT$ is the differential cross section for energy loss T in an elastic ion-target-atom collision

$S_e = S_e(E)$ is the electronic stopping cross section

N = target atom number density

To solve equation (4-1) the F functions are expanded in terms of Legendre polynomials in the angular dependencies η, η', and η''. Equation (4-1) is then multiplied by x^n ($n=0,1,2,\cdots$) and integrated over x to generate a series of moment equations. These integrodifferential equations are solved numerically for $n \leq 3$ or expanded to first order in U_o/E and the first few moments solved for analytically.[43] Finally, the energy deposition distribution is constructed from these moments by use of the Edgeworth expansion in terms of Gaussians and derivatives of Gaussians.[43,49] The sputtering yield for a given ion-target combination may then be written in terms of the energy deposited at the surface:

$$S(E,\eta) = \Lambda \cdot F_{(1)}(0,E,\eta) \tag{4-2}$$

where

$$\Lambda = \frac{3}{4\pi^2} \frac{1}{NC_o U_o} \simeq \frac{0.042}{NU_o[\text{Å}^2]} \tag{4-3}$$

and C_o is a constant related to the Born-Mayer interaction between target atoms (see Sigmund 1969, p. 390).

The energy dependence of sputtering yields is essentially that of the nuclear stopping cross section $S_n(E)$. It is customary, therefore, to introduce the function $\alpha(E,\eta)$ such that

$$F_{(1)}(0,E,\eta) = \alpha(E,\eta)\ N\ S_n(E) \tag{4-4}$$

so that (4-2) may be rewritten as

$$S(E,\eta) = \frac{0.042}{U_o[\text{Å}^2]}\ \alpha(E,\eta)\ S_n(E) \tag{4-5}$$

It is also customary in calculations of α and of nuclear stopping powers to work with the dimensionless energy ε and dimensionless distance ρ given by

$$\varepsilon \equiv \frac{a}{Z_1 Z_2 e^2}\ \frac{M_2}{(M_1+M_2)} \cdot E \tag{4-6}$$

$$\rho \equiv \frac{4M_1M_2}{(M_1+M_2)^2}\ N\pi a^2 \cdot x \tag{4-7}$$

where subscript 1 refers to the projectile and 2 refers to the target and a is the screening parameter in the Thomas-Fermi potential:

$$a \equiv \frac{0.8853}{(Z_1^{2/3} + Z_2^{2/3})^{1/2}} \cdot a_o \tag{4-8}$$

a_o is the Bohr radius.

Equation (4-5) can then be rewritten as

$$S(E,\eta) = 4\pi a Z_1 Z_2 e^2 \frac{M_1}{M_1+M_2} \frac{0.042}{U_0} \frac{1}{[\text{Å}]^2} \alpha(\varepsilon,\eta)\left(\frac{d\varepsilon}{d\rho}\right)_n \qquad (4\text{-}9)$$

It is this form of the yield equation which has proved most useful for calculations to compare with experimental results in Section IVB.

B. Comparison to Results

Equation (4-9) was used to calculate theoretical values of S vs. energy for H_1, He and Ar. The results are tabulated in Tables 7-9 and graphed for H_1 and He in Figs. 27 and 29. The values for the reduced nuclear stopping cross section $s_n(\varepsilon) \equiv (d\varepsilon/d\rho)_n$ are from Schiøtt (1966). The values $\alpha(\varepsilon) \equiv \alpha(\varepsilon,\eta = 0)$ for perpendicular incidence are taken from Weissman and Sigmund (1973) for H_1 and He. For argon sputtering the data presented in Andersen (1974, p. 392) were consulted to arrive at an (energy-independent) value $\alpha(\varepsilon) = 0.5$. A value $U_o = 5.4$ eV for the surface binding energy was taken from Gschneidner (1964).

The energy dependence of H_1 sputtering as predicted by the theory and graphed in Fig. 27 follows the data except for the measured yields at 13 and 20 keV. These two points were determined using 40 keV H_3^+ and 40 keV H_2^+ ion beams. According to Fig. 28 and other sources,[23,50] an H_2^+ ion with energy E gives the same sputtering yield as two H_1^+ ions with energy 1/2E, and similarly for H_3^+. The points at 13 and 20 keV should be reasonable yield measurements for H_1^+, and the reason for disagreement with theory is not known.

For He^+ sputtering the measured sputtering yield also begins to diverge from the theoretical curve at lower energies (Fig. 29). This is tantalizing, but more measurements at lower energy are needed to establish the dependence firmly.

The magnitudes of S as predicted by (4-9) do not agree with the experimentally determined values very well. The theory is high by a factor of about 25 for H_1^+ on sputter-cleaned targets (the curve in Fig. 27 is the prediction by the Sigmund theory multiplied by 10^{-2}). In the case of He^+ ions on sputter-cleaned targets the theoretical curve is high by a factor of $\sim$10 (see Fig. 29). The calculated values of S(E) appropriate to sputtering by argon (Table 9) are higher by a factor of $\sim$3 than the measured values at 40 and 80 keV (Tables 3 and 4). The theoretical predictions appear to approach the empirical values of S as the target-to-ion mass ratio (M_2/M_1) decreases. This is not too surprising as it is a well-known feature of the original Sigmund (1969) theory. Why it should be true of the Weissman and Sigmund (1973) version, in which the approximations appropriate to light-ion sputtering have been made, is unclear.

One can imagine several reasons why the experimentally-determined values of the yield might be reduced. For one thing, surface contamination or oxidation of the targets would reduce the yield. This effect is considered in detail in Appendix C and is expected to be unimportant for the sputter-cleaned targets. The surface roughness would also be expected to influence the yield relative to the predicted yield, since the theory assumes a planar surface. The expectation, and the usual result, however, is that the sputtering yield increases with increasing surface

roughness, since more ions impinge at oblique angles and deposit more energy near the surface. The ion dose probably has some effect as well, but the doses delivered in this experiment are not unusually high or low compared with experiments with heavy ions which the theory fits quite well. The conclusion is that the lack of agreement between theory and this experiment is probably due to inaccuracy of the theory at large M_2/M_1.

C. Chunk Emission

The study of chunk emission from solids under ion bombardment is of recent genesis, and a cogent theory of the emission mechanisms has not yet been formulated. I do not intend to formulate one, but will confine myself to a few brief remarks on the subject.

It is clear that none of the chunks observed in this experiment could have been ejected directly by a single ion, since the energy required to create the necessary free surface is greater than the total ion energy available. To put it in rough quantitative terms, imagine a small, cubic chunk of 10^6 atoms perched on one face on the target surface. The energy required to release the chunk is given roughly by the number of atoms on the attached face (10^4) times the cohesive energy per atom ($\sim$ 5 eV) or 50 keV. Especially when it is considered that the average energy transferred to a primary recoil ^{235}U atom by any of the incident ions is near 100 eV, it is evident that the ejection mechanism must involve some variety of energy accumulation.

Guinan (in Kaminsky et al, 1974, p. 171) suggests a process whereby energy deposited in collision cascades serves as a trigger to

release much larger reserves of energy stored as internal stresses in the material. Cold rolling of the metal, for example, stores considerable energy in various types of dislocations. It appears that energy deposited by cascades in the vicinity of certain dislocations is sufficient to initiate a crack. Continued energy deposition contributes to propagation of such microcracks and leads to chunk emission when cracks intersect the surface. A prediction based on this mechanism is that chunk emission should be enhanced by increased surface roughness. This effect has been observed by Kaminsky[21] and is certainly not contradicted by the amount of chunk emission from the very rough surfaces sputtered in this experiment.

Returning for a moment to the idealized cubic chunk perched on the surface, we observe that as we increase the number n of atoms in such a chunk the energy binding it to the target surface increases as $n^{2/3}$. If we naively expect the probability of emitting a chunk to be inversely proportional to the energy binding it to the surface, we would then look for an $n^{-2/3}$ dependence in the mass distribution of chunks. A look at Fig. 30 reveals that an n^{-1} fit to the distribution is too flat--deviating markedly from the data at larger n. An $n^{-2/3}$ dependence deviates even more, so our naive expectation does not appear to have been very fruitful.

Suppose we now look at the mass distributions and see if any information can be gleaned from them. The distribution of chunk size in the case of argon sputtering (Fig. 32), with a maximum at small n, is suggestive of the sort of distribution of pieces obtained when an object

(such as a glass) is smashed by a sudden blow: lots of small pieces, less tiny ones, and a few large ones. It is conceivable in the case of chunk emission that the "object" is a blister which suddenly ruptures when the internal pressure of gas (accumulating as ion implantation continues) becomes too great. A number of groups have reported[20] blistering (and blister rupturing) of various metals under bombardment by hydrogen and helium ions. No a priori reason is known why the process should not also take place in uranium. Particularly for argon, which has a much lower mobility in uranium than hydrogen, and which does not form compounds with uranium as hydrogen does, gas bubble formation and subsequent blistering may be an important mechanism for chunk emission.

If we do not learn anything immediately from the exponential fit to the chunk size distribution, at least we can use it to calculate a total sputtering yield in chunks. For

$$N(n) = N_o e^{-\lambda n} \tag{4-10}$$

where N is the number of chunks consisting of n ^{235}U atoms (in units of 10^6 atoms), the total number of ^{235}U atoms contained in chunks with size between n_1 and n_2 is simply

$$N_U = \int_{n_1}^{n_2} N(n)\, n\, dn = \int_{n_1}^{n_2} N_o\, n\, e^{-\lambda n}\, dn \tag{4-11}$$

$$\Longrightarrow \quad N_U = \frac{N_o}{\lambda^2}\left[(\lambda n+1)e^{-\lambda n}\right]_{n_1}^{n_2} \tag{4-12}$$

Using the values N_o = 180 and λ = 0.05 for the fit to the distribution of hydrogen-sputtered chunks in Fig. 31, and integrating from n_1 = 10 to n_2 = 100, equation (4-12) gives $N_U = 6.2 \times 10^3$. This is the number of ^{235}U atoms (in units of 10^6) contained in all chunks having sizes between 10^7 and 10^8 atoms found on the 30 cm^2 of mica that was scanned; i.e., $N_U = 2.1 \times 10^8 cm^{-2}$. This is a bit less than 0.1% of the total single-track yield per cm^2 (see Table 6). Integrating instead from n_1 = 0 to $n_2 = \infty$, we obtain $N_U = 2.4 \times 10^8$ atoms cm^{-2}. This exponential fit says, therefore, that most of the total yield of atoms contained in chunks is found in chunks with sizes from 10^7-10^8 atoms. The fact that this estimate of chunk contribution to total sputtering yield (0.1%) is lower than the estimate of 0.3% in Table 6 is due presumably to the exponential fit underestimating the quantity of chunks in the tail of the distribution.

Performing the same calculation for the argon sputtering case of Fig. 32, equation (4-12) yields (with N_0 = 60, λ = 0.03, n_1 = 0, $n_2 = \infty$, and a scanned area of 4 cm^2): $N_U = 1.6 \times 10^{10}$. This is actually 30% of the single-track yield, implying that this fit overestimates the quantity of chunks in the tail of the distribution.

V. SUMMARY

One of the most significant results of this experiment is that it demonstrated the great sensitivity of the technique of detecting fission-fragment tracks in mica for measuring sputtering yields of materials containing ^{235}U. Values of the sputtering yield S as low as 3×10^{-5} were readily measured for proton bombardment of uranium, and it is shown in Appendix A that yields as low as 10^{-6} could be measured for bombardment by keV ion beams of materials doped with 0.1 atomic % ^{235}U. One of the primary limits on the technique is simply the available beam fluence, and the possibility of measuring $S = 10^{-11}$ for such things as photon sputtering of uranium is also discussed in Appendix A. It should be mentioned that the sensitivity of the technique implies that very little of a given target surface is actually sputtered away (less than one monolayer was removed during any sputtering run in this experiment). This in turn implies that extraordinary precautions may be required to avoid reduction of the sputtering yield by surface contamination and that, as is discussed in Appendix C, even a vacuum of 10^{-9} torr may be insufficient to maintain the cleanliness of the target surface during a given sputtering experiment.

The fission-track detection method possesses another important virtue: it facilitates detailed study of chunk emission from targets containing ^{235}U since a neutron-irradiated chunk produces a star-burst pattern in the mica collector sheet (see Figs. 13 & 14), and the number of tracks in the star is proportional to the number of ^{235}U atoms in the chunk. Some of the most exciting results of this experiment concern

the emission of chunks during sputtering of uranium by $^{1}H^{+}$, $^{4}He^{+}$, and $^{40}Ar^{+}$ ion beams with energies in the vicinity of 80 keV. These results are summarized in Tables 5 & 6 and Figs. 30-32. The uranium targets consisted of cold-rolled foils which had been pre-sputtered with 80 keV Ar^{+} ions to a dose of approximately 10^{17} cm^{-2} and which had very rough surfaces (see Figs. 15-21).

Mass distributions for chunks emitted during sputtering by $^{1}H^{+}$ and $^{40}Ar^{+}$ were found to have approximately exponential shapes over the range of sizes seen — from the scanning cutoff at 5×10^{6} atoms/chunk to a few times 10^{9} atoms/chunk (see Figs. 31 & 32). The average size of the chunks seen was close to 5×10^{7} ^{235}U atoms. The sputtering yield in chunks was about .3% of the total sputtering yield for proton bombardment and about 10% in the argon case. By way of comparison, Kaminsky and Das report[22] emission of chunks from niobium during irradiation with 14 MeV neutrons and observed chunk sizes ranging from $\sim 5 \times 10^{6}$ to $\sim 5 \times 10^{12}$ atoms. They also found chunk contributions to the total sputtering yield ranging from zero to about 60% for different areas of targets having various surface finishes. One should not attach too much significance to similarities and differences between the chunk emission results reported here and those reported by Kaminsky since the bombarding particles are quite dissimilar, the doses are 3 - 7 orders of magnitude apart, the energy deposition per primary recoil and per volume differ by several orders of magnitude, and a considerable amount of the chunk emission here may be due to bursting of small blisters containing gas bubbles of the implanted ions.

It was also found that the amount of chunk emmission due to

bombardment by $^{1}H^{+}$, $^{4}He^{+}$, and $^{40}Ar^{+}$ correlated roughly with the sputtering yield in each case. For example, the yield S for argon sputtering of uranium is about 10^{4} times that for H^{+}, and approximately 10^{5} times as many protons as argon ions were required to eject a given amount of uranium in chunks.

Angular distributions for the sputtered uranium are plotted in Figs. 23 - 26. The $\cos^{1/4}\theta$ shapes are due presumably to smearing out, by the very rough target surfaces, of much sharper distributions.

Total sputtering yields are summarized in Tables 3 & 4 and Figs. 27 - 29. Typical values of S, for sputter-cleaned targets, are 3×10^{-4} for 80 keV $^{1}H^{+}$, 10^{-2} for 80 keV $^{4}He^{+}$, and 2 for 80 keV $^{40}Ar^{+}$ ion beams. Calculations of S based on the theory due to Sigmund[43] and Weissman and Sigmund[49] overestimate the results by approximately a factor of 3 in the argon case, by a factor of ~10 in the helium case, and by a factor of nearly 25 in the case of proton bombardment. There are several things which could contribute to this discrepancy. For one, the theory assumes a planar surface, but the surfaces being sputtered in this experiment are very rough (see Section IIIA). While roughening a smooth surface generally increases the yield, it has been demonstrated[55] that an extremely rough surface can reduce the yield considerably. This may well account for a factor of 3 reduction in the yield as compared to theory. Another important consideration is that the theory tends to overestimate the sputtering yield for large ratios of target atomic weight to projectile atomic weight, which probably explains much of the discrepancy in the hydrogen and helium cases. For comparison, Furr and Finfgeld[15] reported yields for H^{+} on gold approximately 5 times lower

than the theoretical values calculated by Weissman and Sigmund[49], and Summers, et al,[46] found values of S for H^+ on niobium that were 8 to 9 times lower than theory predicts[49]. One other possible source of discrepancy is that the real target surfaces incorporate a certain amount of contamination, due to adsorption and due to implantation of the ions themselves, which the theoretical calculations ignore.

One last result from this experiment derives from sputtering runs made with molecular hydrogen beams (see Fig. 28). Consistent with the findings of others[15,16,23], it was found that, for the few energies investigated, the sputtering yield from an H_n^+ molecule having energy E is the same as that from n $^1H^+$ ions having energy E/n.

APPENDIX A

Sensitivity of the Fission Track Detection Technique

In this appendix I would like to discuss the intrinsic sensitivity of the fission-track detection method for measuring the sputtering yield of ^{235}U and to suggest possible extensions of the technique. The primary limit to the sensitivity of the technique is the ^{235}U background in the mica itself. Good (but readily available) mica such as was used in this experiment has an effective surface contamination of $\sim 10^{8}$ ^{235}U atoms/cm^2 (equivalent to $\sim$2.5 ppb). This permitted keeping the level of background tracks below 1% while measuring a sputtering yield S of $\sim 10^{-4}$ for 100 keV H_1^+ on ^{235}U with a fluence of 5×10^{15} protons and an irradiation of the mica with 10^{16} neutrons/cm^2. This sensitivity implies that the technique could be used to measure sputtering yields down to $S = 10^{-4}$ for materials doped with 0.1% (atomic) ^{235}U and bombarded with $\sim 10^{17}$ beam particles. In that case the background level of tracks in the mica would be at about the 50% level. It would of course be necessary to allow for non-stoichiometric effects in such a sputtering of very small amounts of material from a surface doped with something as heavy as ^{235}U.

If one wishes to push the technique to measure smaller sputtering yields, the most obvious approach is to increase the fluence of beam particles, either by running for long periods of time or by increasing the beam current. In the latter case one may run into the problem of excessive heating of the target and begin to evaporate, rather than sputter, material. We found it possible to run as much as 10 $\mu A/cm^2$ of 100 keV H_1^+ on 0.025 mm uranium foil without excessive heating, which

implied 5 hours to accumulate 10^{17} beam particles. Metals more conductive than uranium would allow higher beam currents, as would operation at lower beam energies. Finfgeld et al,[10] for example, have sputtered thin metal foils with H^+ and D^+ beams of a few keV at beam current densities around 1 mA/cm^2 for beam currents of $\sim$100 μA. Such a beam current allows accumulation of 10^{19} projectiles in 5 hours and makes possible the measurement of $S = 10^{-6}$ for materials doped with 0.1% (atomic) ^{235}U.

One can also gain a bit in the density of sputtered material collected by decreasing the distance from target to collector foil. For backsputtering it is difficult to gain a great deal due to practical limits set by the aperture required in the foil holder to admit the beam and by the finite beam size itself. For transmittance sputtering these practical limits do not apply, since the catcher foil may be placed very close to the target. In that case the density of collected ^{235}U atoms is simply S x beam fluence x doping fraction, and $S = 10^{-8}$ could easily be measured for a beam fluence of 10^{20}cm^{-2} and 0.1% (atomic) doping. This would also be true for backsputtering by particles with enough energy to pass through a catcher foil placed immediately in front of the target. In that case one would use a foil with low ^{235}U content to collect the sputtered material and then place the foil on the surface of a mica sheet during the neutron irradiation. Good results have been achieved using high purity aluminum for such catcher foils.

The great sensitivity of this technique may also prove useful in the investigation of such exotic forms of sputtering as electron and

photon sputtering, which are expected to have very low yields. As an example, photon sputtering of ^{235}U is being looked for in Kellogg Laboratory. The UV light source employed emits 3×10^{15} 4.88 eV photons $cm^{-2}sec^{-1}$ at a distance of 4 cm (Barbara Cooper, private communication). Requiring that 10^{8} ^{235}U per cm^{-2} be collected on the mica catcher foils (to be above intrinsic ^{235}U background) in a period of 10^{6} seconds implies, via the formula

$$N_t = \frac{N_p S}{2\pi r^2} \quad , \tag{A-1}$$

that $S < 10^{-11}$ could be measured. In fact, substituting $N_t = 10^{8} cm^{-2}$, $r = 4$ cm, and $N_p = 3 \times 10^{15} \times 10^{6} = 3 \times 10^{21}$ in (A-1) yields a measurable S value of 3×10^{-12}.

It is evident that, in the cases of photon and electron beams at least, the possibility of very large beam fluences implies that extremely low values of S are subject to measurement. Ultimate limits may be set by such competing processes as self-sputtering of the uranium target by fission fragments or by α's from decay of ^{234}U.

APPENDIX B

Ultra-High Vacuum Technique

The aim of this appendix is to pass on to the next generation of Caltech graduate students some of the practical knowledge I have learned concerning ultra-high vacuum technique. That which I have not learned fills many volumes of the extensive literature on the subject. Two excellent gateways to that literature, which are very valuable sources of information in their own right, are High Vacuum Technology (Roth 1976)[37] and the chapter on vacuum in the Handbook of Thin Film Technology (Maisel and Glang, ed, 1970).[27] The first chapter of Roth contains a list of the primary journals dealing with vacuum, the transactions of the important vacuum conferences and most (if not all) of the books that have ever been written about vacuum. I would recommend taking a close look at this book before undertaking any extensive work involving ultra-high vacuum.

The technology necessary for producing systems possessing considerable experimental utility and operating in the range of 10^{-9}-10^{-10} torr is well established. Several firms sell the type of components incorporated in the system utilized in this experiment. To be useful in ultra-high vacuum the materials used to construct these components must have low intrinsic outgassing characteristics. In addition, they must have low vapor pressures at the baking temperature (400°-500°C) required to effectively drive off gases adsorbed when the system is at atmospheric pressure. This requirement eliminates such metals as lead, zinc, and cadmium from consideration and implies that brass should never be admitted to an UHV system. Stainless steel is the primary material employed, and other materials

commonly used include oxygen-free high-conductivity (OFHC) copper (primarily for metal-seal gaskets), dense glasses like Pyrex (primarily for viewports), and certain ceramics (primarily for electrical insulation). Common alloys of aluminum in rolled or extruded form can be used in ultra-high vacuum if they are well-cleaned and baked (see Roth 1976, p. 142, 332 and Power and Robson 1962). For a while both the target plate and collimation cylinder in the sputtering assembly were 6061 aluminum, and no difficulty in attaining 10^{-9} torr was experienced. In fact, one can place small quantities of any material in the vacuum provided the pumping speed is adequate to compensate for the outgassing. Roth (1976, p. 142) gives a nomogram for matching pumping speed and outgassing properties to achieve the desired pressure. Pragmatically speaking most materials are still prohibited in a system of the size used in this experiment, but it has proved feasible to introduce considerable amounts of materials not normally recommended for UHV work. It was possible, for example, to reach 10^{-9} torr in the normal pumpdown time with 225 cm^2 of unbaked muscovite mica catcher foils installed.

Selection of suitable materials is not in itself sufficient to guarantee attainment of ultra-high vacuum. It is also necessary to reduce the outgassing rates of these materials. There are two steps in such a process. First, the materials are carefully cleaned to minimize the amount of gas brought into the system. Second, after being installed, they are baked at low pressure to drive off gas adsorbed on the surface and to decrease the concentration of dissolved gases which diffuse into the vacuum from the bulk material.

Rapid pumpdown is greatly facilitated by thorough cleaning of pieces before introducing them into the UHV system. This is particularly important if one hopes to add parts to the system and pump down to $\sim 10^{-9}$ torr quickly without baking. It has proved possible to do so with this system provided the parts constitute a fairly small fraction of the system's surface area. A set of cleaning procedures that have been used successfully in Kellogg for a few years appears in Table 10. For most materials the procedures consist of a degreasing step, an etching bath to remove oxides and other porous surface material which adsorb gases well, rinses to remove the various solvents, and a final methanol rinse to reduce the amount of water adsorbed on the surface and to remove any lingering grease. More information on cleaning (including other recipes for etch baths, more detail on degreasing, and so forth) can be found in section 9.4 of Espe (1970) and section 7.2 of Roth (1976).

A chemical cleaning process that is commercially available is DS-9 sold by the Diversey Co. of Chicago. It consists of three baths, one of which is an etching solution. Milleron[32] reports an outgassing rate for stainless steel of $\sim 10^{-12}$ torr - $\ell\, cm^{-2} sec^{-1}$ after treatment with DS-9 and 12 hr of pumping, but no baking. This is a very low outgassing rate without baking. I would be surprised to find that the treatment for stainless steel specified in Table 10 results in quite as low an outgassing rate.

If it is necessary (as it usually is) to reduce the outgassing rate below that obtained after cleaning, by far the most effective

method is heating in vacuum. Power and Robson[34] obtained outgassing rates of 3×10^{-14} torr ℓ cm^{-2}sec^{-1} for stainless steel and 2×10^{-14} for 99% aluminum shim after 16 hr of baking at 400°C and P $\sim 10^{-9}$ torr. Outgassing of the same samples was about 2×10^{-10} torr-ℓ-cm^{-2}sec^{-1} after 24 hr of pumping at 10^{-9} torr without baking. The rate of degassing increases very rapidly with temperature, being about ten times greater for outgassing stainless steel at 400°C than at 300°C (as shown in Calder and Lewin 1967; this is an excellent reference on the theory and results of baking stainless steel). Most of the UHV system used in this experiment is bakeable to at least 400°C. As a practical matter the rate of degassing must be kept low enough so the ion pump does not stall, which means that 400°C must normally be approached gradually. The most efficient way to do this is to employ a controller (such as the one built by Bob Weller for Kellogg Lab) which senses the ion pump current and keeps it below an acceptable maximum by regulating the current to the bake-out heaters.

Baking of new components is especially important since a great deal of gas is dissolved in the materials during manufacture. Since gas diffusion constants are much larger at elevated temperature than at room temperature, UHV materials may be effectively degassed irreversibly by baking at 300-400°C. It often requires a few days of baking at such temperature to achieve the lowest possible outgassing rate. Again, the higher the temperature the quicker the results, 1 hour at 1000C° being equivalent to 2500 hours at 300°C.[7] The gas that is the worst offender in this regard is hydrogen. A typical concentration of H_2 in stainless

steel is 0.3 torr $\ell\, cm^{-3}$,[7] and long after all water vapor and other gases have been desorbed from the surface during bake-out H_2 will continue to evolve, comprising 99% of the gas output.[7] Since the diffusive release of hydrogen is much less at room temperature, it is theoretically possible to achieve an outgassing rate of $\leq 10^{-16}$ torr ℓ $cm^{-2} sec^{-1}$ for a typical stainless steel component.[7] It is not possible to go much lower with a thin-walled component because of permeation through the walls by hydrogen in the atmosphere.

Once the system has been thoroughly degassed there are a couple of things that can be done to minimize outgassing during subsequent pump-downs. First, the system should be vented with dry nitrogen when it is brought back up to atmospheric pressure. This is to eliminate the condensation of water that occurs when room air is allowed to expand into the vacuum. Adsorbed water vapor is difficult to get rid of without baking.[28] The second thing is to make sure that none of the surfaces which will be in vacuum comes in contact with skin--the grease deposited in a fingerprint acts as a vast gas source in ultra-high vacuum.

When pumping down, the ion pump will start readily at pressures below 10^{-2} torr provided the outgassing from the system is small. In practice, the outgassing load is frequently great enough that the ion pump will not start without difficulty. If the gas load is large the high pump current required causes the pump to heat up, which in turn causes the pump itself to outgas. The increased gas load leads to still higher pump current, and the cycle may run away resulting in shut-down of the pump by the thermal safety relay. Forced air cooling of the pump

helps avoid overheating, but the most effective technique is simply to plug the pump into a Variac and use that to maintain the pump current below some safe level. It is also very helpful to pump the system down below 10^{-4}torr by opening up to beam-line vacuum (with the cold trap filled) before attempting to start the ion pump. This procedure has the additional benefit of prolonging the life of the pump element by decreasing the volume of gas to be pumped.

APPENDIX C

Effect of Adsorption on the Sputtering Yields

I will consider here the question of whether or not the vacuum employed was sufficient to prevent reduction of the sputtering yields due to adsorption of gases onto the target surfaces. The factors which determine the amount of gas adsorbed per time are the partial pressures of the reactive gases in the vacuum system's atmosphere, their sticking fractions on impact with the target surface, and the residence times before adsorbed atoms are vibrated back off the surface.

The sticking fraction is somewhat dependent on temperature and the amount of gas already adsorbed, but for most gases on most metals it is between 0.1 and 1.[29] For a reactive metal like uranium we can assume it is close to 1.

The average residence time is given by[29]

$$\bar{\tau} = \tau_o \, e^{E_d/RT} \qquad \text{(C-1)}$$

where τ_o is the adsorbed atom's period of thermal vibration normal to the surface, and E_d is the energy required to desorb the adatom. τ_o is approximately 10^{-13}sec.[29,38] An E_d of 25 kcal/mole (which is typical of H_2O on metal surfaces) thus gives $\bar{\tau} = 10^5$sec at room temperature. Since uranium is a good getter,[39] and since adsorption energies of the common reactive gases (N_2, O_2, CO_2, etc.) on other getters are normally greater than 25 kcal/mole, we conclude $\bar{\tau} > 10^5$sec for all relevant non-inert gases. The maximum time between sputter-cleaning of a target and

the end of the sputtering data run is a few hours, hence it is apparent that most of the atoms adsorbed on the uranium surface remain during the sputtering run unless sputtered away.

An upper limit to the amount of gas adsorbed on the uran ium surface by the end of a data run can be obtained by assuming all of the residual gas in the system at its base pressure is reactive. The base pressure is $\lesssim 10^{-9}$ torr, and the gas density $n \simeq 3.5 \times 10^{7} cm^{-3}$ at this pressure. The average velocity $\bar{v}$ of the gas particles is given by[36]

$$\bar{v} = \sqrt{\frac{8}{\pi} \frac{RT}{M_{mol}}} \qquad (C\text{-}2)$$

For a molecular weight $M_{mol} = 28$ and $T = 300°K$, $\bar{v} = 4.5 \times 10^{4} cm/sec$. The flux of gas particles impacting the target surface is

$$\Phi = \frac{1}{4} n\bar{v}$$

$$= 4 \times 10^{11} cm^{-2} sec^{-1} \qquad (C\text{-}3)$$

in this case. This implies a time of $2 \times 10^{3} sec$ ($\sim$ 30 min) to adsorb a monolayer on the target surface. In the worst case several monolayers would have been adsorbed between sputter-cleaning and sputtering of a target.

In reality, it is expected that at least 90% of the residual gas in the UHV system is hydrogen and helium.[7,37] This is due primarily to the low pumping speed for helium and to the high emission rate of H_2 from the system's stainless steel walls and from the titanium sublimator filaments. Helium is not adsorbed. Hydrogen is, but the amount that

might be adsorbed is considerably less than the quantity being delivered to the target surface by the ion beam anyway. It is probable, therefore, that less than a monolayer of gas which might affect the hydrogen sputtering yields was adsorbed before the end of the short (15 min) sputtering runs. The masses of the adsorbed gases are so much less than that of ^{235}U that a monolayer of gas added to the top few monolayers of uranium actually being sputtered cannot be expected to reduce the yield of ^{235}U by more than a few percent.

It is possible that a few monolayers may have been adsorbed by the end of the longest (5 hour) runs. This may be responsible for the fact that the long runs gave sputtering yields about 25% lower than the short runs. An idea of the maximum effect adsorption may have can be gained from the observation that the runs on targets which had not been sputter-cleaned (and were thus known to have surface oxidation many monolayers deep) produced sputtering yields roughly a factor of 2 lower than the sputter-cleaned targets.

It has been assumed thus far that the sputter-cleaning of the targets during proton bombardment was not sufficient to ensure an atomically clean surface. Let us look briefly at that assumption. The fact that relevant adsorption energies are on the order of 1 eV/atom[37] and the knowledge of proton sputtering yields for a variety of materials[10,31] make it clear that the desorption yield in this case for such gases as nitrogen and oxygen must be at least 10^{-2}. With a typical ion beam current density of $6 \times 10^{13} cm^{-2} sec^{-1}$, the desorption rate would then be at least $6 \times 10^{11} cm^{-2} sec^{-1}$, which is approximately the adsorption rate for

air at 10^{-9} torr (eq. C-3). Given that most of the residual gas is hydrogen and helium, it appears that the targets actually became substantially cleaner during hydrogen ion bombardment.

All things considered, it is very unlikely that the hydrogen sputtering yields in the short runs were reduced by more than a few percent, as an upper limit, by effects due to gas adsorbed on the target surface.

Since the argon and helium runs were very short (< 60 sec) and took place immediately after sputter-cleaning, and since the sputtering rates are so much higher than those of hydrogen, there was no effect on these yields due to adsorbed gas.

APPENDIX D

Neutron Fluence Determination Using NBS Neutron-Irradiated Standards

The National Bureau of Standards has available glass wafers containing precisely known quantities of uranium and thorium which have been irradiated with carefully determined fluences of neutrons. Identical non-irradiated standards are also available which the user may include with samples being neutron irradiated. The user's neutron fluence may subsequently be determined by comparison, after etching both standards and counting the etch pits due to fission tracks in each. The basics of this technique are covered in NBS Special Publication 260-49: "Standard Reference Materials: Calibrated Glass Standards for Fission Track Use".[8] I will simply summarize them and add some information of a practical nature.

The first step is to decide which of the four available uranium concentrations (nominally 500 ppm, 50 ppm, 1 ppm and .07 ppm) is appropriate for the anticipated neutron dose, bearing in mind that the uranium is <0.7 atom % ^{235}U. It was found that SRM 963 (1 ppm) gave a convenient density of tracks when exposed to 10^{16}-10^{17} n/cm^2 and etched according to NBS recommendations (75 sec in 16% HF at 20°C).

Once a blank wafer has been irradiated, both it and comparison standards must either be broken or ground to reveal an internal surface free of fission track contamination from the environment. Fracturing immediately yields a smooth internal surface which can be etched without further treatment. Unfortunately, the fractured surface is not flat and is rather inconvenient to scan under the microscope. Grinding and

polishing requires more time and effort but, done properly, yields a smooth, flat surface which is conducive to easy scanning. The details of grinding and polishing proceduresdeveloped by the author are presented next.

The initial step, and it is an important one, is to round off the edge (about 1/64" will do) of the face of the wafer to be ground. Next, at least 30μ of the face is removed by hand grinding directly on a smooth glass surface using a slurry of water and 5μ alumina. With firm pressure from one finger and 3-4 small circular motions per second, 30μ can easily be removed in less than 5 minutes. 30μ is removed because it is greater than the longest fission-fragment range. The first reason for rounding off the edge of the wafer is to avoid big scratches on the surface made by tiny fragments of glass which chip off a sharp edge during the grinding operation. The reason for grinding directly on a sheet of glass is that if one attempts to grind on a piece of polishing paper, it will take close to forever to remove 30μ.

After a brief ultrasonic cleaning, polishing can now begin. Low speed polishing is necessary to avoid heat buildup, which causes track fading.[8] I found the Mini-Met polisher (manufactured by Buehler, Ltd. of Evanston, Ill.) to be quite useful for this step. The polishing may also be done by hand if one has the patience and endurance. If one employs the Mini-Met, it is necessary at this juncture to either fabricate a sample holder sized to the NBS wafers or to glue them to 1" glass wafers, which fit the standard Mini-Met holder. The latter option was chosen by the author and offered the additional advantage of a convenient

handle for manipulating the wafer without worrying about marring its surface. It was found that 1" glass wafers, 1/16" thick (which are commonly used for mounting petrographic thin sections) are readily available and are ideal. Cyanoacrylate cement gave a quick, strong bond between the glass wafers.

The first of two polishing operations utilizes a slurry of water and 1μ alumina on (Texmet®) polishing cloth. One hour of polishing with the Mini-Met set at its lowest speed and third-from-lowest pressure gave an adequate surface finish without noticeable heating of the standards. The second reason for rounding off the edge of the wafer will now become obvious if it has not been done, for the sharp edge will dig into the polishing cloth and cause the standard to roll around on its edge rather than riding around with its full surface in contact with the polishing surface.

If the polished surface is viewed with phase-contrast microscopy at this point, many 1μ-wide scratches and a fairly small population of 1μ pits will be evident. If the standard is etched at this point, these tiny pits will etch to about the size of typical fission-fragment track etch pits and will make accurate track counting difficult. It is standard practice,[11] therefore, to give the surface a final polishing using 0.3μ alumina. Another brief ultrasonic bath precedes the 0.3μ polishing, which is performed on very soft polishing cloth (Microcloth® is used with the Mini-Met). With the same settings as above, the Mini-Met produced a surface virtually devoid of 1μ pits in 30 minutes.

A final brief ultrasonic bath, distilled water rinse, and filtered-air blow drying leaves the sample clean and ready to be etched.

It is imperative that care be taken not to mar the polished surface until after it is etched. Wiping it with a Kimwipe, for example, produces enormous numbers of 1μ pits which will interfere with track counting.

The etch recommended by the NBS (75 seconds in 16% HF at room temperature) gave excellent results. Track etch pits were typically 3-4μ across and were easily counted in reflected light using phase-contrast microscopy at 400X. This technique is recommended for the great clarity it imparts to etch pits and other surface features. Also, the colors are very beautiful. More importantly, it allows accurate discrimination against etch pits which are not due to fission tracks. This is based on the fact that the 75-second etch is short enough that most of the fission tracks have not been etched all the way to the end and are thus sharp-pointed cones.[11,13] Pits which were present before etching were not sharp-bottomed to begin with and are nicely-rounded pits afterwards. These rounded bottoms reflect light in a characteristic manner which is different from the characteristic reflection from sharp-bottomed pits. The difference between the two types of reflection is most apparent when the microscope is focused up and down through the depth of the pits. As a rounded bottom is brought into focus, the reflection coalesces symmetrically and uniformly into a bright but somewhat diffuse spot which is essentially the same shape as the pit and whose size is a considerable fraction of the pit's. When a sharp-bottomed pit is brought into focus, the reflections move around in a nonuniform manner and coalesce into a spot which is more intense and

better defined, at least at one end, than in the previous case. For oblong track pits a criss-crossing of reflections (due to second order reflections from the cone walls, I suppose) as the focus is moved up and down is generally observed. For large cones seen end on there is very little reflection at all.

In studying the difference between track pits and spurious pits, I found it useful to grind and partially 1μ polish an un-irradiated standard. After giving it the standard etch many pits were visible which were not due to tracks and a graphic comparison to a well-polished, irradiated, and etched standard, where most of the pits were due to tracks, could be made.

Since tracks crossing the surface have lengths anywhere from zero to full range, tracks shorter than some length will be etched all the way to the end and become round-bottom pits which are not counted. This technique cannot therefore yield directly an absolute neutron fluence from a single user-irradiated glass standard. However, if both user- and NBS-irradiated wafers receive identical etches and are counted carefully following identical counting criteria, very accurate fluences relative to the NBS values may be determined. Identical etches are required because the density of revealed tracks is a strong function of the etching time and etchant dilution.

One final detail is that one must choose between the two NBS-irradiated standards supplied in each package of standards if one desires neutron fluence values better than $\sim$10%. This is because one of them (RT-3) was exposed to neutrons in a position in the NBS reactor

having a higher proportion of fast neutrons than the other (RT-4). This is indicated by different cadmium ratios for the gold and copper flux-monitor foils in the two positions.[8] If the neutron flux is well thermalized during irradiation of the user's blank standard, then RT-4 would be the wafer to compare to. Wafers from position RT-3 would give a better approximation to neutron energy distributions nearer to core. To give a quantitative example, the cadmium ratio for the gold foil monitors is 10.2 in position RT-3 and 87 in position RT-4 and is 3.3 (Bruce Taylor, private communication) in the center of the UCLA reactor core. A standard exposed in the center of the UCLA reactor and compared to an RT-3 wafer would slightly underestimate the effective flux.

VII. REFERENCES

1. Almén, O. and G. Bruce, 1961, NIM 11, 257,279.
2. Andersen, H., 1974, in V. Vujnović (ed.) 7th Yugoslav Symposium and Summer School on the Physics of Ionized Gases (Institute of Physics of the University of Zagreb), p. 361.
3. Bethe, H. and J. Askin, 1953, in O. Segne (ed.) Experimental Nuclear Physics (John Wiley & Sons, New York), p. 166.
4. Bhandari, N. et al., 1971, Earth Planet. Sci. Lett. 13, 191.
5. Biersack, J., D. Fink and P. Mertens, 1974, J. Nucl. Mat. Met. 53, 194.
6. Burnett, D. and D. Woolum, 1974, Earth Planet. Sci. Lett. 21, 153.
7. Calder, R. and G. Lewin, 1967, Brit. J. Appl. Phys. 18, 1459.
8. Carpenter, B. and G. Reimer, 1974, NBS 260-49: "Calibrated Glass Standards for Fission Track Use."
9. Espe, W., 1966, Materials of High Vacuum Technology (Pergamon Press, New York) Vol. 1: "Metals and Metalloids".
10. Finfgeld, C. et al., 1974, AEC Report ORO-3557-15.
11. Fleischer, R., P. Price and R. Walker, 1975, Nuclear Tracks in Solids (University of California Press, Berkeley).
12. Ibid, p. 318.
13. Fleischer, R. and P. Price, 1964, J. Geophys. Res. 69, 331.
14. Flint, O., J. Polling and A. Charlesby, 1954, Acta Metall. 2, 696.
15. Furr, A. and C. Finfgeld, 1970, J. Appl. Phys. 41, 1739.
16. Grønland, F. and W. Moore, 1960, J. Chem. Phys. 32, 1540.

17. Gschneidner, K., 1964, Solid State Phys. 16, 275.

18. Haines, E., private communication.

19. Kaminsky, M., 1974, Proc. 5th Int. Conf. on Plasma Physics and Controlled Nucl. Fusion Res., IAEA No. CN-33, p. 287.

20. Kaminsky, M., H. Wiedersich and K. Zwilsky (eds), 1974, Proc. Conf. Surface Effects in Controlled Thermonuclear Fusion Devices and Reactors in J. Nuc. Mat. Met. 53.

21. Kaminsky, M. and S. Das, ibid, p. 162.

22. Kaminsky, M. and S. Das, 1975, Proc. 6th Symp. on Eng. Prob. Fus. Res., IEEE No. 75CH1097-5-NPS, p. 1141

23. Kenknight, C. and G. Wehner, 1964, J. Appl. Phys. 35, 322.

24. Kittel, C., 1971, Introduction to Solid State Physics (Wiley & Sons, New York), p. 39.

25. Lindhard, J., M. Scharff and H. Schiøtt, 1963, Kgl. Danske Videnskab, Selskab Mat.-Phys. Medd. 33, No. 14.

26. Lindhard, J., V. Nielsen, M. Scharff and P. Thomsen, 1963, Kgl. Danske Videnskab. Selskab Mat.-Phys. Medd. 33, No. 10.

27. Maisel, L. and R. Glang (eds), 1970, Handbook of Thin Film Technology (McGraw-Hill, New York), Ch. 2: "High Vacuum Technology".

28. Ibid, p. 2-44.

29. Ibid, p. 2-41.

30. Mayer, J. and J. Ziegler (eds), 1973, Ion Beam Surface-Layer Analysis, Thin Solid Films 19.

31. McDonnell, J. and D. Ashworth, 1972, Space Res. XII, 333.

32. Milleron, N., 1967, IEEE Trans. Nucl. Sci. NS-14 (3), 794.

33. Nash, D., D. Matson, T. Johnson and F. Fanale, 1975, J. Geophys. Res. 80, 1875.

34. Power, B. and F. Robson, 1962, Transactions of the Second International Vacuum Congress (Pergamon Press, Oxford), p. 1175.

35. Price, P. and R. Walker, 1963, J. Geophys. Res. 68, 4847.

36. Reif, F., 1965, Fundamentals of Statistical and Thermal Physics (McGraw-Hill, New York), p. 268.

37. Roth, A., 1976, Vacuum Technology (North-Holland, New York).

38. Ibid, p. 174.

39. Ibid, p. 262.

40. Schiøtt, H., 1966, Kgl. Danske Videnskab. Selskab Mat.-Fys. Medd. 35, No. 9.

41. Seitz, M., R. Walker and B. Carpenter, 1973, J. Appl. Phys. 44, 510.

42. Sigmund, P., 1968, Can. J. Phys. 46, 731.

43. Sigmund, P., 1969, Phys. Rev. 184, 383.

44. Sigmund, P., 1972, Rev. Roum. Phys. 17, 823,969,1079.

45. Sigmund, P., M. Matthes and D. Phillips, 1971, Rad. Effects 11, 39.

46. Summers, A., N. Freeman and N. Daly, 1971, J. Appl. Phys. 42,4774

47. Switkowski, Z., P. Haff, T. Tombrello and D. Burnett, 1977, J. Geophys. Res. (in press)

48. Thompson, M., 1968, Phil. Mag. 18, 377.

49. Weissman, R. and P. Sigmund, 1973, Rad. Effects 19, 7.

50. Weissman, R. and R. Behrisch, 1973, Rad. Effects 19, 69.

51. Wickramasinghe, N., 1972, Mon. Not. Roy. Astro. Soc. 159, 269.

52. Winterbon, K., 1972, Rad. Effects 13, 215.

53. Winterbon, K., P. Sigmund and J. Sanders, Kgl. Danske Videnskab. Selskab Mat.-Fys. Medd. 37, No. 14.

54. Yonts, O., C. Normand and D. Harrison, 1960, J. Appl. Phys. 31, 447.

55. Ziegler, J., J. Cuomo and J. Roth, 1977, Appl. Phys. Lett. 30, 268

TABLE 1

Neutron fluxes measured by the National Bureau of Standards for fission track glass standards SRM963 (see p. 25).

Table 1

SRM 963 Fission Track Glass Standard

Wafer Number Identification	NBS Reactor Position	Neutron Flux Mean Value and Standard Deviation[a] ($\times 10^{13}$ n·cm^{-2}·sec^{-1})[b]	Tolerance Intervals[c] (95%)	(99%)
		Cu Foil		
614001-614040	RT-4	1.26 ± 0.026	±0.06	±0.09
614041-614090	RT-4	1.24 ± 0.026	±0.06	±0.09
614091-614125	RT-4	1.26 ± 0.026	±0.06	±0.09
614126-614165	RT-3	5.38 ± 0.17	±0.42	±0.60
614166-614215	RT-3	5.10 ± 0.17	±0.42	±0.59
614216-614251	RT-3	5.14 ± 0.17	±0.42	±0.60
		Au Foil		
614001-614040	RT-4	1.41 ± 0.024	±0.06	±0.09
614041-614090	RT-4	1.36 ± 0.024	±0.06	±0.08
614091-614125	RT-4	1.44 ± 0.024	±0.06	±0.09
614126-614165	RT-3	6.03 ± 0.059	±0.15	±0.21
614166-614215	RT-3	5.97 ± 0.059	±0.15	±0.21
614216-614251	RT-3	6.13 ± 0.059	±0.15	±0.21

[a] Standard deviations refer to individual metal foils.

[b] Irradiation was performed at a power of 10 megawatts; 80 seconds in RT-3, or 120 seconds in RT-4.

[c] A 95 percent tolerance interval is estimated to include the measurement of approximately 95 percent of all individual wafers of the population of wafers. Thus, the probability is approximately 95 percent that any individual wafer measurement will lie inside the 95 percent tolerance interval. A similar definition holds for 99 percent tolerance interval.

TABLE 2

Determination of total fluence received by NBS glass standard SRM-A during neutron irradiation at UCLA reactor by comparison to known fluences received by NBS fission track glass standards SRM963 (RT-3 and RT-4) (see p. 25).

Fields of view were areas 260μ x 260μ on the standard glass wafers as seen under phase-contrast microscopy at 400X.

Neutron fluences for SRM-A are obtained by multiplying the NBS-determined fluences for RT-3 and RT-4 by the ratio of tracks counted on SRM-A to the number counted on the corresponding RT-standard.

Neutron fluences as determined by the NBS for glass standards RT-3 and RT-4 are obtained from Table 1 by multiplying the neutron flux mean values for the appropriate wafers by the times they were irradiated in the NBS reactor (from footnote b). The serial numbers of the particular wafers used in this experiment are 614016 for RT-4 and 614141 for RT-3.

TABLE 2

	SRM-A	RT-3	RT-4
Fields of View Counted	20	40	80
Total Number of Tracks Counted	750	732	556
Tracks per Field of View	37.5	18.3	6.95
Track Density Ratio: SRM-A/RT-		2.05	5.40
Neutron Fluence (n/cm^2) as determined by NBS with			
Au foils:		4.82×10^{15}	1.69×10^{15}
Cu foils:		4.30×10^{15}	1.51×10^{15}
Neutron Fluence for UCLA Reactor Run by comparison of SRM-A to RT-			
Au foils:		9.88×10^{15}	9.13×10^{15}
Cu foils:		8.82×10^{15}	8.15×10^{15}

TABLE 3

Sputtering yields of ^{235}U due to bombardment by ion beams at normal incidence to the targets. Yields "S" are atoms of ^{235}U emitted per incident atom. With a $\cos^{1/4}\theta$ fit to the angular distribution data, S is calculated from

$$S = \frac{8\pi r^2}{5} \frac{N_t^o}{N_p N_n \sigma_f}$$

where N_t^o = number of fission tracks per cm^2 on collector foil at $\theta = 0°$

N_p = number of incident atoms

N_n = neutron fluence = $1.46 \times 10^{15} cm^{-2}$

σ_f = 582 bn

r = 3.7 cm

Most targets contained 99.71% ^{235}U but a few (marked 93 in the % ^{235}U column) contained 93.32% ^{235}U, which necessitated a correction when computing S.

Quoted errors on the values of S are overall errors including uncertainty due to counting and error in determination of N_n.

TABLE 3

Run	Ion Beam	% ^{235}U	N_p	N_t^o	S(atoms/atom)
Sputter-cleaned targets:					
3-3	40 keV H_1	99	10^{17}	3.9×10^5	$3.2 \pm 0.5 \times 10^{-4}$
3-4	60 keV H_1	"	"	2.7×10^5	$2.7 \pm 0.4 \times 10^{-4}$
2-4	80 keV H_1	"	"	2.5×10^5	$2.0 \pm 0.3 \times 10^{-4}$
2-6	100 keV H_1	"	"	2.0×10^5	$1.6 \pm 0.25 \times 10^{-4}$
2-5	120 keV H_1	"	"	1.8×10^5	$1.5 \pm 0.25 \times 10^{-4}$
Targets cleaned only HNO_3:					
1-4	40 keV H_1	93	"	2.1×10^5	$1.8 \pm 0.2 \times 10^{-4}$
1-2	60 keV H_1	99	"	1.3×10^5	$1.0 \pm 0.15 \times 10^{-4}$
1-3	80 keV H_1	"	"	1.1×10^5	$8.9 \pm 0.15 \times 10^{-5}$
1-1	100 keV H_1	93	"	8.9×10^4	$7.7 \pm 0.10 \times 10^{-5}$
1-5	120 keV H_1	99	"	8.3×10^4	$6.7 \pm 0.07 \times 10^{-5}$
Targets not cleaned at all:					
3-6	40 keV H_1	99	"	3.6×10^4	$2.9 \pm 0.6 \times 10^{-5}$
3-5	60 keV H_1	99	"	5.4×10^4	$3.9 \pm 0.6 \times 10^{-5}$
Sputter-cleaned target:					
2-3	80 keV Ar	99	2.0×10^{12}	4.7×10^4	1.9 ± 0.4

TABLE 4

Sputtering yields of ^{235}U due to bombardment by ion beams at normal incidence to the targets. Yields "S" are atoms of ^{235}U emitted per incident atom (rather than per incident ion). With a $\cos^{1/4}\theta$ fit to the angular distribution data, S is calculated from

$$S = \frac{8\pi r^2}{5} \frac{N_t^o}{N_p N_r \sigma_f}$$

where N_t^o = number of fission tracks per cm^2 on collector foil at $\theta = 0°$

N_p = number of incident atoms

N_n = neutron fluence = $1.37 \times 10^{16} cm^{-2}$

σ_f = 582 bn

r = 3.7 cm

All targets in runs in series 4-7 contained 99.7% ^{235}U.

Errors on the values of S are overall errors including uncertainty due to counting and error in determination of N_n.

TABLE 4

Run	Ion Beam	N_p	$N_t^o(cm^{-2})$	S(atoms/atom)
5-5	40 keV H_3	1.5×10^{16}	7.0×10^5	$4.0 \pm 0.5 \times 10^{-4}$
5-6	40 keV H_2	1.0×10^{16}	4.8×10^5	$4.2 \pm 0.5 \times 10^{-4}$
5-4	40 keV H_1	5.0×10^{15}	3.0×10^5	$5.2 \pm 0.7 \times 10^{-4}$
7-6	50 keV H_1	2.5×10^{15}	1.5×10^5	$5.2 \pm 0.7 \times 10^{-4}$
4-6	80 keV H_1	5.0×10^{15}	1.6×10^5	$2.8 \pm 0.3 \times 10^{-4}$
4-4	100 keV H_1	"	1.5×10^5	$2.6 \pm 0.4 \times 10^{-4}$
4-5	120 keV H_1	"	1.4×10^5	$2.4 \pm 0.3 \times 10^{-4}$
7-2	80 keV H_2	"	3.2×10^5	$5.5 \pm 0.8 \times 10^{-4}$
7-3	100 keV H_2	"	2.9×10^5	$5.0 \pm 0.6 \times 10^{-4}$
7-4	120 keV H_2	"	2.7×10^5	$4.7 \pm 0.6 \times 10^{-4}$
7-5	120 keV H_3	7.5×10^{15}	3.6×10^5	$4.2 \pm 0.5 \times 10^{-4}$
6-6	40 keV He	3.0×10^{14}	4.7×10^5	$1.3 \pm 0.15 \times 10^{-2}$
6-5	60 keV He	"	5.0×10^5	$1.4 \pm 0.15 \times 10^{-2}$
6-2	80 keV He	"	4.2×10^5	$1.2 \pm 0.15 \times 10^{-2}$
6-3	100 keV He	"	3.3×10^5	$9.4 \pm 0.10 \times 10^{-3}$
6-4	120 keV He	"	3.6×10^5	$1.0 \pm 0.10 \times 10^{-2}$
4-3	40 keV Ar	1.0×10^{12}	2.0×10^5	1.7 ± 0.5
4-2	80 keV Ar	"	2.3×10^5	2.0 ± 0.5

TABLE 5

The number of fission stars consisting of a number of fission tracks N_t, in four ranges, produced by total doses N_p of various ion beams bombarding uranium metal targets. In each case the numbers were determined by careful scanning with a transmitted-light microscope of the specified area on mica detectors which recorded the ^{235}U distribution on the sputtering collector foils.

$\overline{N}_t$ is the median star size in each case, and $\overline{N}_U$ is the number of atoms in the corresponding chunk. (See Section IIID).

The entry marked "Blank" gives the results of scanning the back of the mica with the 80 keV Ar^+ data bands on it.

TABLE 5

Ion Beam	N_p	Area Scanned (cm^2)	Number of Stars with N_t = 5-24	25-49	50-74	> 75	$\bar{N}_t$	$\bar{N}_U$
40 keV H_1	10^{17}	6	27	8	1	3	15	1.5×10^7
60 keV H_1	"	"	17	4	2	3	20	2.0×10^7
80 keV H_1	"	"	71	35	9	26	25	2.5×10^7
100 keV H_1	"	"	126	37	17	30	20	2.0×10^7
120 keV H_1	"	"	133	30	12	21	15	1.5×10^7
60 keV H_1	5×10^{15}	3	3	2	0	0	-	-
80 keV H_1	"	"	1	0	0	0	-	-
100 keV H_1	"	"	13	0	0	0	10	10^6
120 keV H_1	"	"	1	0	0	0	-	-
80 keV He	3×10^{14}	1.8	27	12	2	4	20	2.0×10^6
100 keV He	"	"	8	5	0	3	25	2.5×10^6
120 keV He	"	"	2	1	0	3	-	-
80 keV Ar	2×10^{12}	4	178	76	39	66	25	2.5×10^7
Blank	-	3	1	1	0	0	-	-

TABLE 6

A comparison of chunk emission data for H_1^+, He^+, and Ar^+ ions on uranium. The total number of chunks counted in each case is given, as well as the number/cm^2 on the micas. The ion beam fluence is the total fluence delivered to a given target, and which produced the stated number of chunks/cm^2. The mean number of ^{235}U atoms per chunk and the number of single atoms/cm^2 are averages over all the data bands counted to produce chunk data for each of the three ion species (e.g., ten data bands for 40-120 keV H_1^+ were scanned).

See p.51

TABLE 6

	H	He	Ar
Chunks counted	612	67	359
Ion beam fluence	10^{17}	3×10^{14}	2×10^{12}
Chunks/cm^2	20	12	90
<Atoms/chunk>	4.3×10^{7}	5.3×10^{6}	6.6×10^{7}
Single atoms/cm^2	3.2×10^{11}	4.6×10^{10}	5.5×10^{10}
Chunk contribution to sputtering yield	$\sim$.3%	$\sim$.1%	$\sim$10%

TABLE 7

Sputtering yields of ^{235}U under bombardment at normal incidence by H_1^+ ions with energy E, as calculated using equation (4-9). ε and ρ are the dimensionless energy and range respectively (see Section IVA). $\alpha(\varepsilon)$ values are from Weissman and Sigmund (1973). The dimensionless nuclear stopping cross-section $s_n(\varepsilon) \equiv (d\varepsilon/d\rho)_n$ values are from Schiøtt (1966). A value of U_o = 5.4 eV was used for the surface binding energy.

See p.46

TABLE 7

H_1^+ Sputtering of ^{235}U

E (keV)	ε	ρ	$\alpha(\varepsilon)$	$s_n(\varepsilon)$	S(E)
5	.38	.06	2.8	.411	6.4×10^{-2}
10	.76	.09	2.35	.378	4.9×10^{-2}
15	1.14	.11	2.0	.345	3.8×10^{-2}
20	1.52	.13	1.75	.313	3.1×10^{-2}
40	3.04	.18	1.3	.236	1.7×10^{-2}
60	4.56	.22	1.0	.193	1.1×10^{-2}
80	6.09	.25	0.8	.165	7.3×10^{-3}
100	7.62	.29	0.7	.144	5.9×10^{-3}
120	9.14	.31	0.65	.137	4.7×10^{-3}

$$\varepsilon = 7.62 \times 10^{-2} \text{ E (keV)}$$

$$\rho = 1.39 \times 10^{-4} \zeta \text{ (}\mu\text{gm cm}^{-2}\text{)}$$

TABLE 8

Sputtering yields of ^{235}U under bombardment at normal incidence by He^+ ions with energy E, as calculated using equation (4-9). ε and ρ are the dimensionless energy and range respectively (see Section IVA). $\alpha(E)$ values are from Weissman and Sigmund (1973). The dimensionless nuclear stopping cross-section $s_n(\varepsilon) \equiv (d\varepsilon/d\rho)_n$ values are from Schiøtt (1966). A value of U_o = 5.4 eV was used for the surface binding energy.

See p.46

TABLE 8

He^+ Sputtering of ^{235}U

E (keV)	ε	ρ	$\alpha(\varepsilon)$	$s_n(\varepsilon)$	S(E)
20	.742	.358	2.35	.38	.39
40	1.48	.535	1.7	.32	.23
60	2.23	.675	1.5	.27	.18
80	2.97	.795	1.3	.24	.14
100	3.71	.901	1.2	.22	.11
120	4.45	.998	1.0	.20	.09

$$\varepsilon = 3.71 \times 10^{-2} E \text{ (keV)}$$

$$\rho = 5.30 \times 10^{-4} \zeta \text{ (}\mu\text{gm cm}^{-2}\text{)}$$

TABLE 9

Sputtering yields of ^{235}U under bombardment at normal incidence by Ar^+ ions with energy E, as calculated using equation (4-9). ε and ρ are the dimensionless energy and range respectively (see Section IVA). $\alpha(\varepsilon)$ value of 0.5 is from Andersen (1974) p. 392. The dimensionless nuclear stopping cross-section $s_n(\varepsilon) \equiv (d\varepsilon/d\rho)_n$ values are from Schiøtt (1966). A value of U_o = 5.4 eV was used for the surface binding energy.

See p.46

TABLE 9

Ar^+ Sputtering of ^{235}U

E (keV)	ε	ρ	$\alpha(\varepsilon)$	$s_n(\varepsilon)$	S(E)
20	.064	.20	0.5	.34	5.2
40	.129	.32	"	.39	5.9
60	.193	.43	"	.40	6.2
80	.257	.52	"	.41	6.3
100	.322	.61	"	.41	6.3
120	.386	.70	"	.41	6.2

$$\varepsilon = 3.22 \times 10^{-3} \text{ E (keV)}$$

$$\rho = 3.22 \times 10^{-3} \zeta \text{ (}\mu\text{gm cm}^{-2}\text{)}$$

TABLE 10

Cleaning procedures used to prepare materials for use in ultrahigh vacuum (see Appendix B). Recipes for the acid dip solutions are given in the next table.

TABLE 10

Cleaning Procedures for Parts to be Used in Ultrahigh Vacuum

Ceramics: Ultrasonic rinse in clean methanol; hot air dry

Copper: Vapor degrease in trike*, detergent wash, acid dip (50% HCl at room temperature for 1-3 min), water rinse, methanol rinse, acetone rinse, warm air dry

Copper Wire: Vapor degrease in trike, detergent wash (Labtone), acid dip (50% HCl at room temperature for 1-3 min), water, methanol, and acetone rinses while brushing with SST brush, warm air dry

Gold: Acid dip in aqua regia ($3HCl + HNO_3$)

Aluminum: Vapor degrease in trike, dip in 10% NaOH solution saturated with common salt for 15-50 sec, rinse; if discolored wash in 20-30% HNO_3, rinse in running water 3-5 min, dip in 12% H_2SO_4, HaOH solution again for 1 min, rinse in running water, methanol rinse, warm air dry

Glass Parts: Vapor degrease in trike, potassium dichromate saturated solution 35 cc in 1 liter concentrated H_2SO_4, or CrO_3 saturated solution instead of potassium dichromate; n.b. slowly stir the acid into the chromate or trioxide solution; use at 110°C (solution should be red), deionized water rinse, ultrasonic methanol bath, warm air dry

Stainless Steel: Vapor degrease in trichloroethylene (10-15 min), rinse in warm tap water, dip in stainless steel cleaning solution no.2 for 8 min, rinse in cold deionized water, dip in stainless steel cleaning solution no.3 for 10-15 min, rinse in tap water, rinse in deionized water, dip in methanol (ultrasonic cleaner), hot air dry

Titanium: Dip in titanium cleaning solution (30 sec, inspect, and repeat until surface is smooth and clean), rinse in deionized water, rinse in methanol, hot air dry

*trichloroethylene

TABLE 11

Acid dip solutions called for in table of cleaning procedures

TABLE 11

Stainless Steel Solution No. 2

	% by volume	minimum	maximum	specific gravity
HNO_3-nitric acid	19.0	18.0	20.0	1.4078
HCl-hydrochloric acid	1.1	1.0	1.2	1.16
HF-hydrofluoric acid	2.2	2.0	2.4	1.258
H_2O-deionized water	77.7	balance		

Makeup: Fill tank somewhat less than half full with deionized water, add acids in above order, while stirring. Fill up with water.

Stainless Steel Solution No. 3

HNO_3-nitric acid	50.0	46.0	50.0	1.4078
H_2O-deionized water	balance			

Makeup: Fill tank somewhat less than half full with deionized water, slowly pour in HNO_3, while stirring. Fill up with water.

Titanium Cleaning Solution

HNO_3-nitric acid	25.0	23.0	30.0	1.4078
HF-hydrofluoric acid	2.0	1.5	2.1	1.258
H_2O-deionized water	balance			

FIGURE 1

The sputtering assembly.(see p.11) A cross-section of the apparatus is sketched in Fig. 2. The assembly is mounted on an 8" OD UHV flange.

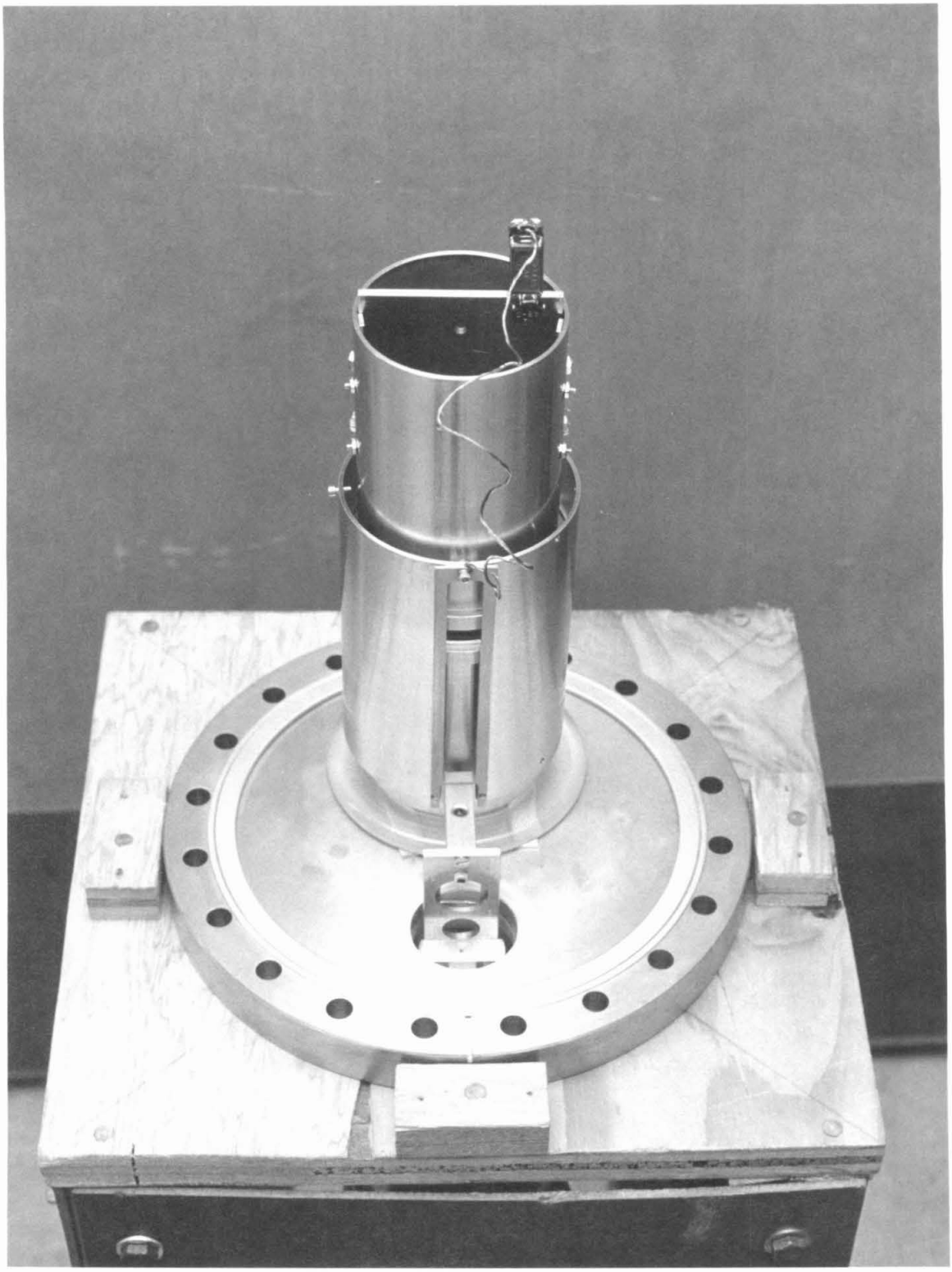

FIGURE 2

Cross-sectional view of the sputtering apparatus pictured in Fig. 1.
(See p.9)
Bars bracketing edges of target plate ensure that it remains perpendicular to beam at all times.

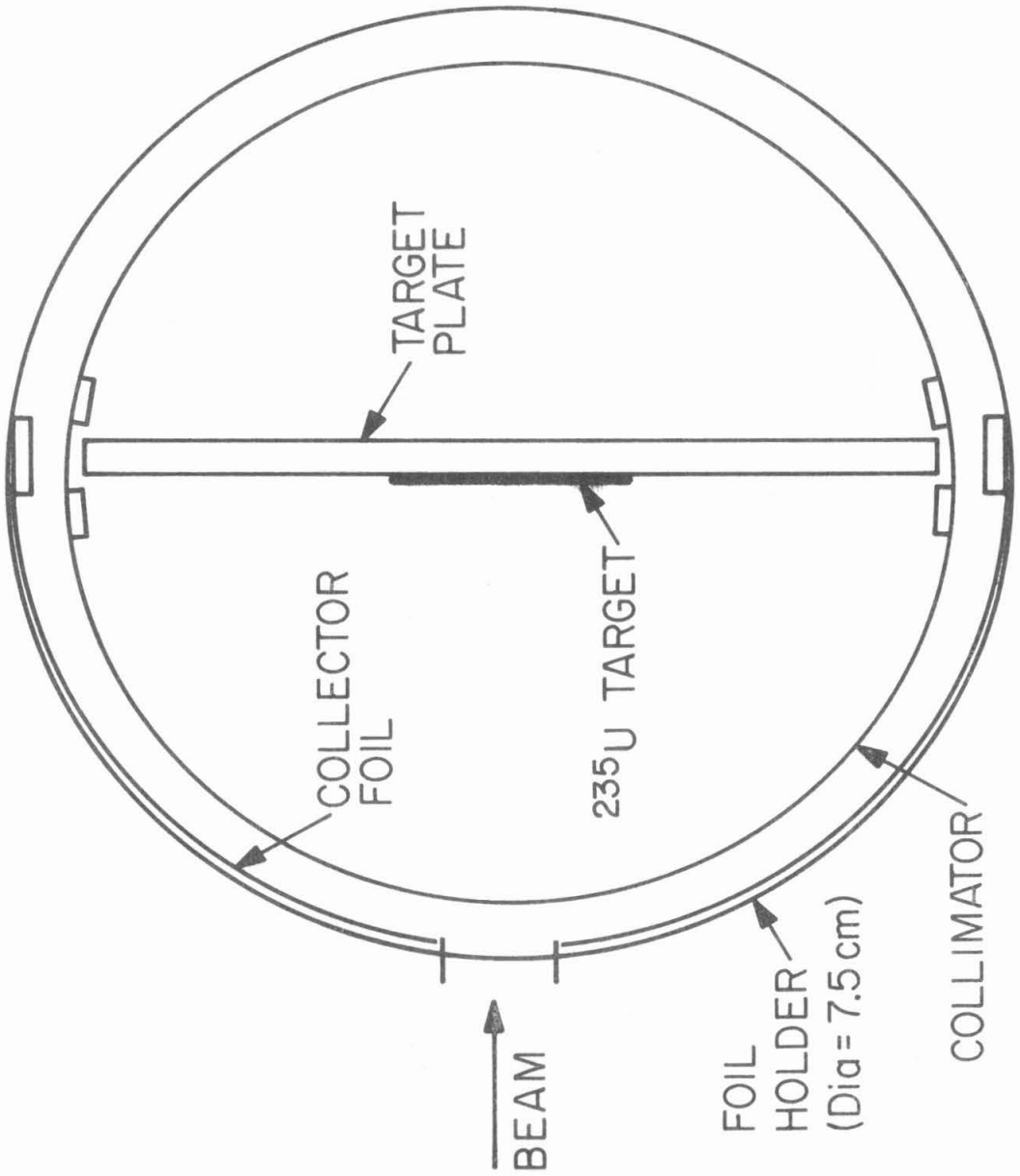
TARGET PLATE
COLLECTOR FOIL
^{235}U TARGET
BEAM
FOIL HOLDER (Dia = 7.5 cm)
COLLIMATOR

FIGURE 3

The arrangement of the bands of sputtered uranium resulting from moving catcher foils to different postions behind 1 cm horizontal slot in collimator cylinder. (see Figs. 1 & 2 and p.9) Viewpoint is that of target, so labels on the backs of catcher foils appear backwards. Labels are drawn as for runs in series 1. Beam enters between left and right foils.

Uranium sputtered during sputter-cleaning of targets is collected on foils labelled GL & GR. All dimensions in cm.

0.1
1.5
6
5
4
3
2
1
UL1
UR1
LL1
LR1
GL1
GR1
3.8
1.0

FIGURE 4

The manipulators for positioning the targets and catcher foils.

(see p.11)

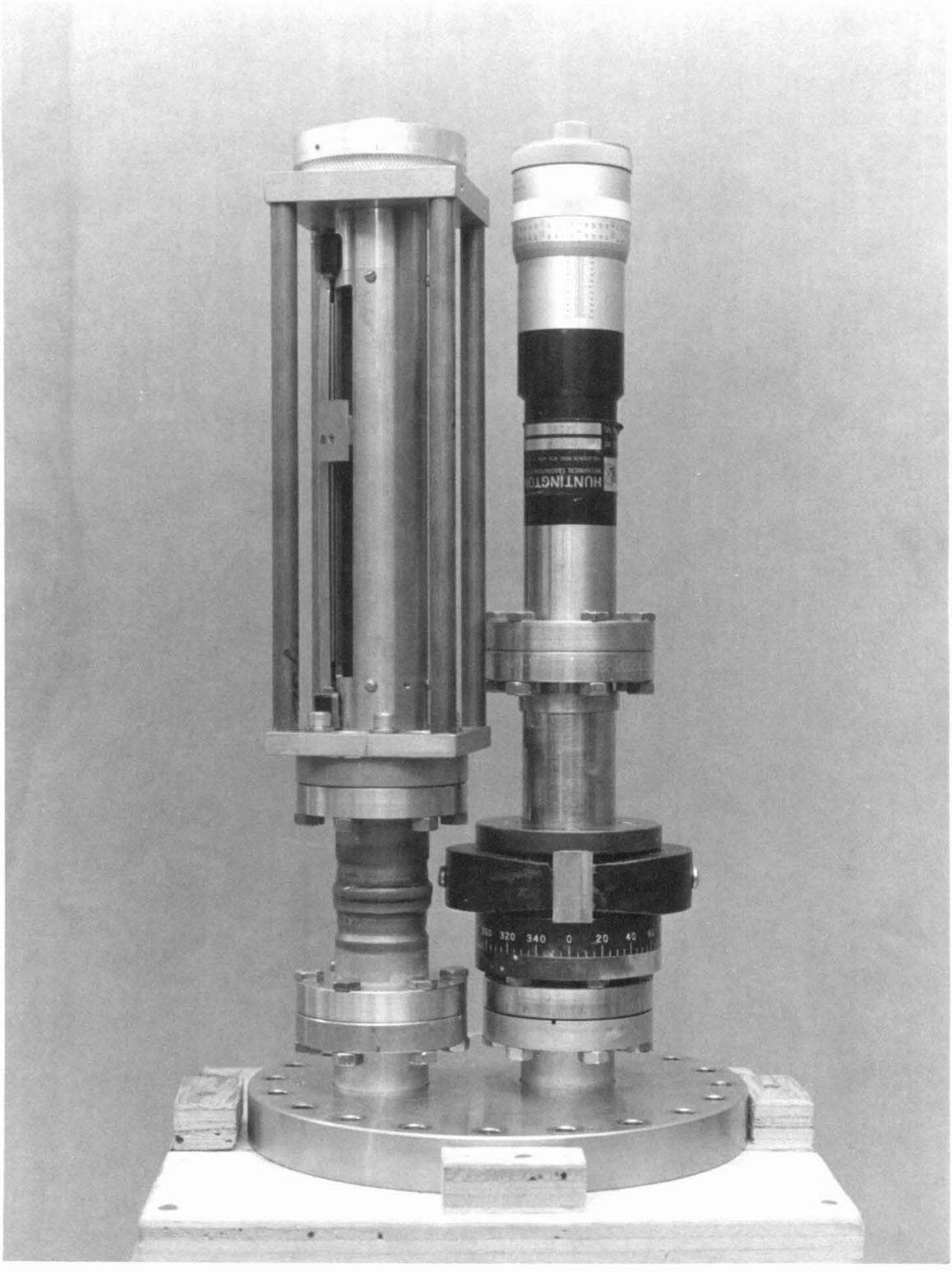
HUNTINGTON
320 340 0 20

FIGURE 5

The vacuum side of the sputtering assembly mounting flange with the assembly removed. (see p.11)

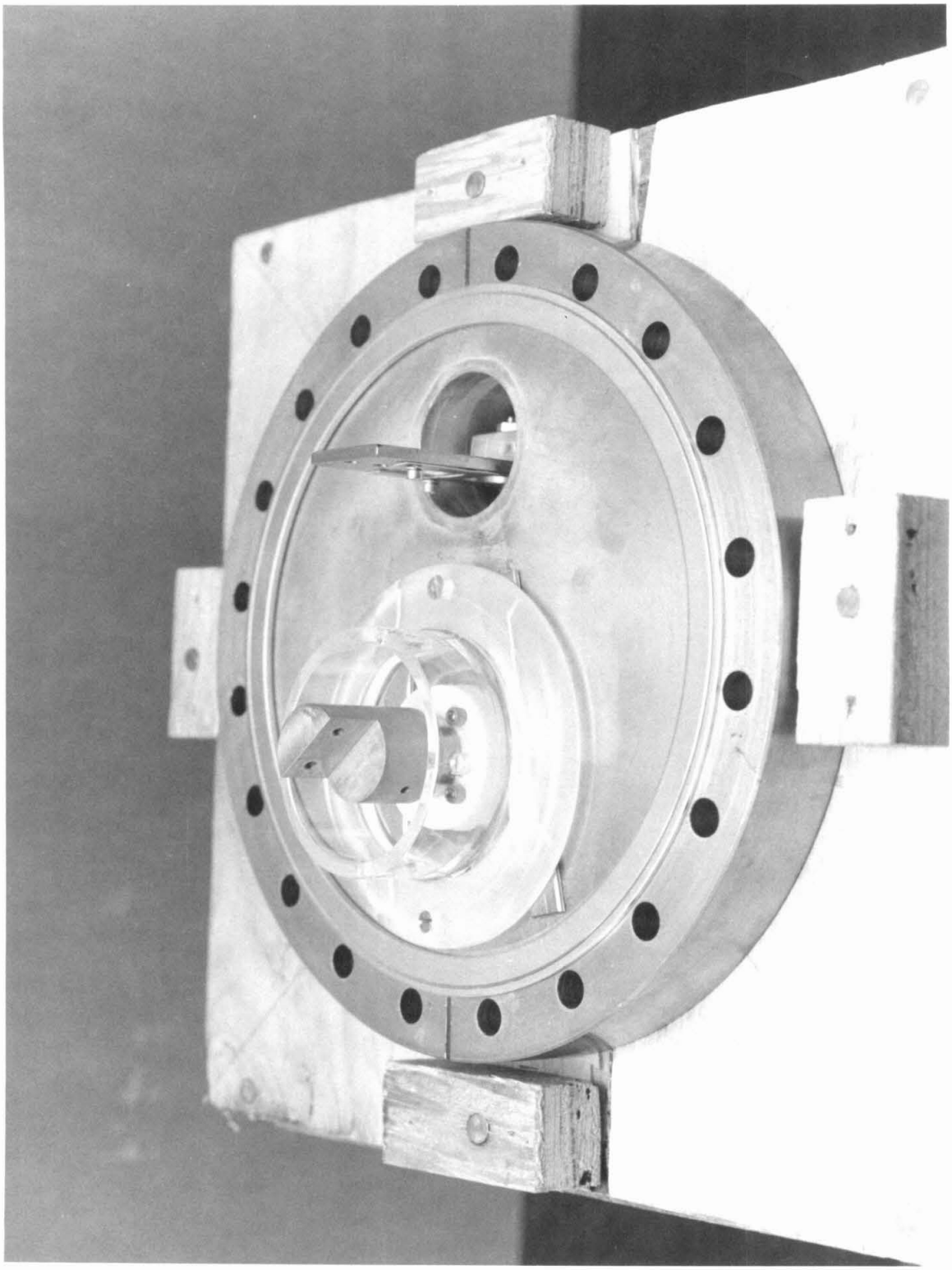

FIGURE 6

Target plate. (see p.11)

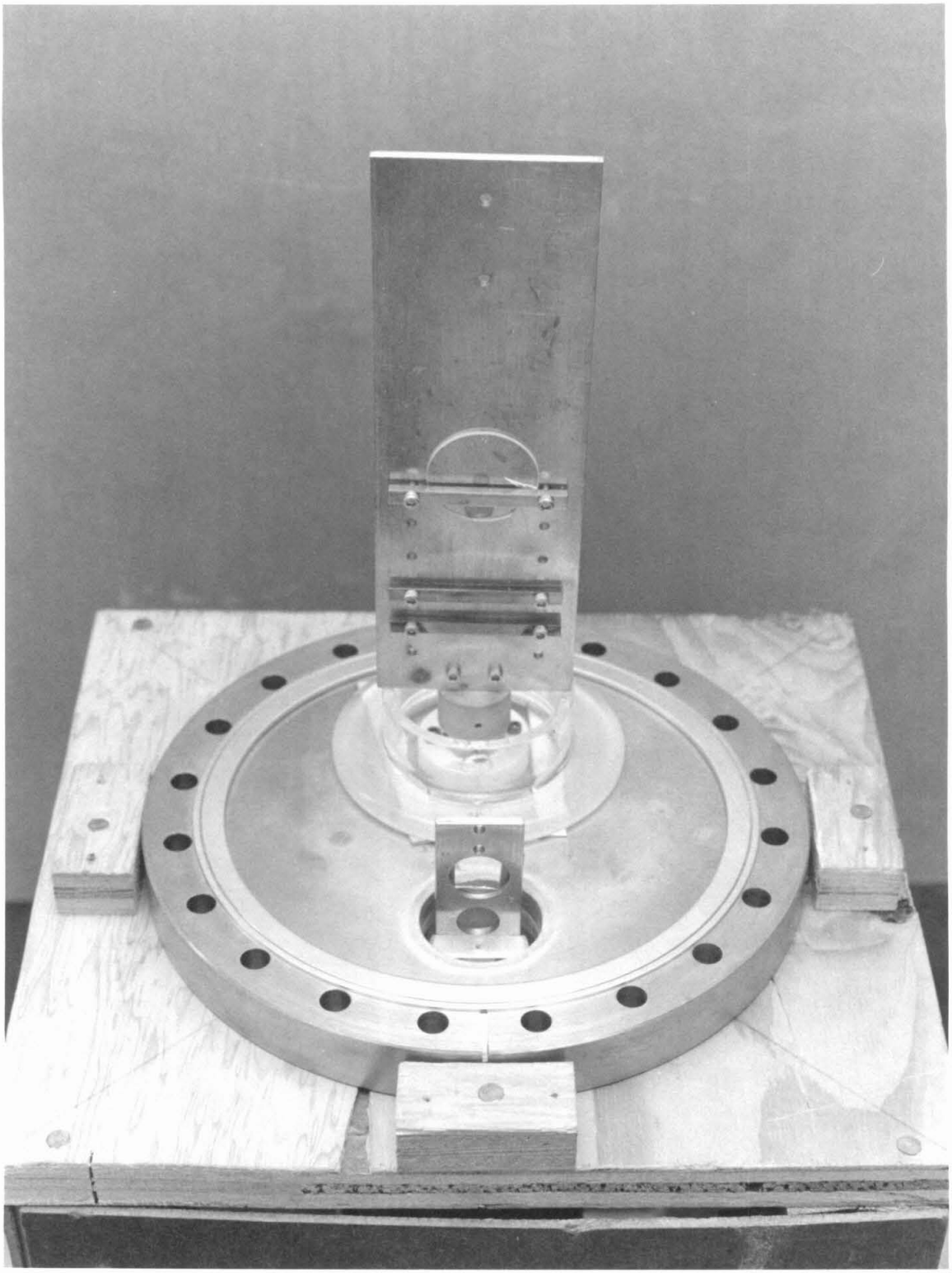

FIGURE 7

Collimation cylinder added to assembly. (see p.12)

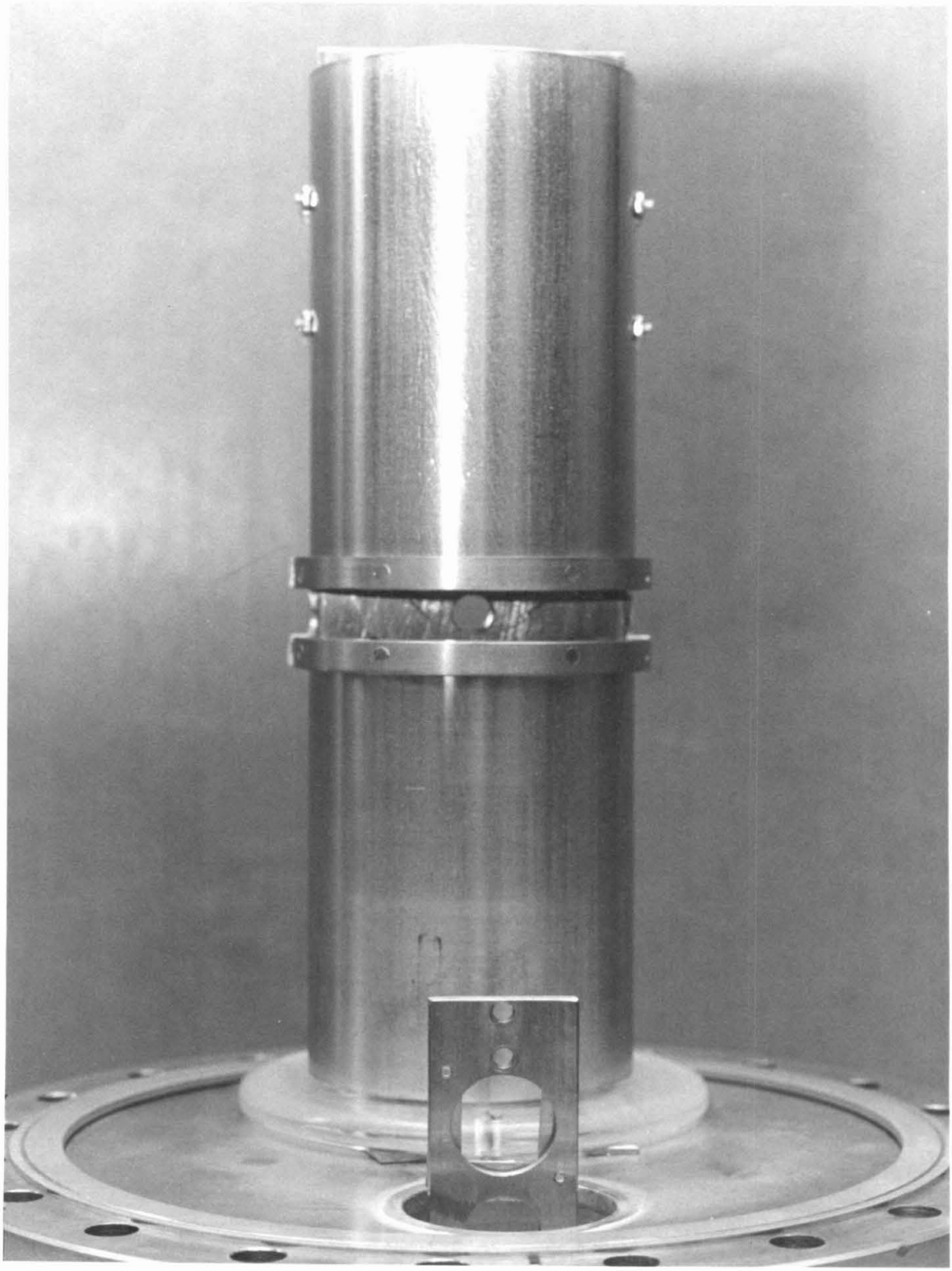

FIGURE 8

Complete sputtering assembly. (see p.12)

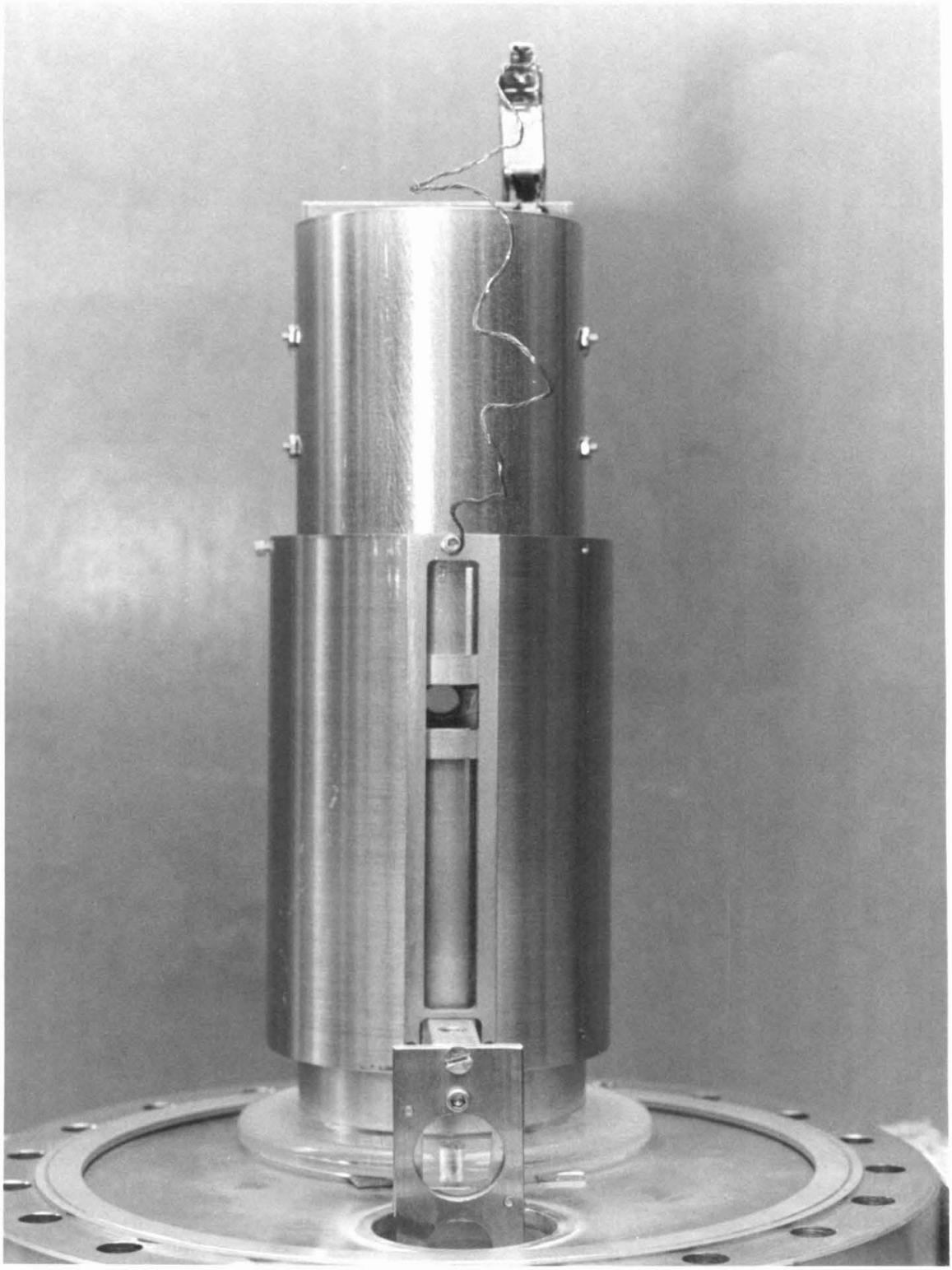

FIGURE 9

The ultra-high vacuum system. (see p.12) Essential components are sketched in Fig. 10. The entire assembly may be adjusted vertically and horizontally for purposes of alignment to ion beam.

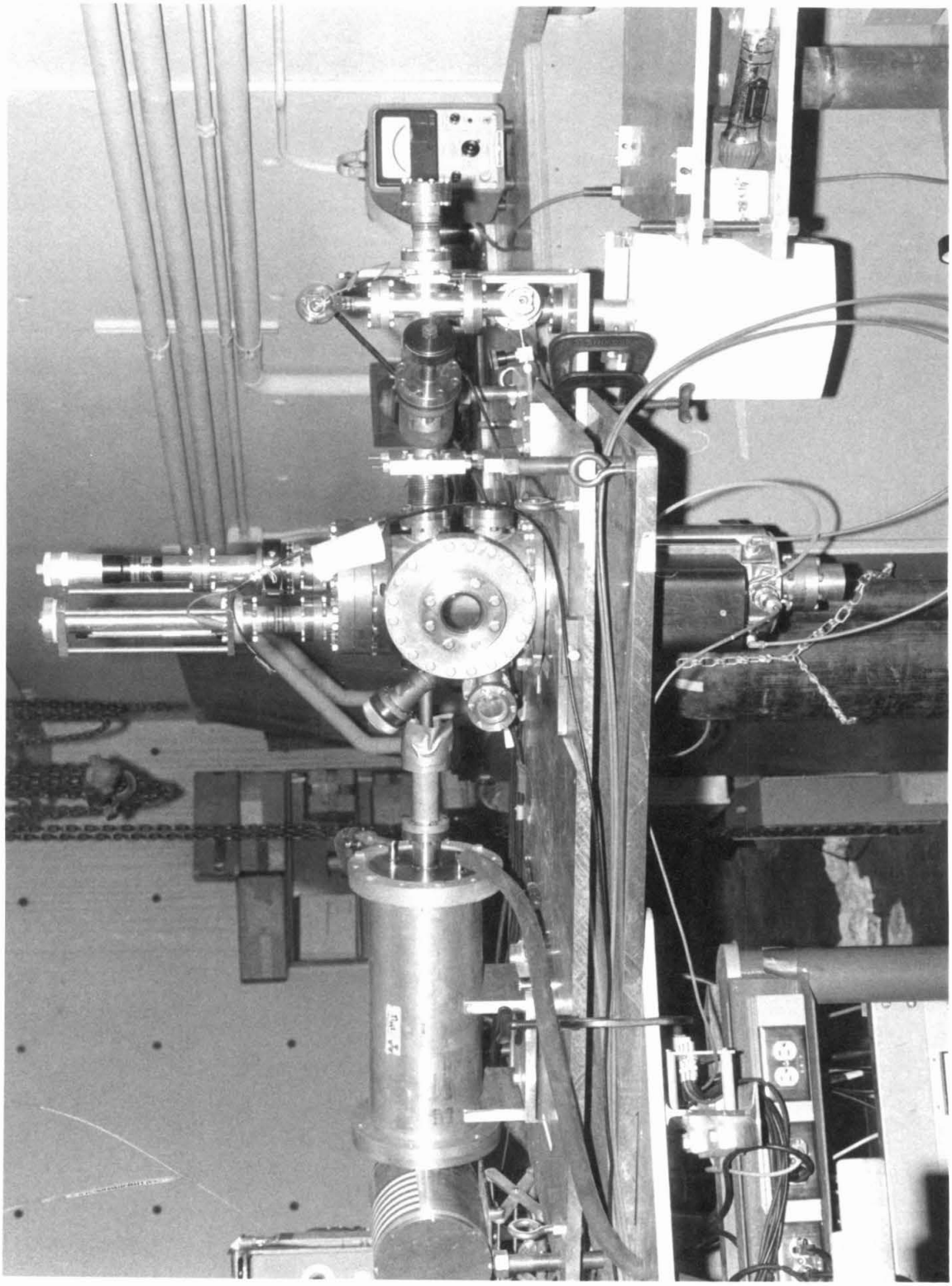

FIGURE 10

Sketch of UHV system pictured in Fig. 9.

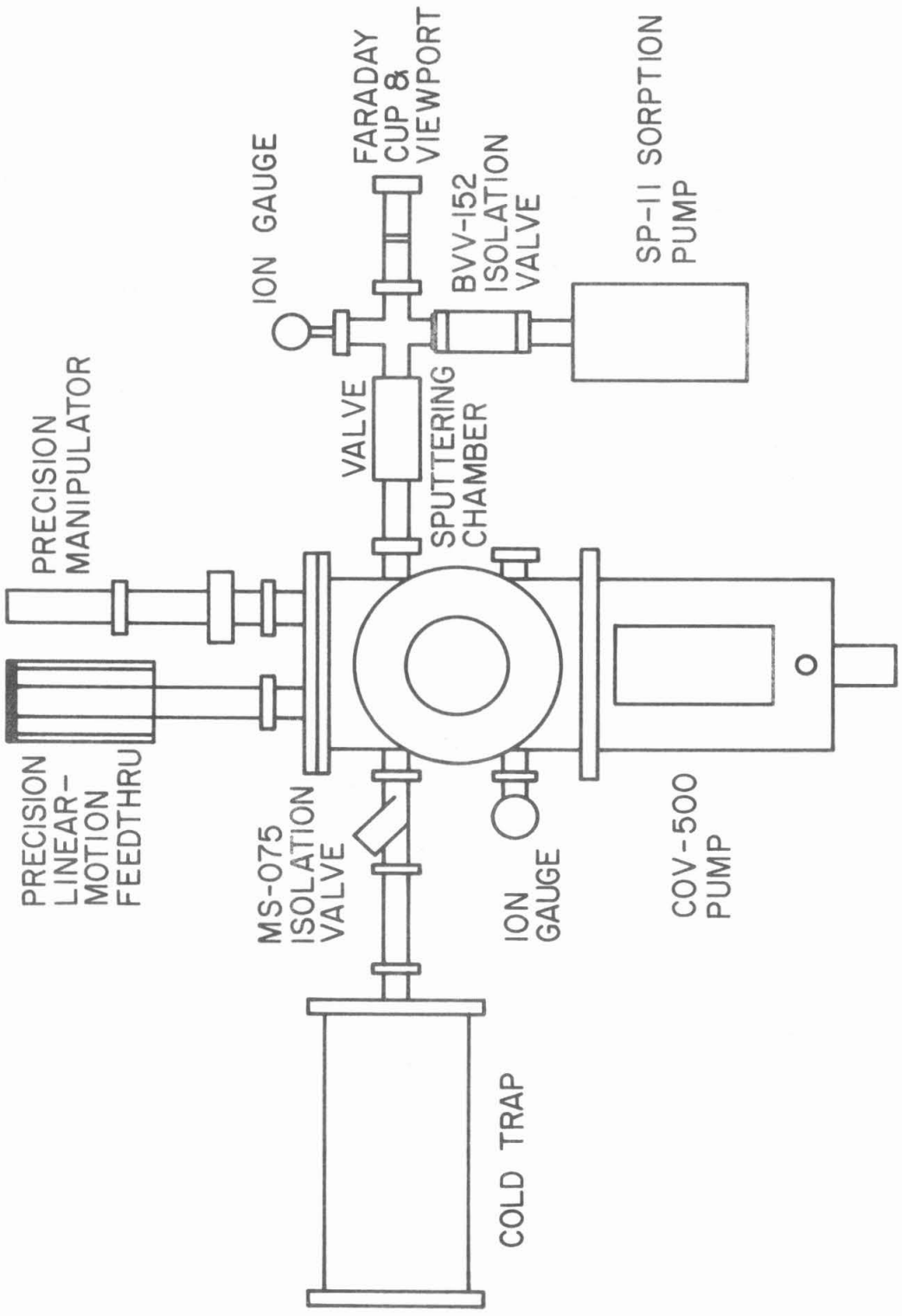
ION GAUGE
FARADAY CUP & VIEWPORT
BVV-152 ISOLATION VALVE
SP-11 SORPTION PUMP
PRECISION MANIPULATOR
VALVE
SPUTTERING CHAMBER
PRECISION LINEAR-MOTION FEEDTHRU
MS-075 ISOLATION VALVE
ION GAUGE
COV-500 PUMP
COLD TRAP

FIGURE 11

The ion source and beam line. (see p.15) Essential components are sketched inFig. 12. The ultra-high vacuum system is just out of the photo at right.

FIGURE 12

Plan view of complete beam line pictured inFigs. 9 & 11. Not drawn to scale.

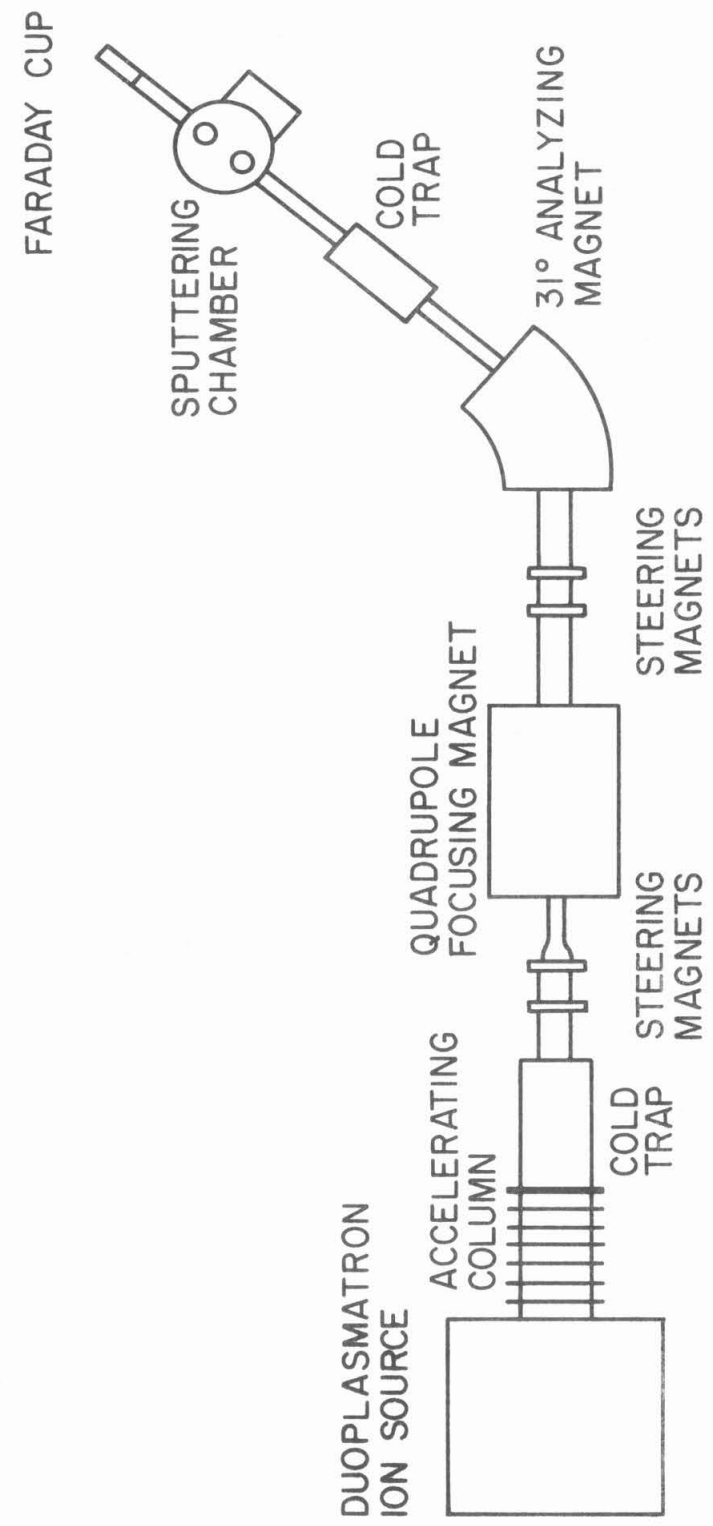
FARADAY CUP
SPUTTERING CHAMBER
COLD TRAP
31° ANALYZING MAGNET
STEERING MAGNETS
QUADRUPOLE FOCUSING MAGNET
STEERING MAGNETS
COLD TRAP
ACCELERATING COLUMN
DUOPLASMATRON ION SOURCE

FIGURE 13

Fission-fragment tracks in mica after 15 minutes etch in 48% HF (see p.26). The photo was made in transmitted light at a magnification of about 450X and enlarged by a factor of two. The fission star is fairly typical of the many observed in this experiment but is somewhat smaller than average (see Section IIID).

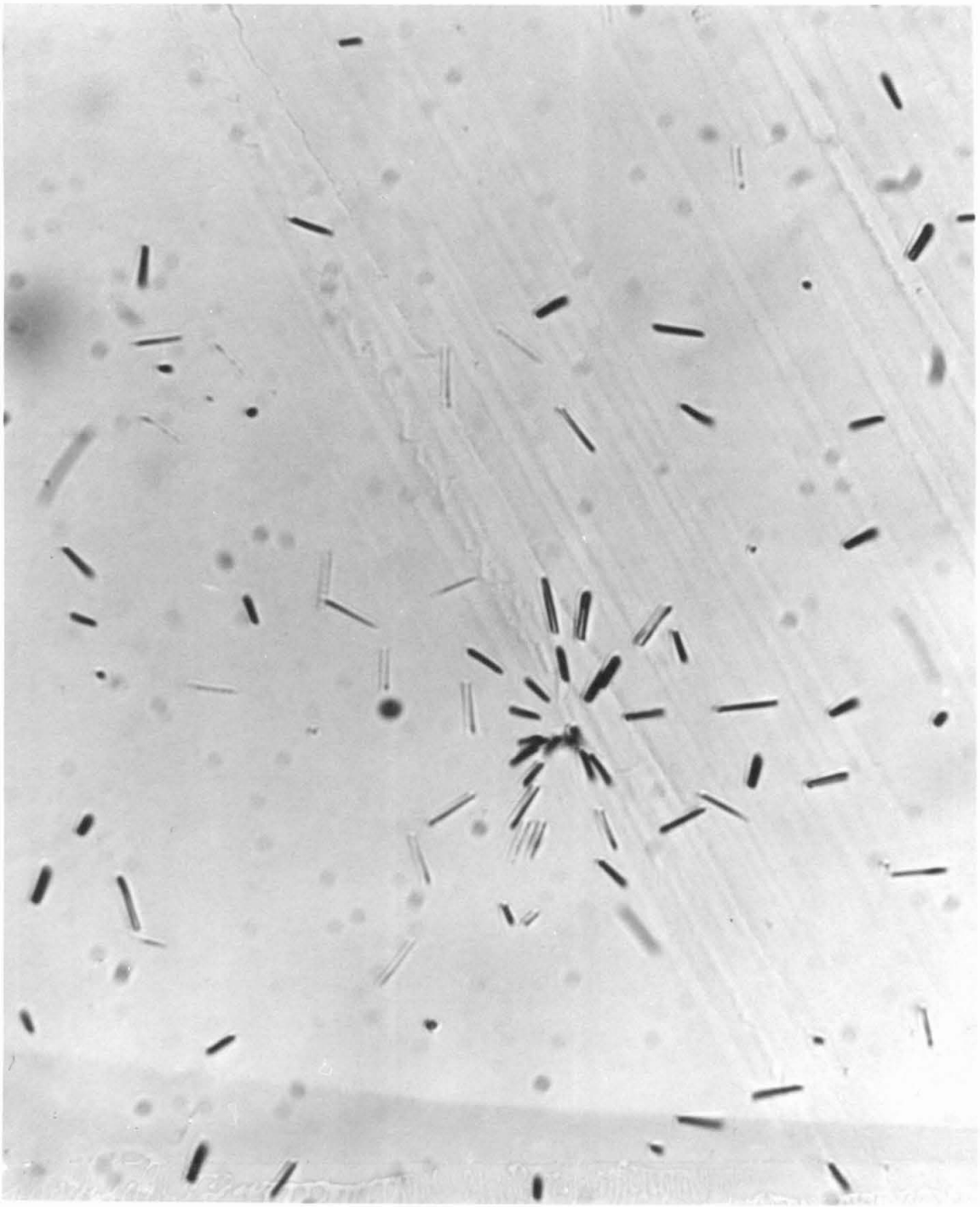

FIGURE 14

A larger-than-average fission star seen at 1000X. (see p.26 and Section IIID).

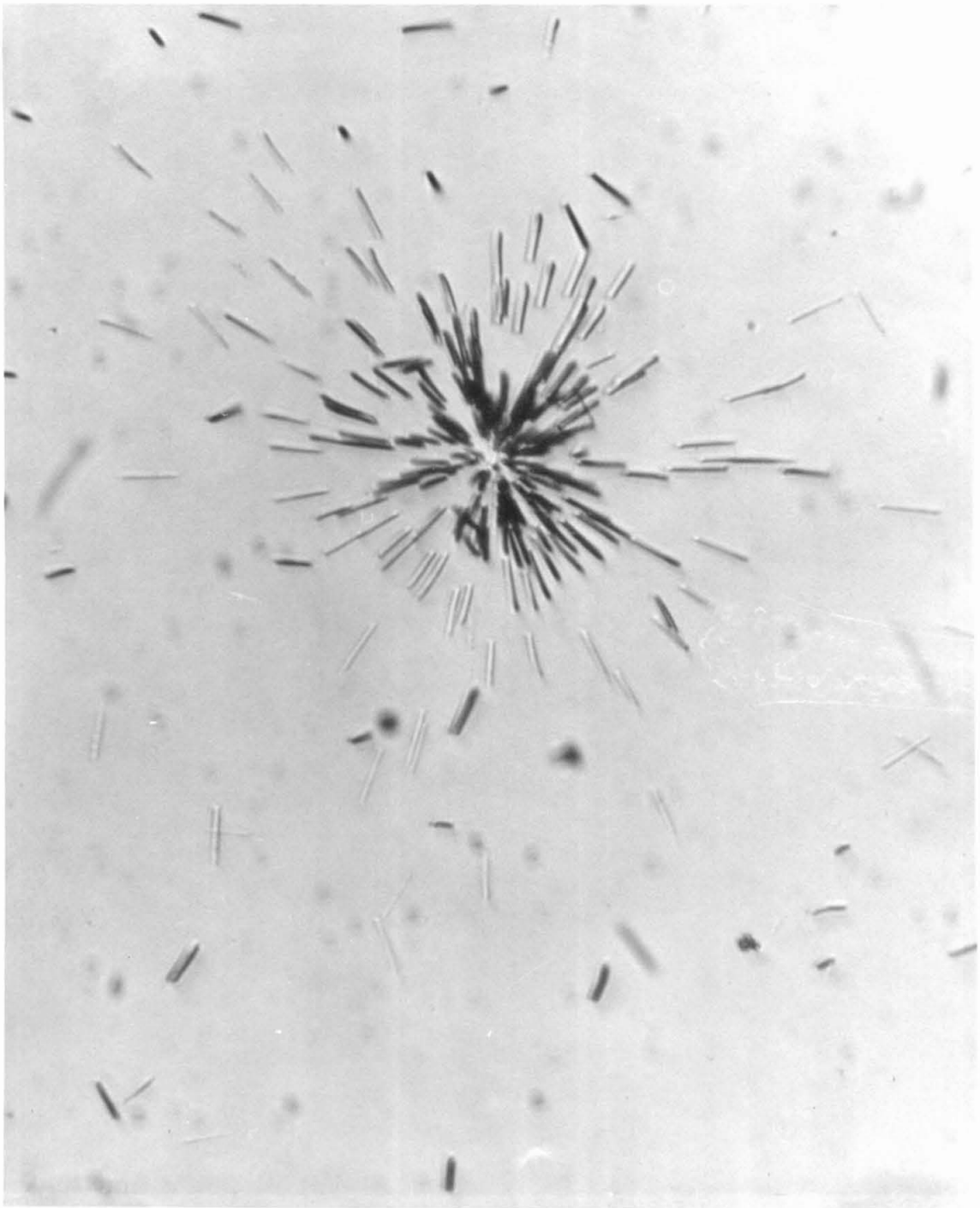

FIGURE 15

Scanning electron micrograph of uranium foil target at 240X.

(see p.28)

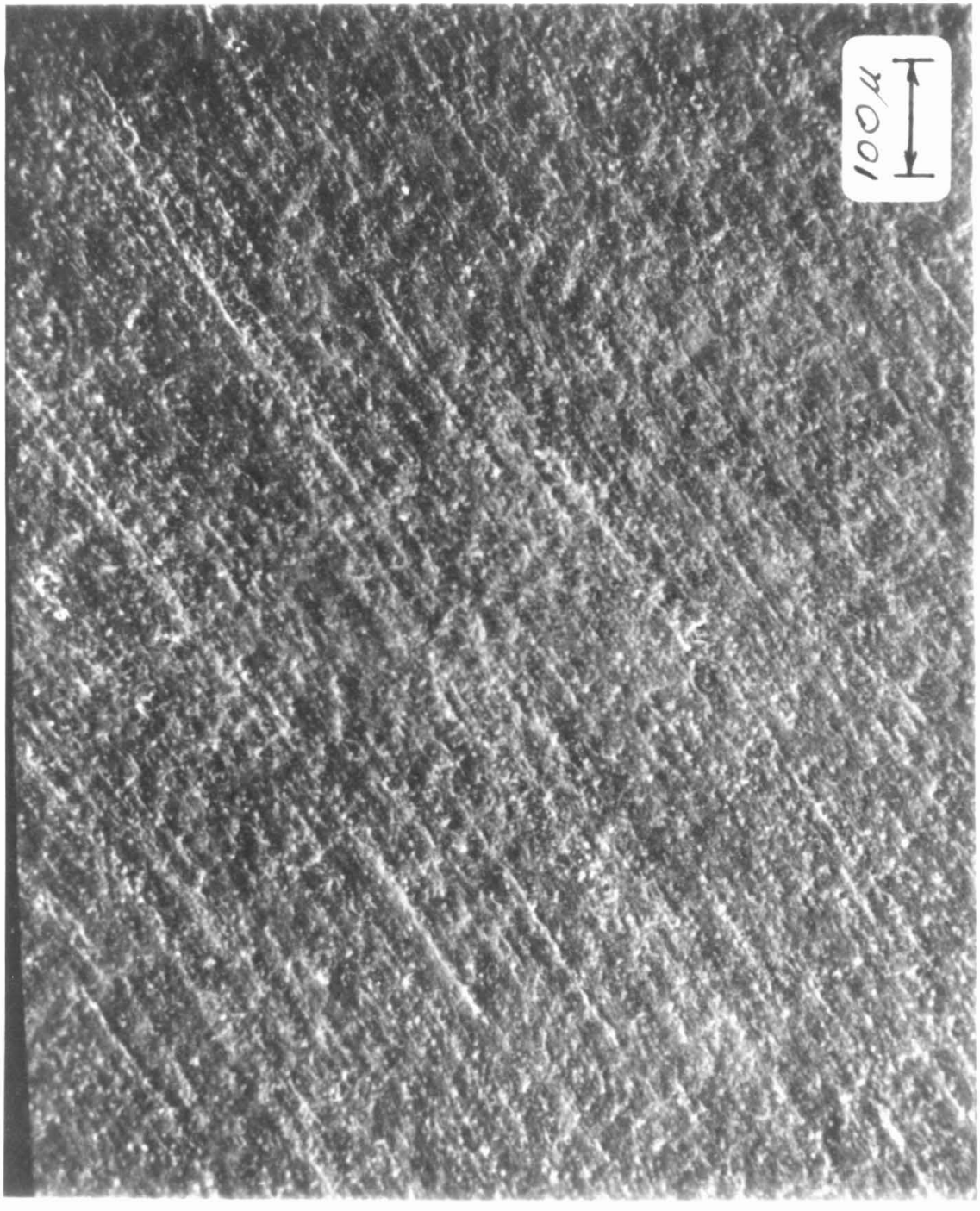
100μ

FIGURE 16

SEM of uranium target at 2400X. (see p.28) This area of target has not been sputtered, but was cleaned in HNO_3.

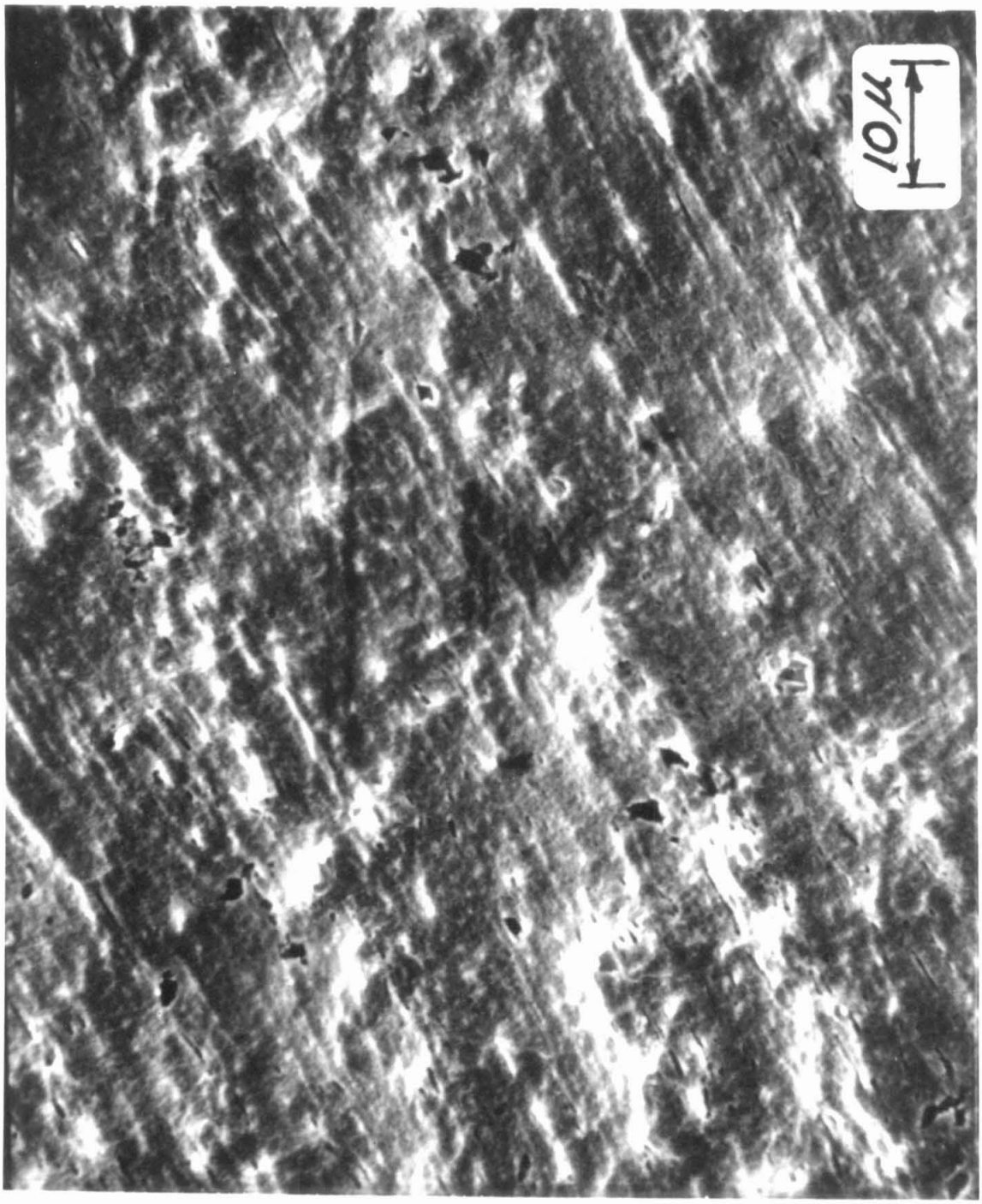
10μ

FIGURE 17

Same area as Fig. 16 at 8400X.

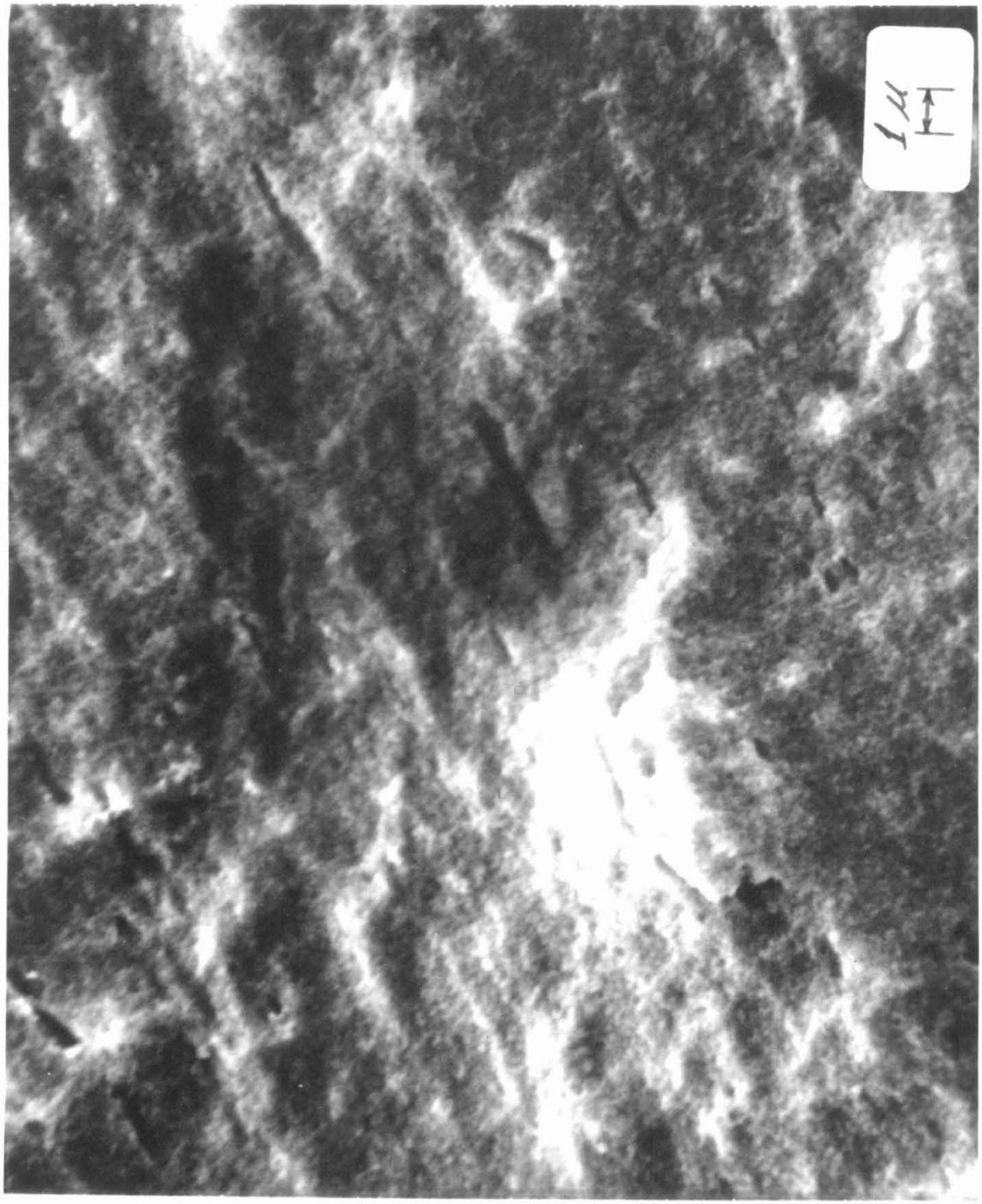
1μ

FIGURE 18

SEM at 8400X of uranium target which has been sputtered by 3×10^{17} 80 kev Ar^+ ions per cm^2. (see p.28)

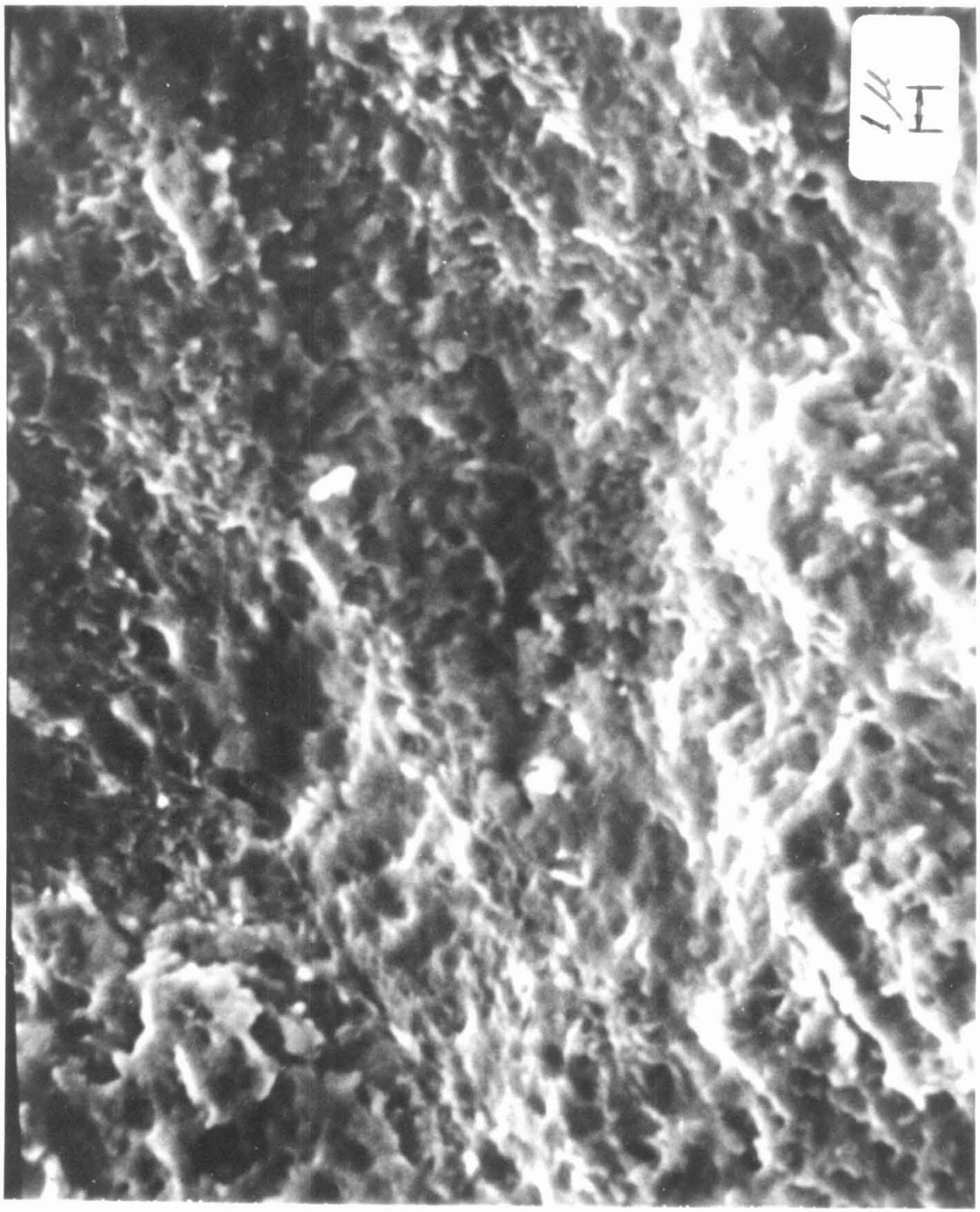
1μ

FIGURE 19

The same area as Fig. 18 at 2400X.

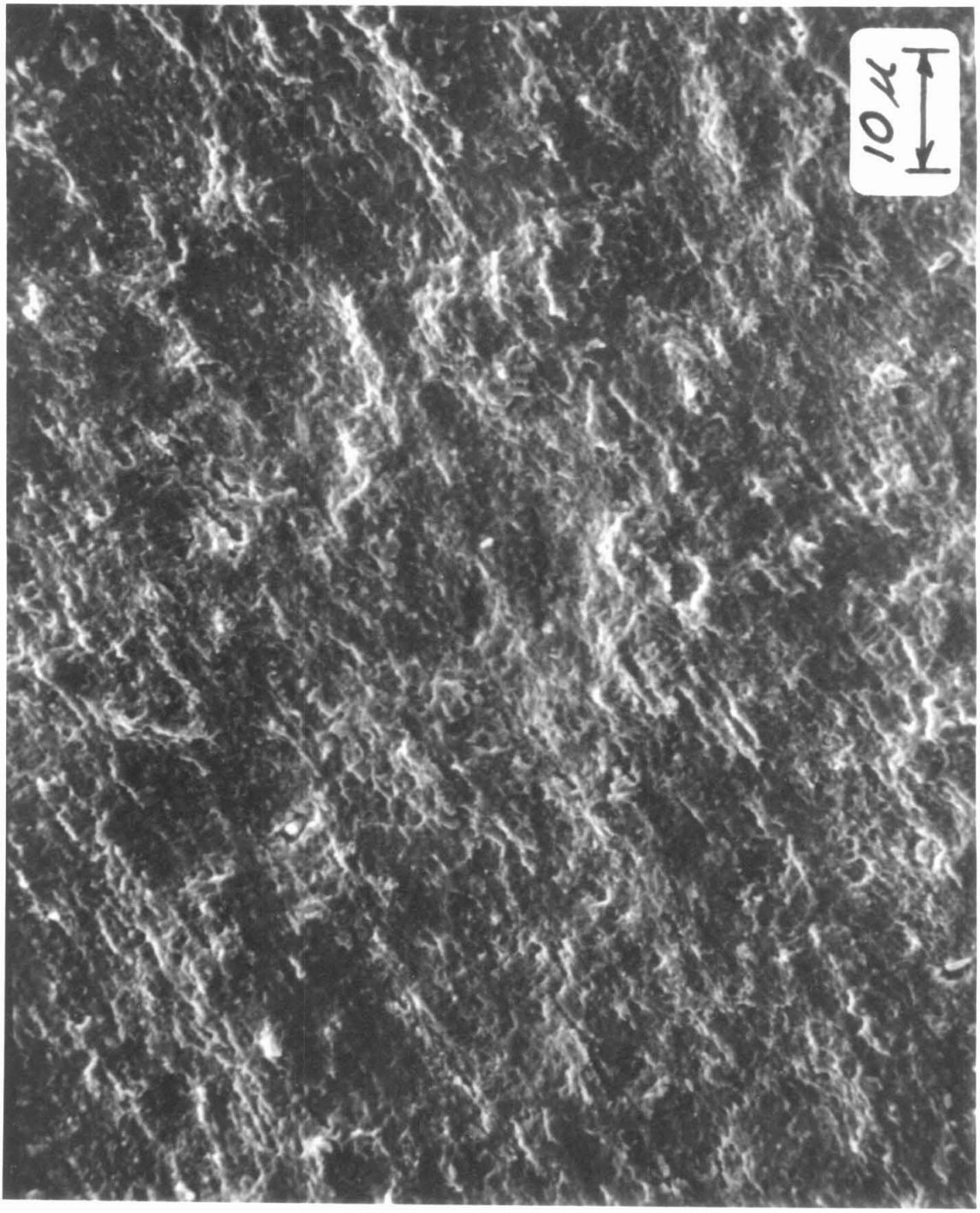
10μ

FIGURE 20

An area similar to the one in Fig. 19 at 2400X.

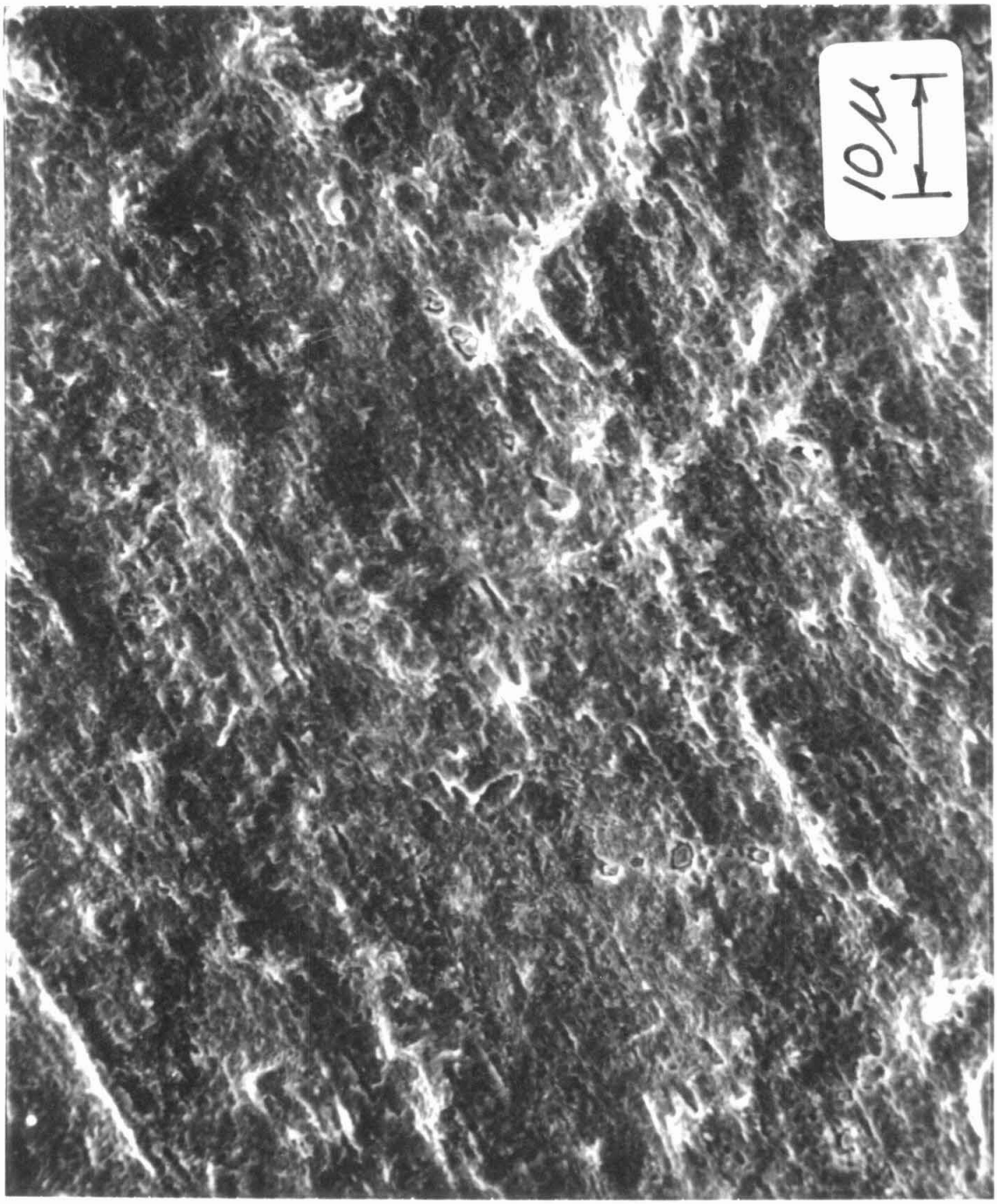
10μ

FIGURE 21

Another un-sputtered area of the target at 2400X. (see p.29)

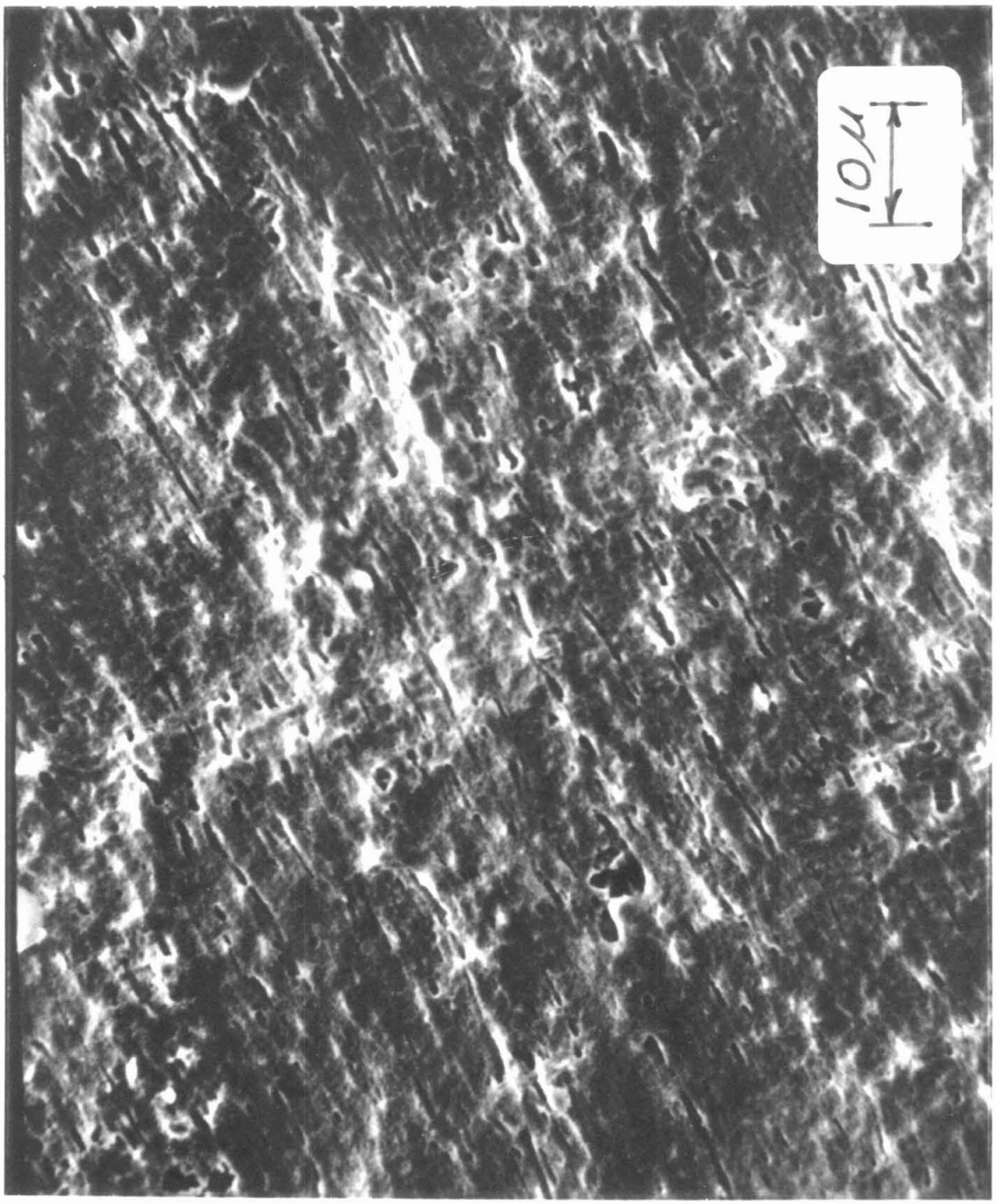
10μ

FIGURE 22

Scanning electron micrograph at 800X of uncleaned uranium target.

(see p. 29)

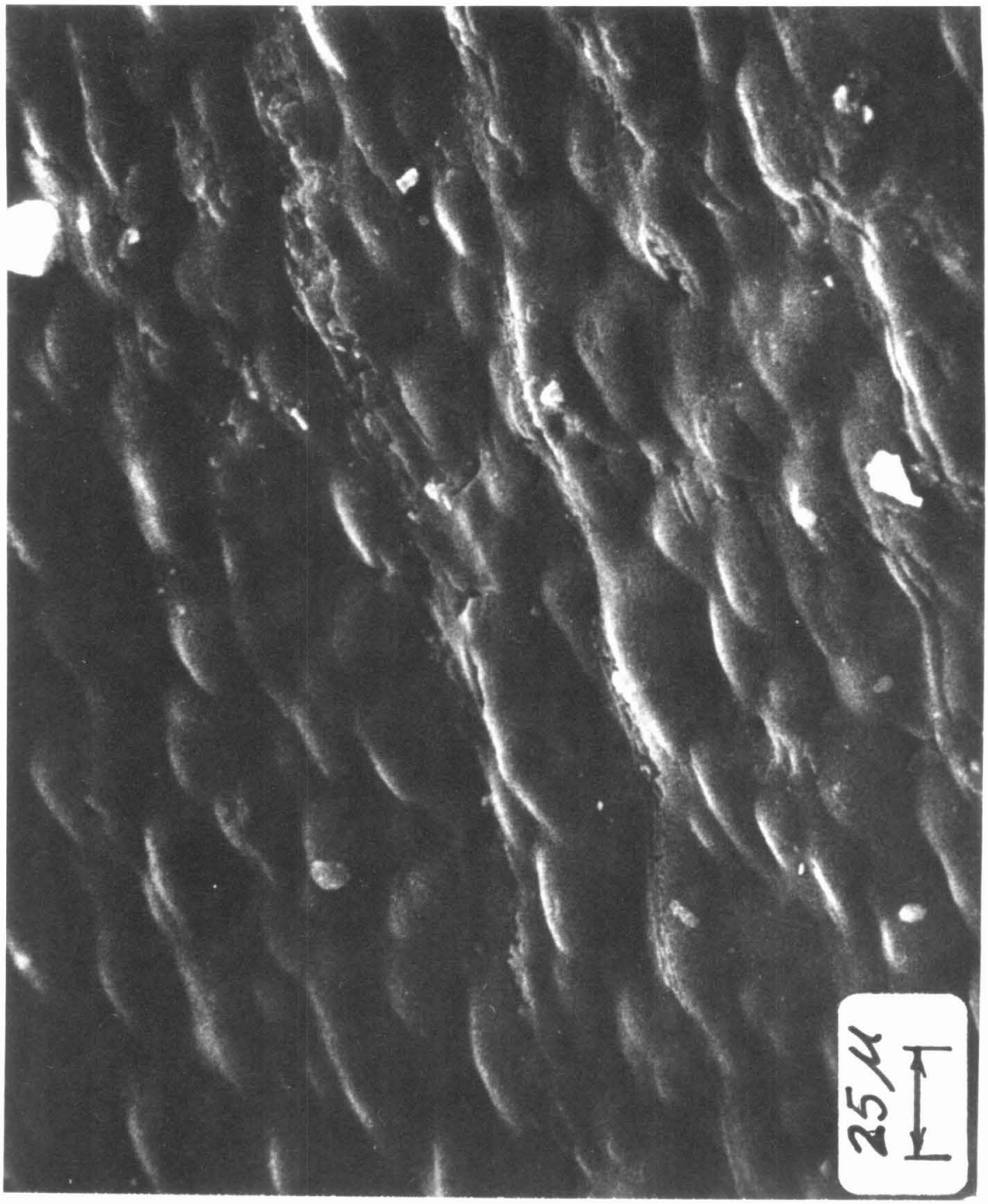
25μ

FIGURE 23

Angular distribution of ^{235}U atoms sputtered by 40 kev H_1^+ ions at perpendicular incidence to target. (see p.30)

N_t= actual number of tracks counted per 130μ x 148μ field of view in the microscope.

N_t^o= number of tracks per field of view extrapolated to $\theta = 0^o$.

θ= sputtering angle relative to incident beam direction.

Error bars indicate uncertainty due to counting statistics only. Angular distributions were found to be symmetric about the incident beam direction.

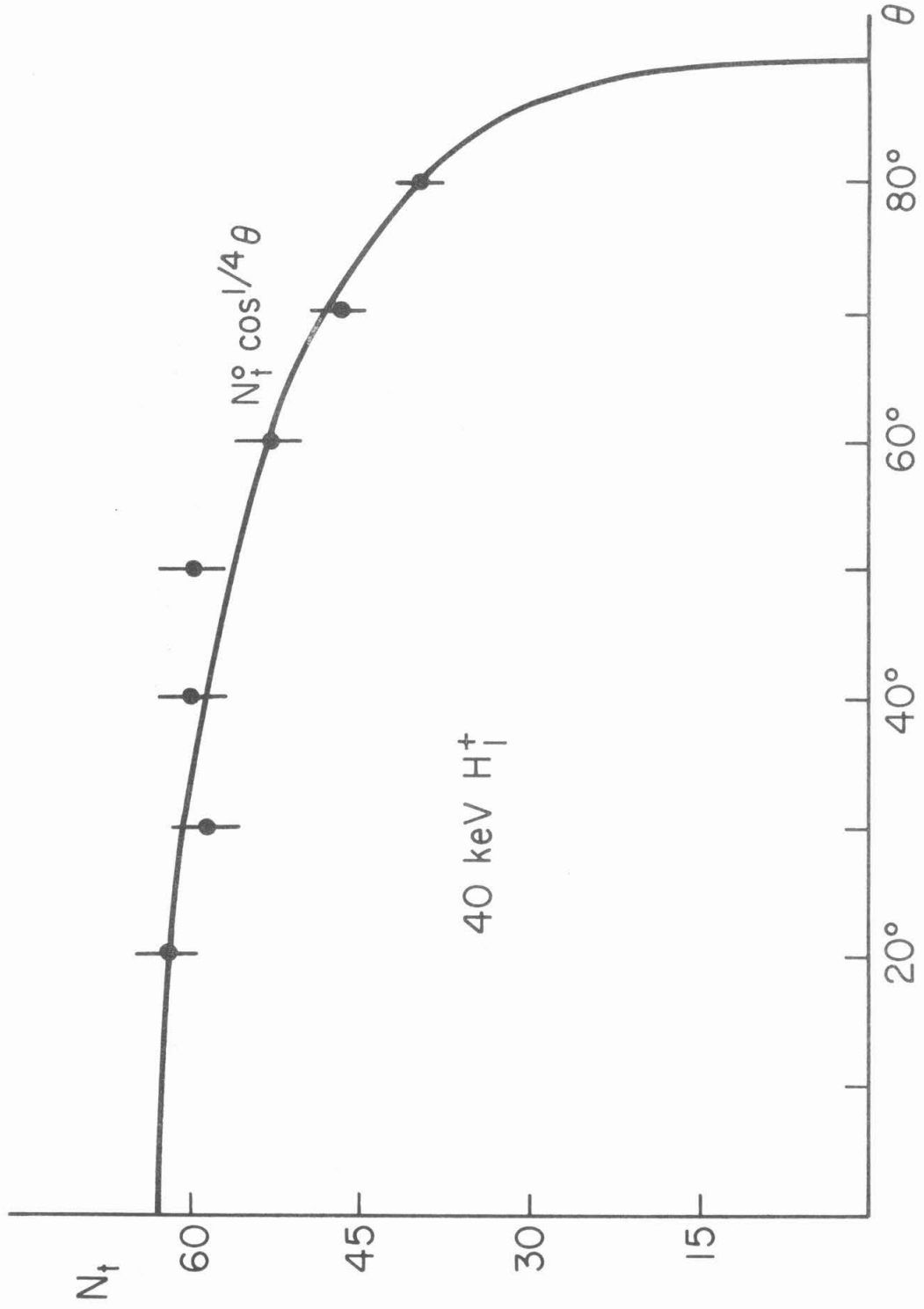
N_t
60
45
30
15
$N_t^\circ \cos^{1/4}\theta$
40 keV H_1^+
20°
40°
60°
80°
θ

FIGURE 24

Angular distribution of ^{235}U atoms sputtered by 50 kev H_1^+ (see p. 30) Other information as in Fig. 23.

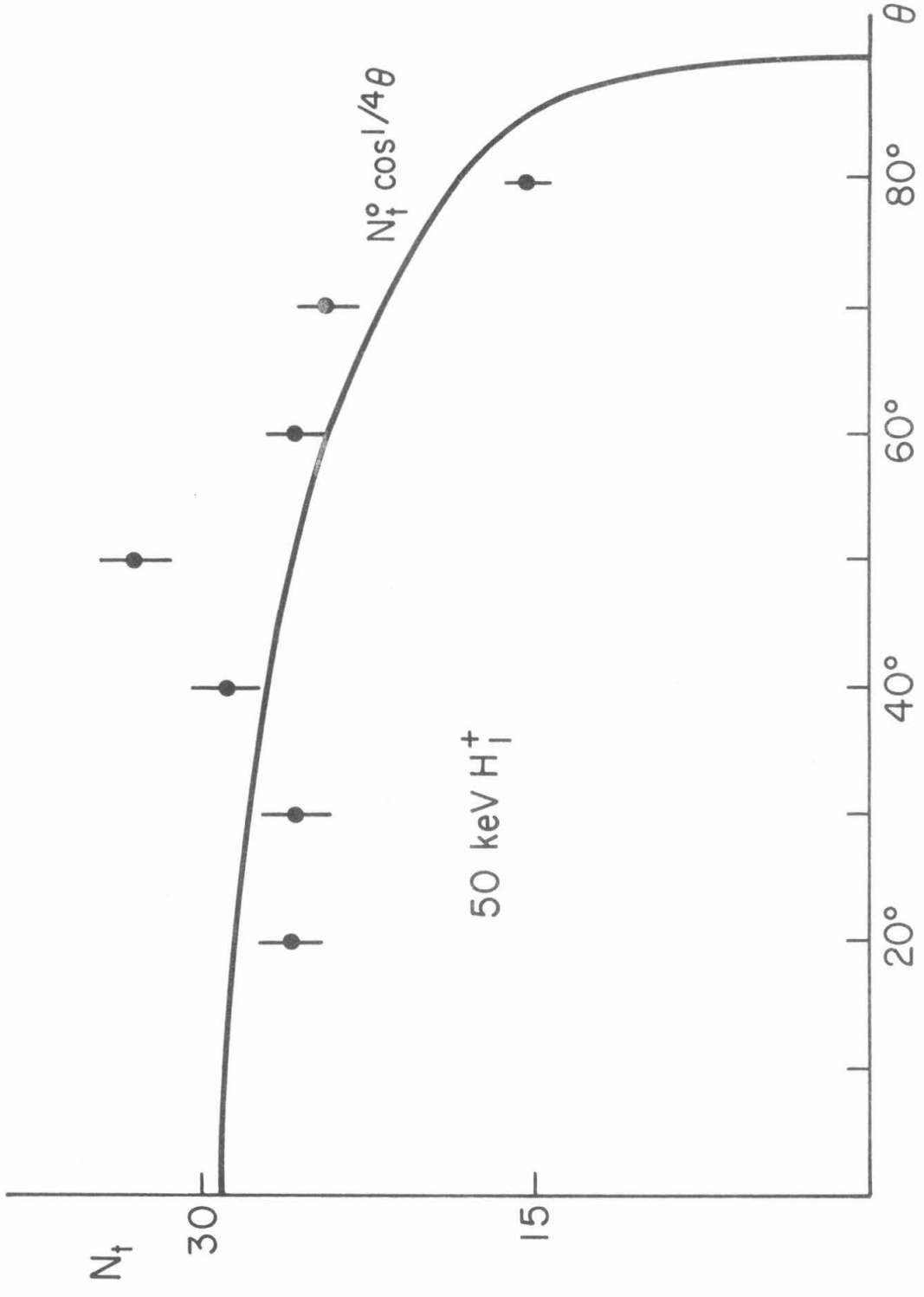
N_t
30
15
$N_t^\circ \cos^{1/4}\theta$
50 keV H_1^+
20°
40°
60°
80°
θ

FIGURE 25

Angular distribution of ^{235}U atoms sputtered by 40 keV H_2^+. (see p.30)

Other information as in Fig.23.

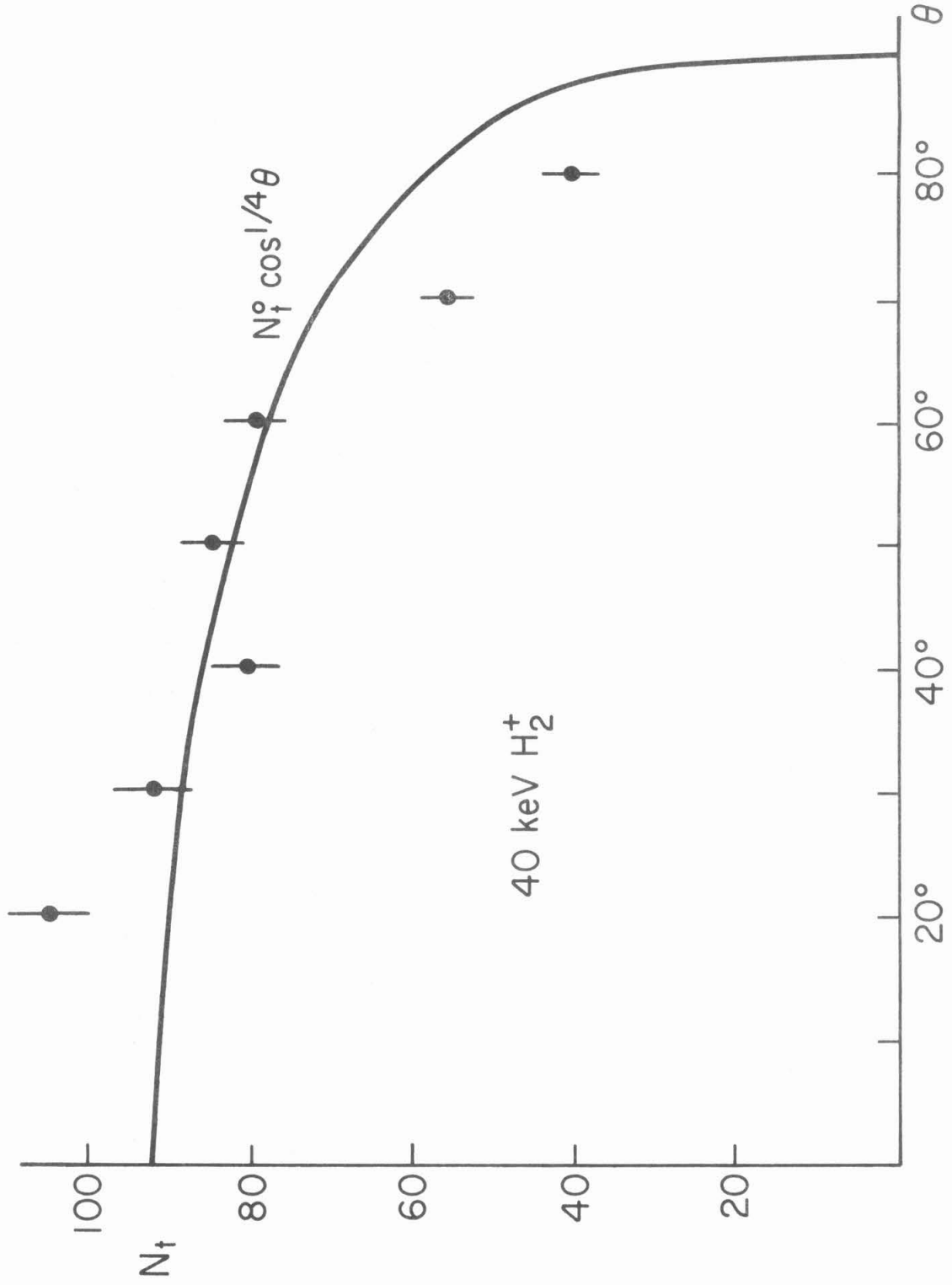
N_t
100
80
60
40
20
20°
40°
60°
80°
θ
$N_t^\circ \cos^{1/4}\theta$
40 keV H_2^+

FIGURE 26

Angular distribution of ^{235}U atoms sputtered by 120 keV He^+.
(see p. 30) Other information as in Fig. 23.

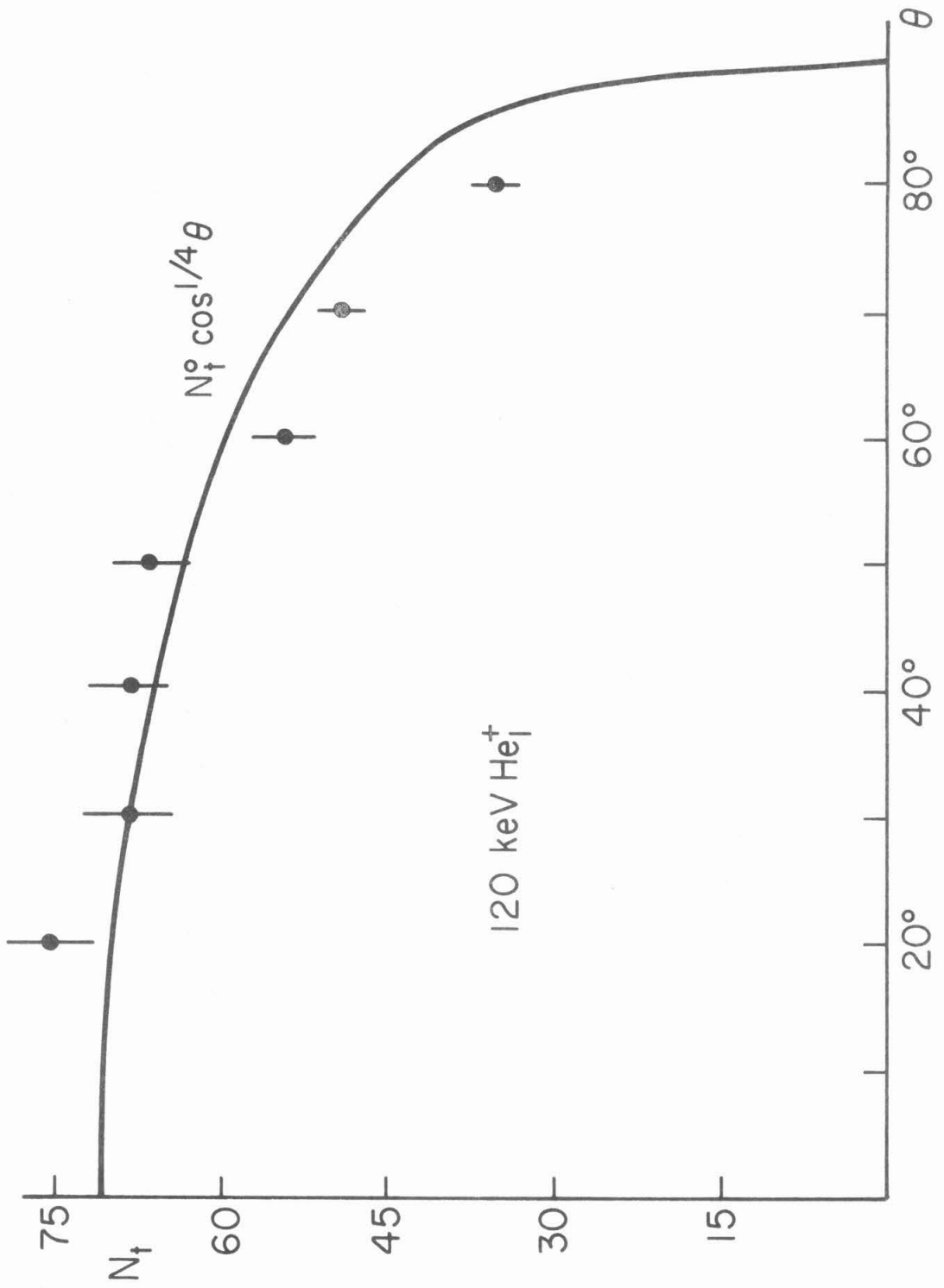
75
60
45
30
15
$N_\uparrow$
$N_\uparrow^\circ \cos^{1/4}\theta$
120 keV He_I^+
20°
40°
60°
80°
θ

FIGURE 27

Sputtering yields S (in units of 10^{-2}) of ^{235}U under bombardment by protons with energies from 13 to 120 keV. (see Section IIIC and Tables 3&4). Yields in upper two sets of points were from targets that had been sputter-cleaned with an argon beam. (see p.17)

Errors are discussed in Section IIIE.

The curve is S(E) calculated from the Sigmund theory (see Sections IVA and IVB), but multiplied by 10^{-2}.

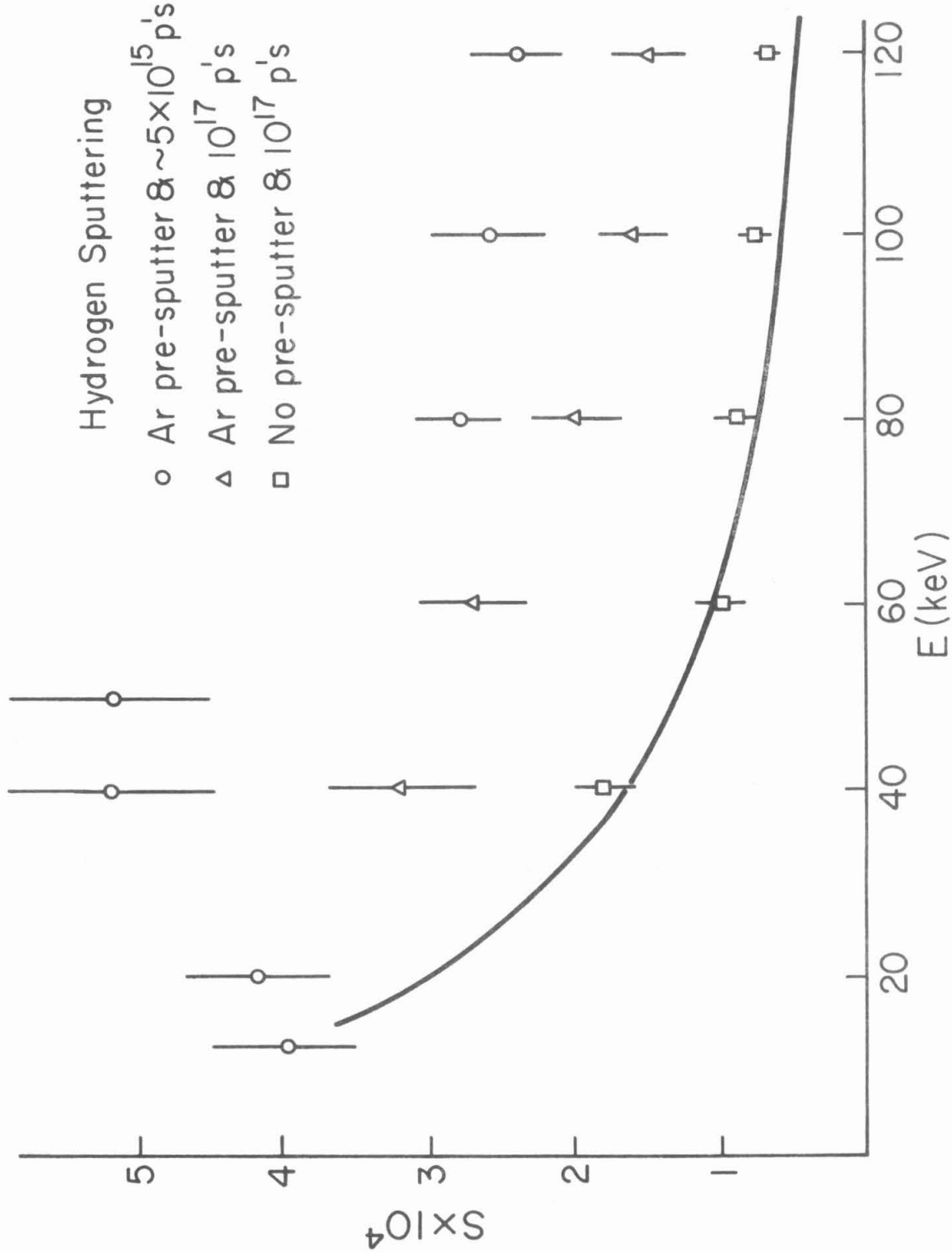
Hydrogen Sputtering
○ Ar pre-sputter & ~5×10^15 p's
△ Ar pre-sputter & 10^17 p's
□ No pre-sputter & 10^17 p's
S×10^4
5
4
3
2
1
20
40
60
80
100
120
E (keV)

FIGURE 28

Sputtering yields S of ^{235}U atoms emitted per incident proton under bombardment by H_1^+, H_2^+ and H_3^+ (see Section IIIC). Energies are per proton. Targets had been sputter-cleaned in all cases except for the 60 keV H_1^+ data point, which was obtained by scaling up 60 keV point from middle data set to upper set in Fig. 27.

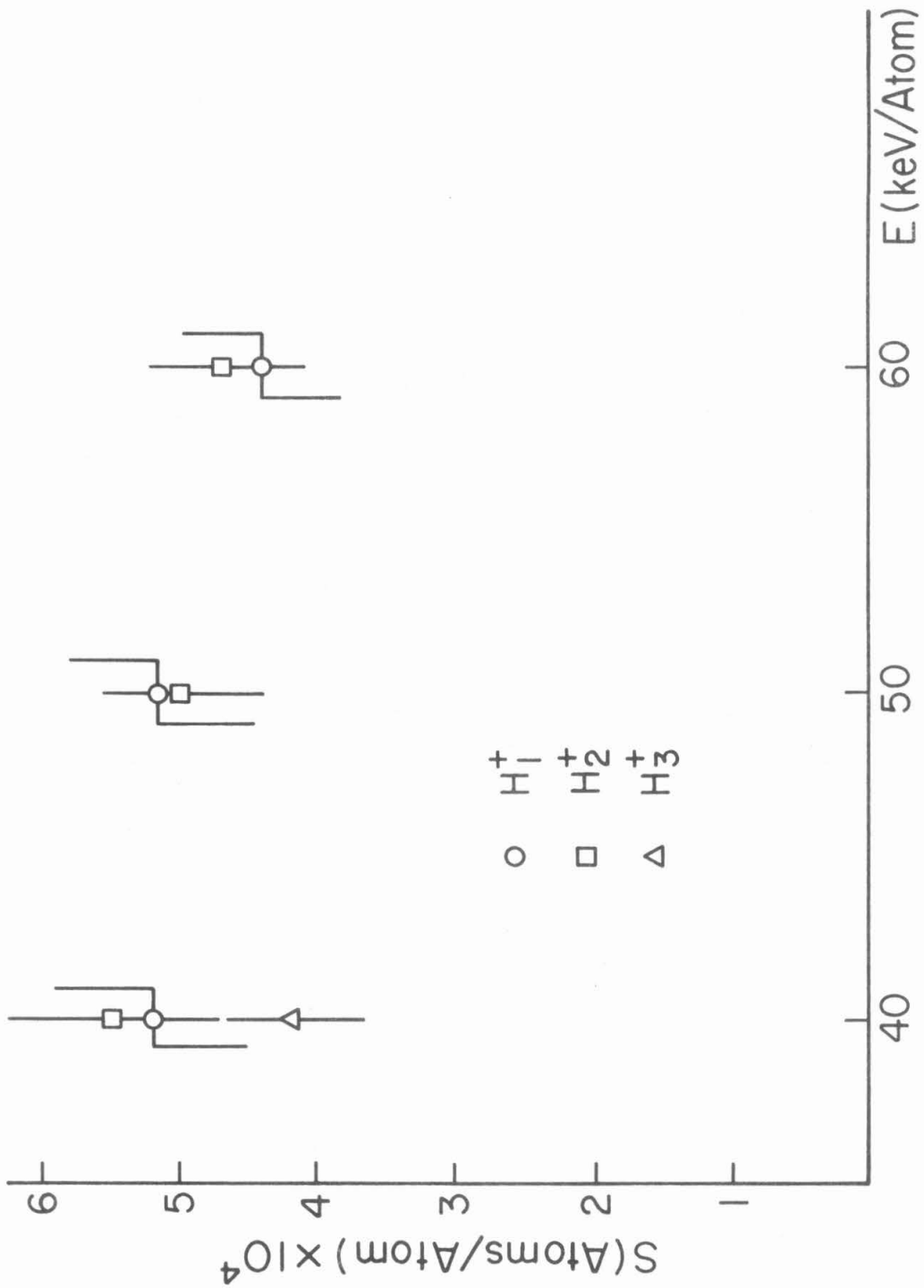
S(Atoms/Atom) x10⁴
6
5
4
3
2
1
40
50
60
E(keV/Atom)
H1+
H2+
H3+

FIGURE 29

Sputtering yields S of ^{235}U under bombardment by 20 - 120 keV He^{+}.

(see p. 33)

Curve is S(E) as calculated from Sigmund theory (see Sections IVA and IVB), but multiplied by 10^{-1}.

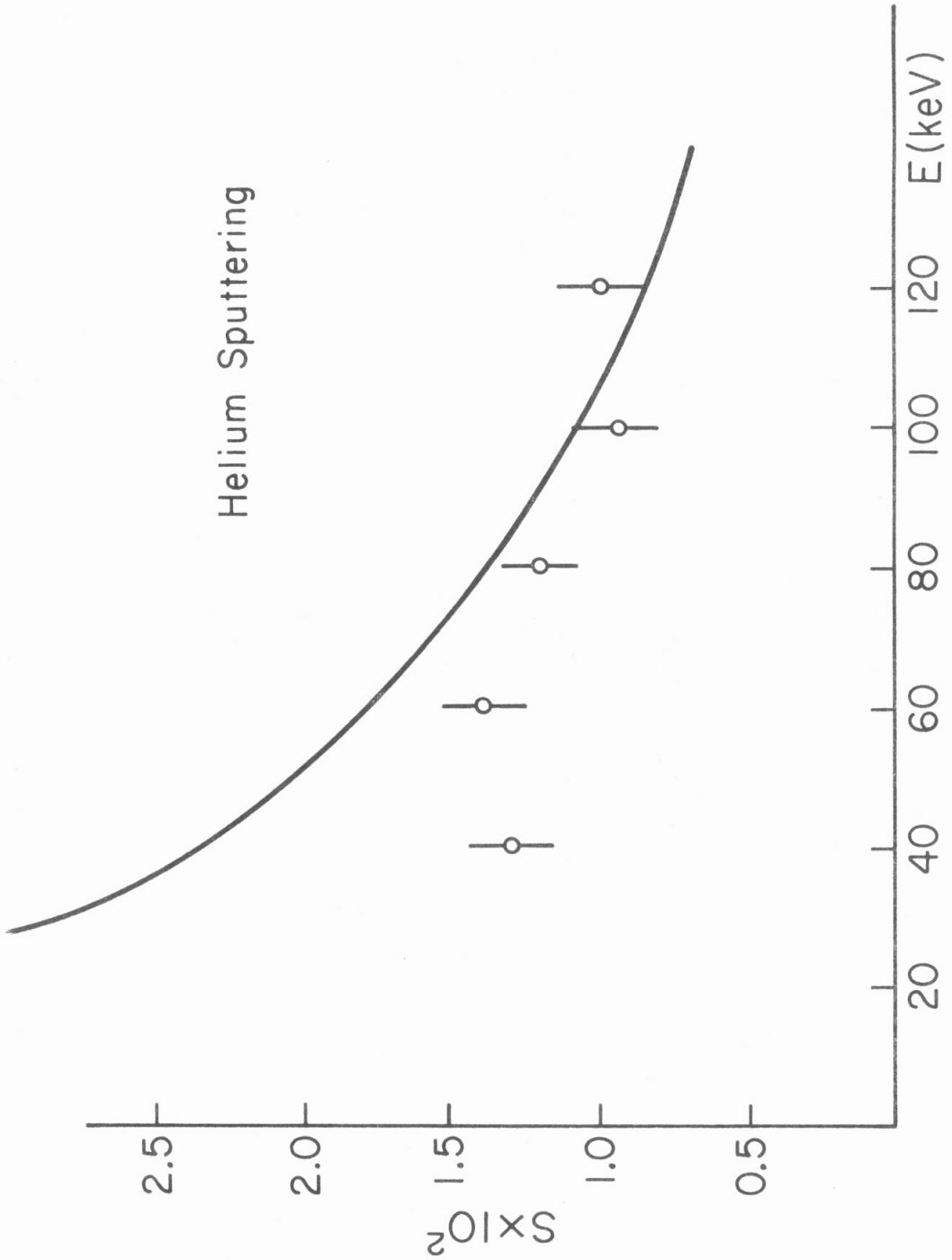
Helium Sputtering
S x 10²
2.5
2.0
1.5
1.0
0.5
20
40
60
80
100
120
E(keV)

FIGURE 30

Size distribution of 612 chunks emitted during proton sputtering of pre-sputtered uranium targets. Data was accumulated during five sputtering runs with H_1^+ ion energies of 40-120 keV. (see Table 5 and p.34) The bars at the right show the number of chunks containing 10^8-$2x10^8$ ^{235}U and > 2×10^8 ^{235}U atoms.

The two curves are visual fits to the histogram; a= 2.5×10^4 cm^{-2} & b= 10^3 cm^{-2}.

n is the actual number of tracks produced in mica by a given chunk due to neutron irradiation.

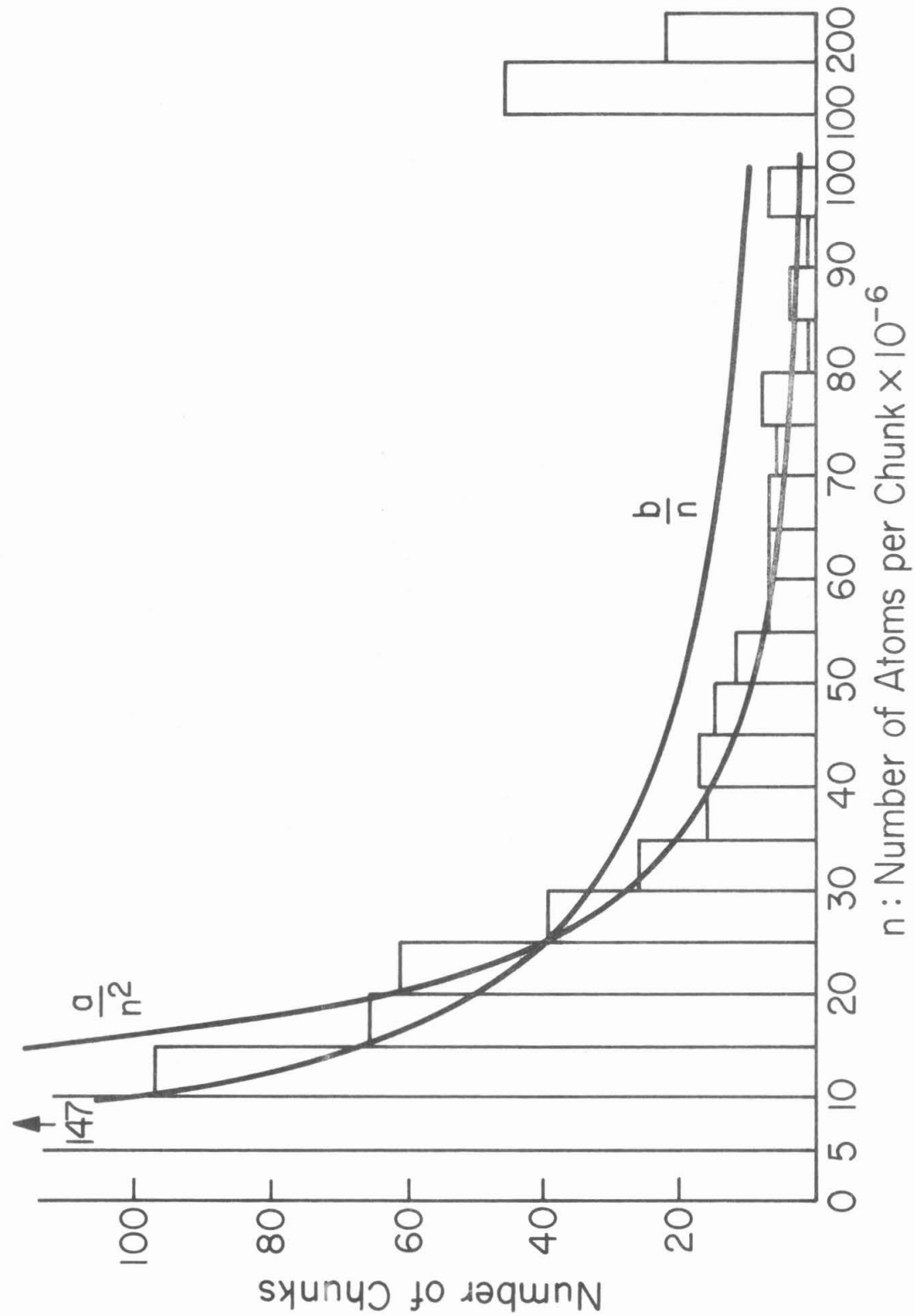
Number of Chunks
100
80
60
40
20
0 5 10 20 30 40 50 60 70 80 90 100 100 200
n : Number of Atoms per Chunk × 10⁻⁶
147
a/n²
b/n

FIGURE 31

The same data as Fig. 30 on an expanded scale. The curve is a visual fit to the data; $N_o = 180$ and $\lambda = 0.05$. (see Sections IIIE and IVC)

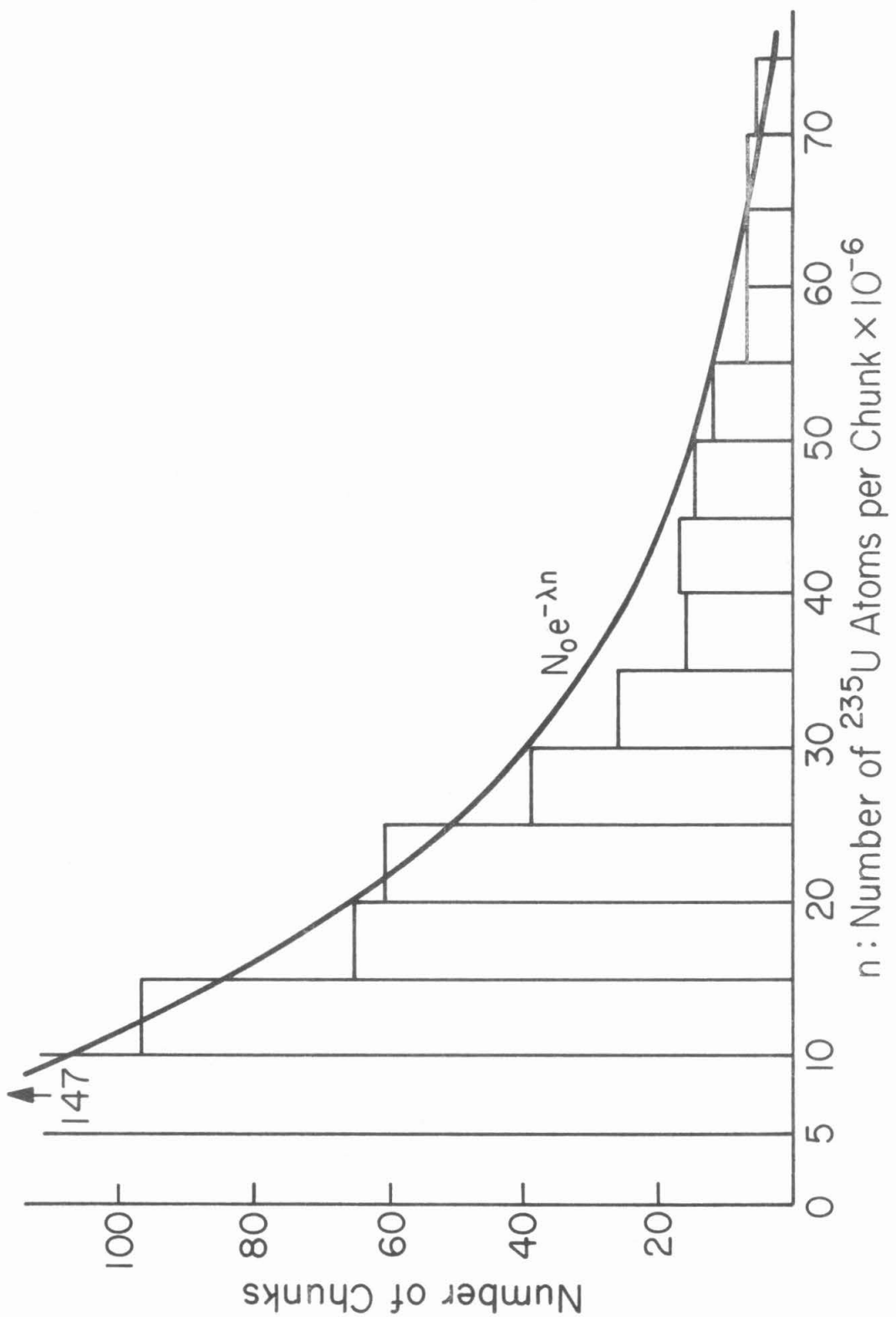
Number of Chunks
100
80
60
40
20
0
5
10
20
30
40
50
60
70
147
$N_0e^{-\lambda n}$
n : Number of ^{235}U Atoms per Chunk $\times 10^{-6}$

FIGURE 32

Size distribution of 359 chunks emitted during 80 keV Ar^+ sputtering of a pre-sputtered uranium target. (see Table 5 and p. 35)

The bars at the right show the number of chunks containing 10^8 - 2 x 10^8 ^{235}U atoms and > 2 x 10^8 ^{235}U atoms.

The curve is a visual fit to the histogram; N_o= 60 and λ= 0.03. (See Section IVC)

n is the actual number of tracks produced in mica by a given chunk due to neutron irradiation.

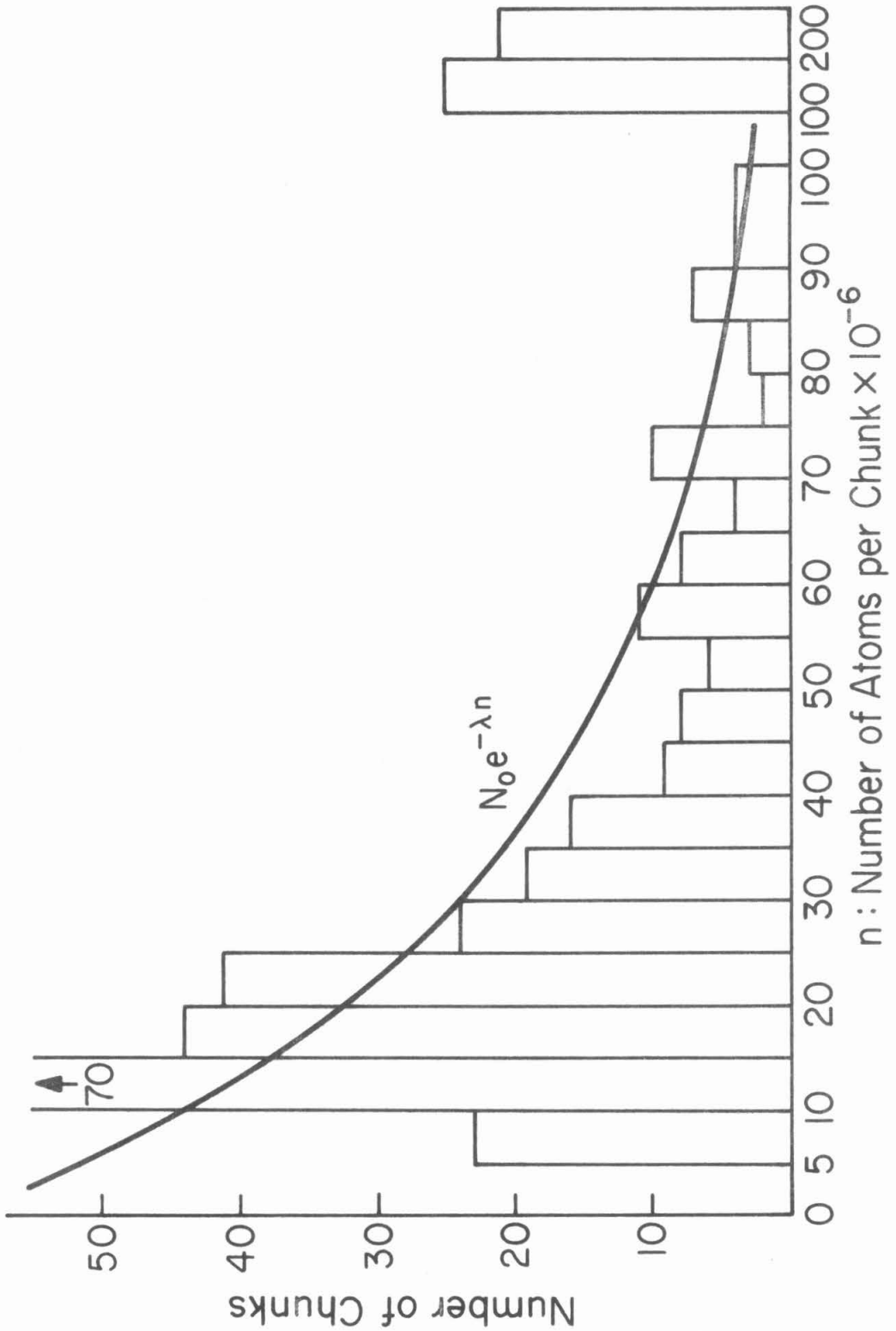
Number of Chunks
50
40
30
20
10
0 5 10 20 30 40 50 60 70 80 90 100 100 200
n : Number of Atoms per Chunk × 10^{-6}
$N_0e^{-\lambda n}$
70